Tiago Rodrigo da Costa Coelho

Licenciatura em Bioquímica

Unveiling paracrine dissemination and toxicity of neuronal TrkB-ICD via secretome signalling in Alzheimer's disease

Dissertação para obtenção do Grau de Mestre em
Bioquímica para a Saúde

Orientadora: Maria José de Oliveira Diógenes Nogueira, PhD – Instituto de Medicina Molecular João Lobo Antunes | Instituto de Farmacologia e Neurociência, Faculdade de Medicina da Universidade de Lisboa

Co-orientadora: Dora Maria Tuna de Oliveira Brites, PhD – iMed.Ulisboa | Instituto de Investigação do Medicamento, Faculdade de Farmácia da Universidade de Lisboa

Co-orientador Interno: Hugo Vicente Miranda, PhD – CEDOC | NOVA Medical School, Faculdade de Ciências Médicas da Universidade Nova de Lisboa

Maio de 2021

Tiago Rodrigo da Costa Coelho

Licenciatura em Bioquímica

Unveiling paracrine dissemination and toxicity of neuronal TrkB-ICD via secretome signalling in Alzheimer's disease

Dissertação para obtenção do Grau de Mestre em
Bioquímica para a Saúde

Orientadora: Maria José de Oliveira Diógenes Nogueira, PhD – Instituto de Medicina Molecular João Lobo Antunes | Instituto de Farmacologia e Neurociência, Faculdade de Medicina da Universidade de Lisboa

Co-orientadora: Dora Maria Tuna de Oliveira Brites, PhD – iMed.Ulisboa | Instituto de Investigação do Medicamento, Faculdade de Farmácia da Universidade de Lisboa

Co-orientador Interno: Hugo Vicente Miranda, PhD – CEDOC | NOVA Medical School, Faculdade de Ciências Médicas da Universidade Nova de Lisboa

Júri:

Presidente: Prof. Doutor António Sebastião Rodrigues
Arguente: Prof. Doutora Teresa Faria Pais
Vogais: Prof. Doutora Maria José de Oliveira Diógenes Nogueira
Prof. Doutora Maria Teresa Nunes Mangas Catarino
Prof. Doutora Teresa Faria Pais

Faculdade de Ciências Médicas da Universidade Nova de Lisboa

Maio de 2021

2021

Unveiling paracrine dissemination and toxicity of neuronal TrkB-ICD via secretome signalling in Alzheimer's disease

Tiago Coelho

UNIVERSIDADE NOVA DE LISBOA

Unveiling paracrine dissemination and toxicity of neuronal TrkB-ICD via secretome signalling in Alzheimer's disease

This work was funded by Santa Casa da Misericórdia MB37-2017 and FCT/Ministério da Ciência, Tecnologia e Ensino Superior (MCTES), through the Fundos do Orçamento de Estado UID/BIM/50005/2019, awarded to Maria José Diógenes, Twinning action (SynaNet) from the EU H2020 Programme, PhD fellowship PD/BD/114441/2016, to João Fonseca-Gomes, PTDC/MED-NEU/31395/2017 and LISBOA-01-0145-FEDER-031395 to Dora Brites, by FCT-UIDB/04138/2020 and UIDP/04138/2020, to iMed.ULisboa. and PhD fellowship FCT/SFRH/BD/128738/2017 to Gonçalo Garcia.

Publications

While developing this master project, I was also invited to collaborate in other works, now published (*1* and *2*).

1. Belo RF, Martins MLF, Shvachiy L, **Costa-Coelho T,** Almeida-Borlido CD, Fonseca-Gomes J, Neves V, Miranda HV, Outeiro TF, Coelho JE, Xapelli S, Valente CA, Heras M, Bardaji ER, Castanho MARB, Diógenes MJ, Sebastiao AM (2020). The neuroprotective action of amidated-kyotorphin on amyloid β peptide-induced Alzheimer's disease pathophysiology. *Frontiers in Pharmacology Neuropharmacology,* **11** (2020)

2. Miranda-Lourenço C, Ribeiro-Rodrigues L, Fonseca-Gomes J, Tanqueiro SR, Belo RF, Ferreira CB, Rei N, Ferreira-Manso M, Almeida-Borlido CD, **Costa-Coelho T**, Freitas CF, Zavalko S, Mouro FM, Sebastião AM, Xapelli S, Rodrigues TM, Diógenes MJ (2020). Challenges of BDNF-based therapies: from common to rare diseases. *Pharmacological Research*, **162** (2020)

Beyond that, I was also able to present a poster (*3*) and an oral communication (*4*) regarding this thesis:

3. **Costa-Coelho T,** Fonseca-Gomes J, Ferreira CB, Sebastião AM, Brites D, Diógenes MJ – "Unveiling paracrine dissemination and toxicity of neuronal TrkB-ICD via secretome/exosome signaling in Alzheimer's disease" – 5th Meeting Mind-Brain College (12th-13th November 2019, Lisbon)

4. **Costa-Coelho T,** Fonseca-Gomes J, Garcia G, Ferreira-Manso M, Savchak OK, Pinto S, Sebastião AM, Brites D, Diógenes MJ – "Vesicle dissemination of neuronal TrkB-ICD in secretome: relevance in Alzheimer's disease pathophysiology" – 51st Reunião da Sociedade Portuguesa de Farmacologia (SPF) (17th -19th February 2021, Lisbon)

“Monsters are real, and ghosts are real too. They live inside us, and sometimes, they win.”

- Stephen King -

“Once you’ve met someone you never really forget them. It just takes a while for your memories to return.”

- from “Spirited Away”, by Hayao Miyazaki -

“É saber relativizar e respirar!”

- João Gomes -

“Stat sua cuique dies
Stat sua cuique dies
Maél is mé tó féran
Ὤλετο μέν μοι νόστος
Ὤλετο μέν μοι νόστος
C'est pour cela que je suis née
この道や 行く人なしに
この道や 秋のくれ
C'est pour cela que je suis née
Ne me plaignez pas
C'est pour cela que je suis née”

- “I Was Born For This” from Journey, by Austin Wintory -

Acknowledgments

"The most important things are the hardest to say. They are the things you get ashamed of because words diminish them -- words shrink things that seemed limitless when they were in your head to no more than living size when they're brought out. But it's more than that, isn't it? The most important things lie too close to wherever your secret heart is buried, like landmarks to a treasure your enemies would love to steal away. And you may make revelations that cost you dearly only to have people look at you in a funny way, not understanding what you've said at all, or why you thought it was so important that you almost cried while you were saying it. That's the worst, I think. When the secret stays locked within not for want of a teller but for want of an understanding ear."

— Stephen King —

In the midst of mania and madness... where should I begin?

Who would know that a single year would impact and shape me into a new person, one that stops being afraid of emotions, one that stops raising walls, a person that tries its best to overcome its own insecurities! These past 365+ days were different!

A short memoire of heartfelt words forever attached to this work, is in my opinion, the most fitting way to convey the much needed appreciation while trying to make justice to all of those who have helped me in this last year; those who I have burdened; those who stood by my side when I was at my lowest; those who have celebrated my victories; THOSE, simply put! Having said that, one should not measure their importance by this tribute, but by knowing the bonds we share.

It must be said that the work presented in this thesis could have not been made without the help and support of those mentioned ahead. I feel truly honored to have worked with such brilliant and kind people. With this, I would like to express my deepest gratitude to:

Starting off strong, I would like to thank the one who welcomed me with open arms, **Maria José Diógenes**, hereinafter **Mizé**! I still cannot fathom the idea that I am part of a team driven by the one area that, for almost a decade now (yes, 14-year-old Tiago would be thrilled if he knew!), I dreamt about: Neuroscience. Not only that, but in the field that most excites my inner scientist, neurodegeneration. Thank you for inspiring me to be a better scientist, for the dedication, for all the little times you had

and still wanting to catch up and for all the memories caught in those timeless pictures. You were right, they are and will always be precious memories! These were priceless gifts that I can never repay. If I was to be a blank canvas, you would be the guiding brush that, with each stroke, allowed me to make my own path. Of course that no painting, or journey for that matter, is free of ups and downs, but your motivation, persistence, friendship, and motherly love would always lead me to find solace and try again! There were stressful times where you would set aside your work to help me out; to cheer me on; to praise me and to brainstorm with me. I am extremely proud and grateful to have you as my supervisor, but more importantly to have you as a friend and as a second mother figure that I can count on! It was on March 25th, 2019 that it had become official, from that day onward I had been introduced to a new family. A family that I now treasure deeply in my heart. In your own words: "Bem vindo a bordo!". Thank you Mizé!

My deepest gratitude's to Professor **Ana Sebastião**, the captain of our incredible group, for allowing me to do research in the Neuronal Communications and Synaptopathies Unit and for giving all the necessary conditions so that we can perform science comfortably. Always present to make comments, suggestions and giving ideas, advocating that science is making bridges and joining forces between different areas of expertise. A true leader!

With that, I must thank my dear co-supervisor, Professor **Dora Brites**. It is not a matter of how many times, or how many hours I am with someone, but how does that person behave and connect with me. Since our first meeting, I have nothing but respect for you and for your amazing, dare I call them, crazy ideas! Always striving for more, an unstoppable thirst for knowledge, a trait of whom truly loves what it does. Thank you for the wisdom, guidance, resources, and especially the much-needed advice for the path I was about to walk. I hope we will continue to cross paths in the future!

To the one person without whom none of this would had happened, my internal supervisor and friend, **Hugo Vicente Miranda**. I still remember when I asked you for advice and you suggested me who is now my wonderful supervisor. For all of your advices and trustworthy opinions, thank you!

To the one and only Professor **Teresa Catarino**, my former enzymology teacher and now my current master coordinator, the happy virus of all coordinators! Thank you for accepting me in this wonderful master program, for all the honesty and advices throughout my academic years. You were always a lighthouse, a friend that guides in times of distress. Also, to Professor **Sebastião Rodrigues** for all the help and guidance regarding the last stretch in this master program.

Heads-up, for this one is about to be long and yet short at the same time. This was also one of the hardest to write as it brought up and reminded me of several moments in this last year. Very rarely do I find someone whose personality makes me open up, specially someone who I just met, as I tend to be extremely shy around new people. For that, I have to thank you **João**, the unsung hero of this work! At first glance it was clear that your outgoing personality would clash with my calm, reserved nature… and it did, multiple times in the beginning. Your over-the-top eccentricities would always short-circuit my brain, leaving me speechless. But time took its course and bit by bit I felt that I could rely on you. Soon enough I was also preaching the doctrine of "certoooooo", even if as a(n) (un)fortunate reflex; even if you were not around. But throughout this journey not all was bliss, there were times where I felt confuse, lonely and even lost. The feeling of being trapped in an endless loop that starts to consume ones will, replacing it with self-loathing. You experienced it even though I tried to hide it. You have seen a side of me that very few have before, a side that I am not proud of, a side that I deeply try to hold within me. I failed. I was not able to. And, even though I stopped believing in myself at a point, you did not! You saw strength where I saw weakness, resilience where I saw loss, hope where I saw failure. There were times where I pointlessly and stubbornly kept thinking where things went wrong, and you systematically continued looking over me. I thank you for forcing me out of the lab when I needed most; for giving me a shoulder to cry; for supporting me; for all the wanted and unwanted help. There were times where I had to let off some steam, and you were there to listen and shoulder me. Likewise, if there is anything you ever need, just know that you can count on me! I would like to apologize for all the burden I have put you up to. I (tried to) know how busy you were, and attempted not to give you more work, because I know that like me, you always try to help (even when overloaded). I am also sorry for not being as outspoken as I wanted but do know that I cherish(ed) every moment of our friendship. All in all, I am sorry for everything! If I had to name a single moment that I will hold dear, it would be the hug – it meant a lot! You made me grow not only as a scientist but also as a person, showing me that determination is needed no matter the scenario. And also, you taught me the valuable lesson of "relatiza", and that the next day will always shine brighter than the one before. There is a lot more that I could write about, but I also know that summarizing everything on paper will never be enough… I do not know what the future has in store for you or me but nonetheless, despite what title you ceaselessly renounce – my unofficial co-supervisor, my mentor, my role model – there is one you cannot escape: you are my friend, and a very dear one! Love you older bro!

To another person who I admire, the LTP nemesis, **Rita**. As the original member of the official Rita Fanclub, and your friendly neighbor, I cannot not dedicate a special section to you. I have already told you that besides the big bosses, you and the later are the two people who I respect the most. Your determination, humbleness and critical judgment are essential goods in a scientist's kit to success. Even though you did not have to, you took me under your wing and shared your knowledge, gave me critics, advices, tips and tricks. You took your "free time" and taught me to be a better scientist, its hardships (moment of silence for the lost Hoechst) and its delights. Thank you for the trust, I will not disappoint!

Starting off novel experiments in the lab can be daunting and overwhelming, but thanks to the extracellular vesicle crew - **Gonçalo Garcia and Sara Pinto** - I had the confidence and guts to do it. There were times where the path was still foggy, but it began to clear itself with your help. Thank you for staying by my side!

It is time to speak of someone who has been on this same journey with me. I know that these past 2 years might have seemed and felt like a turmoil! But look at us now **Kat**, doing what we wanted! Aside from all the backlashes, discussions, and sleepless nights over works, you have to admit that we make a hell of a good team! Thank you for all the support you gave me when I was lacking and for all the innovative ideas when my mind was too clouded to think. From the pointless conversations in the culture to the mindless rants at the end of the day (beginning…middle… all the time). Thank you for your friendship! PhD?

To my dear northern, Yoshi-loving friend **Mafalda** *aka* **Mafs**! Thank you for always challenging me to up do myself. For all the help you willingly and unwillingly (sorry) offered! For an extra set of hands to pipette and wash those endless plates and an extra head to think. This year took its toll on us, whether due to failed experiments, late nights at the lab or even social isolation, but like partners in crime (even though you are a Gryffindor), we supported each other and conquered what we set out to do! PhD?

Who would have thought that a person who says "o enzima" would ever become my friend…? I AM JOKING! Now, do not get offended, but it is "a enzima". Grammatical nonsense aside (even though I am right!), I thank you **Carolina**! For always speaking up, for your caring personality and supportive attitude. For always offering me help and catching up about the latest manga series chapters. Let's go PhD?

It is known that the brain needs sugar to work, and so this journey assembled an adenosinergic system dopping team, **Daniela, Joana,** Sara, Kat and Mafs**.** Still cannot process the amount of coffee breaks one needs to go through the day (I

counted 3 in a single morning!), but nonetheless, those were also short breaks to laugh and unwind from everything lab-related. Thank you for making this experience more fun. Coffee break?

A special thanks to Mizeses: Mizé, João, Rita**, Bia, Catarina, Sara, Nádia, Leonor,** Mafalda, Carolina**, Céline, Svitlana, Francisco** and **Sara Oliveira** for giving me a comfortable place to bond and grow. In that regard, a special thanks to the remaining **ASeb Lab members**!

To all the **mice** that were used and evaluated in this project, thank you. I am hopeful that your contribution will move this research line forward and sprout fruitful outcomes in the future!

Importantly, we must not forget those who cheer for us from the sidelines, as the majority of them have accompanied me from other points in time. These are friendships that lasted and that endured (some older, some newer).

To **Miguel (primo), Mike, Repolho, Neto, Luís, Babs, Gabs, Cravidão, André, Sara, João, Paloma, Raquel, Paulo, Ju, Daniela, Diogo, Francisca, Muri, Philip, Vera, Rita, Gonçalo, Salomé and Inês**, for all the memories, adventures (in both realms), traditions, laughs, games, movies, low IQ (and high IQ) moments… and many other things. These are some of the people that one is proud to have by their side. Those who stay and bring out the best in you. Thank you!

Finally, some warm words to my close family: **mãe, pai, irmão, tio, avó (and to those who are not here today – avó e tia** specially -, but I am sure would be proud). Thank you! Thank you for always being there not matter the scenario, for helping me not matter the problem, for supporting me no matter my choices, for praising me no matter my outcomes, for acknowledging me no matter my decisions… for everything! Life will continue to present its challenges, but with your help, I will continue to move forward and make you all proud. Love you all!

Lastly (I promise) an unusual message from the present me (currently writing this) to the **future me**: Grow up (in the good sense)! Treasure every moment people around give you and be more outspoken. Do not let measle hindrances such as shyness get in-between you and your friends, for that will hurt you later on. Take it all in, good and bad. Cherish and make everlasting memories with those dear to you and learn from your mistakes. Grow up to be the best version of (our)yourself. I truly feel that the Tiago writing this is much different from the Tiago 1 year ago. Today I see myself as a much stronger person, having embodied a set of traits of those who I shared this last year with.

In the midst of mania and madness… one has to be mindful of the journey, and what journey this has been!

What will come next?

All figures and timelines were created using **BioRender.com**

Abstract

The brain-derived neurotrophic factor (BDNF) is a neurotrophin that binds to the TrkB full-length receptor (TrkB-FL), triggering cascades responsible for neuroprotection. This BDNF/TrkB-FL system is known to be impaired in Alzheimer's disease (AD) due to an amyloid-β-mediated TrkB-FL cleavage, leading to the formation of two fragments, a membrane-bound truncated receptor (TrkB-T') and an intracellular domain fragment (TrkB-ICD). TrkB-ICD has tyrosine kinase activity, promotes cognitive impairments, and modifies gene expression. Notwithstanding, its intracellular clearance mechanisms remain elusive. Importantly, TrkB-ICD has been detected in cerebrospinal fluid of humans, questioning its release pathway. Interestingly, AD pathological features may be disseminated by extracellular vesicles (EVs) such as exosomes and microvesicles, which by incorporating harmful mediators, can drive intercellular propagation of inflammatory, misfolded proteins and toxic factors. Although AD remains as an untreated disorder, our lab designed a peptide, TAT-TrkB, capable of preventing TrkB-FL cleavage. As such, this project aimed at: i) explore TrkB-ICD cellular clearance mechanisms; and ii) evaluate the efficacy of TAT-TrkB in 5xFAD, an AD mouse model.

Data with TrkB-ICD-expressing SH-SY5Y cells corroborated that TrkB-ICD is a stable fragment with a half-life of approximately 6-8 h. Studies evaluating the contribution of both the proteasome and autophagy pathways in TrkB-ICD clearance did not completely elucidate its degradation mechanisms, so far. We pioneered the discovery of TrkB-ICD in microvesicles, and exosomes released by SH-SY5Y cells. This is a remarkable observation that may imply that TrkB-ICD can be disseminated among cells. propagating its toxicity. The experiments performed to evaluate TAT-TrkB efficacy in the 5xFAD AD mouse model were done in the context of a pilot study and did not provide a coherent conclusion, prompting us to redesign this *in vivo* study in future work. Nevertheless, the obtained data strongly suggest that TAT-TrkB may have a beneficial role in learning and memory, as evaluated by the Morris Water Maze test.

Keywords: Alzheimer's disease, TrkB-FL, TrkB-ICD, extracellular vesicles, TAT-TrkB peptide, 5xFAD model

Resumo

No sistema nervoso, o fator neurotrófico derivado do cérebro (*Brain-derived Neurotrophic Factor*-BDNF), é uma neurotrofina que, quando ligada ao seu recetor completo (TrkB-FL), promove neuroproteção. Todavia, na doença de Alzheimer (Alzheimer's disease-AD) o péptido amilóide-β (Aβ) promove a clivagem do TrkB-FL, levando à formação de um novo recetor truncado (TrkB-T') e de um fragmento intracelular, TrkB-ICD. Este fragmento possui atividade tirosina cinase e é capaz de alterar a expressão génica e promover comprometimento cognitivo. Contudo, desconhece-se quais os mecanismos intracelulares pelos quais é degradado. Curiosamente, o nosso laboratório detetou a presença deste fragmento no líquido cefalorraquidiano de doentes com AD, postulando a hipótese de que possa ser libertado por vesículas extracelulares (*extracellular vesicles*-EVs). Estas vesículas, muito envolvidas na sinalização intercelular, foram já associadas à transmissão de mediadores de toxicidade na AD, disseminando proteínas e outros agentes tóxicos. A falta de tratamento nesta doença, impulsionou o nosso laboratório a desenvolver um péptido TAT-TrkB, capaz de prevenir a clivagem do TrkB-FL, restaurando os efeitos protetores da sinalização BDNF/TrkB-FL. Desconhecendo-se os mecanismos de depuração do TrkB-ICD e os efeitos do novo composto, TAT-TrkB, este projeto propôs-se a: i) elucidar possíveis mecanismos de depuração celular do TrkB-ICD; e ii) estudar a eficácia do TAT-TrkB em ratinhos 5xFAD, um modelo de AD com patologia Aβ.

Estudos com células SH-SY5Y a expressar TrkB-ICD corroboraram que o fragmento tem um tempo de semi-vida de 6-8h. A avaliação da possível contribuição da degradação proteasomal e lisosomal não permitiu clarificar relativamente à depuração do fragmento. Identificámos, pela primeira vez, a presença do TrkB-ICD em microvesículas e exosomas de células SH-SY5Y, servindo como uma forma de depuração celular e um possível mecanismo de propagação tóxica intercelular. As experiências realizadas em ratinhos 5xFAD não permitiram apurar a eficácia do TAT-TrkB, pela qual serão redesenhadas. No entanto, dados obtidos pelo teste *Morris Water Maze* sugerem um restauro da aprendizagem e memória.

Palavras-Chave: Doença de Alzheimer, TrkB-FL, TrkB-ICD, vesículas extracelulares, péptido TAT-TrkB, modelo 5xFAD

Table of Contents

Index of figures

Index of tables

Abbreviations

(e)GFP	(Enhanced) Green Fluorescent Protein
(e)NMDAr	(Extrasynaptic) *N*-methyl-$_D$-aspartate receptor
5xFAD	AD mice model carrying 5 different familial AD mutations
AD	Alzheimer's disease
AICD	APP intracellular domain
Akt	Protein kinase B
ALIX	Programmed cell death 6-interacting protein
ALP	Autophagy-Lysosomal pathway
AMPA	α-amino-3-hydroxy-5-methyl-4-isoxazolepropionic acid
APP	Amyloid-beta precursor protein gene
APP	Amyloid-beta precursor protein
ARF1/6	ADP-ribosylation factor 1/6
Atg proteins	Autophagy-related proteins
ATP	Adenosine Triphosphate
Aβ	Amyloid-β
BAD	Bcl-2 antagonist of cell death
BBB	Blood-brain barrier
BDM-PUB	Bayesian Discriminant Method of Prediction of Ubiquitination sites
BDNF	Brain-derived neurotrophic factor
BSA	Bovine Serum Albumin
C57BL/6J	C75 black 6J – common inbred strain of laboratory mice
CA1	*Cornu Ammonis* 1 area
Ca^{2+}	Calcium ion
CaMK	Ca^{2+}/Calmodulin (Ca^{2+}/CaM)-dependent kinases
cAMP	Cyclic adenosine monophosphate
CD9/63/81	Tetraspanin 9/63/81
CHX	Cycloheximide
CMA	Chaperone mediated autophagy
CNS	Central nervous system
CO_2	Carbon dioxide
CREB	cAMP response-element binding protein
CSF	Cerebrospinal fluid
CTR	Control
DAG	Diacylglycerol

DAPI	4',6-diamidino-2-phenylindole
DGAV	Direção Geral de Alimentação e Veterinária
DIV	Days *in vitro*
DLS	Dynamic Light Scattering
DNA	Desoxyribonucleic acid
DOB	Days of birth
DTT	Dithiothreitol
E. coli	*Escherichia coli*
E1	Ubiquitin-activating enzyme
E17-E18	Embryonic day 17-18
E2	Ubiquitin-conjugating enzyme
E3	Ubiquitin ligase
EDTA	Ethylenediaminetetraacetic acid
EPM	Elevated Plus Maze
Erk	Extracellular signal-regulated kinase
ESCRT	Endosomal sorting complex required for transport
EV	Extracellular vesicle
EXO	Exosome
FBS	Fetal Bovine Serum
FDA	US Food and Drug Administration
FDG-PET	Fluorodeoxyglucose-positron emission tomography
GAPDH	Glyceraldehyde 3-phosphate dehydrogenase
GSK-3β	Glycogen Synthase Kinase 3β
GTPases	Family of guanosine triphosphate hydrolase enzymes
h	Hour
HBSS	Hank's Balanced Salt Solution
HCl	Hydrochloric acid
HEK293T	Human Embryonic Kidney 293 cells T
HEPES	N-2-Hydroxyethylpiperazine-N'-2-Ethanesulfonic Acid
HSC70	Heat shock cognate 70 kDa protein
HSP70	Heat shock 70 kDa protein
i.p.	Intraperitoneal injection
ICAM-1	Intracellular Adhesion Molecule 1
ICD-V5	TrkB-ICD-V5
IF	Immunofluorescence
ILV	Intraluminal vesicle

IP_3	Inositol triphosphate
JNK	c-Jun N-terminal kinase
K	Lysine
k	decay rate constant
KCl	Potassium chloride
KH_2PO_4	Potassium dihydrogen phosphate
LC3B	Microtubule-associated proteins 1A/1B light chain 3B
LRRK2	Leucine-rich repeat kinase 2
LTP	Long-Term Potentiation
mA	Milliampere
Map2	Microtubule-associated protein 2
MAPK	Ras-mitogen-activated protein kinase
MCI	Mild Cognitive Impairment
Mg^{2+}	Magnesium ion
MHCI/II	Major Histocompatibility Complex I/II
miRNA	Micro RNA
mM	Millimolar
MOI	Multiplicity of Infection
MRI	Magnetic resonance imaging
mRNA	Messenger Ribonucleic Acid
mTOR	Mammalian target of rapamycin
mV	Millivolt
MV	Microvesicle
MVE	Multivesicular endosome
MWM	Morris Water Maze
$Na_2HPO_4.2H_2O$	Sodium hydrogen phosphate
Na_3VO_4	Sodium orthovanadate
NaCl	Sodium Chloride
NADE	p75NTR-associated cell death executor
NaF	Sodium fluoride
NF-κB	Nuclear factor kappa light chain enhancer of activated B cells
NGF	Nerve Growth Factor.
NIA	National Institute on Ageing
nM	Nanomolar
NRAGE	Neurotrophin Receptor-interacting Melanoma Antigen-encoding protein

NT	Neurotrophin
NT3	Neurotrophin 3
NT4/5	Neurotrophin 4/5
NT6	Neurotrophin 6
NT7	Neurotrophin 7
NTF	Neurotrophic Factor
NTRK2	Neurotrophin tyrosine kinase receptor 2, gene that encodes for TrkB
N-type	SH-SY5Y cells displaying a neuroblastic morphology
ORBEA	Órgão Responsável pelo Bem-Estar Animal
p21	Cyclin-dependent kinase inhibitor 1
p3 fragment	3-kDa APP fragment resulting from α- and γ-secretase cleavage
p53	Tumor protein p53
p62	Sequestosome-1/Ubiquitin-binding protein p62
p75NTR	p75 neurotrophin receptor
PBS	Phosphate buffered saline
PD	Parkinson's disease
PDL	Poly-D-Lysine
PI3K	Phosphatidylinositol 3-kinase
PLCγ	Phospholipase Cγ
pre-pro-NT	Precursor neurotrophin
pro-NT	Immature neurotrophin
PrP^{c}	Cellular Prion Protein
PSEN1/2	Presenilin1/2 gene
PVDF	Polyvinylidene difluoride
Q	L-glutamine
RA	Retinoic acid
Rab	Ras-associated binding family of proteins
Rac1	Ras-related C3 botulinum toxic substrate 1
Ras	Family of small GTPases involved in cellular signal transduction
RIP2	Receptor-interacting protein 2
RIPA	Radio-Immunoprecipitation Assay buffer
RNA	Ribonucleic acid
RT	Room temperature
SDS	Sodium dodecyl sulfate
SDS-PAGE	Sodium dodecyl sulfate polyacrylamide gel
Shc	Shr homologous and collagen-like adaptor

SNARE	Soluble NSF Attachment Protein Receptor complex
SOD-1	Superoxide dismutase 1
S-type	SH-SY5Y cells displaying a non-neuronal substrate adherent morphology
$T_{1/2}$	Half-life
TAT-TrkB	Peptide with a TAT domain fused to the cleavage-targeted TrkB-sequence
TBS-T	Tris-Buffered Saline Tween 20
TCA	Trichloroacetic acid
TDP-43	TAR DNA-binding protein 43
TEM	Transmission Electron Microscopy
Tg	Transgenic
TGN	Trans-Golgi network
TNF	Tumor necrosis factor
TNFR	Tumor necrosis factor receptor
TRAF6	TNR receptor-associated facto 6
Trk	Tropomyosin-related Kinase
TrkA/B/C	Tropomyosin-related Kinase A/B/C
TrkB-FL	TrkB Full-length
TrkB-ICD	TrkB-Intracellular Domain (calpain-generated)
TrkB-ICD-stop	Plasmid expressing for TrkB-ICD
TrkB-ICD-V5	Engineered TrkB-ICD fragment with a V5-tag fused in its C-terminal
TrkB-T'	TrkB Truncated receptor (calpain-generated)
TrkB-T1/T2	TrkB Truncated receptor 1/2
TrkB-TK (+/-)	TrkB tyrosine kinase positive/negative
TrkB-T-Shc	TrkB truncated receptor with a Shc binding site
TrkB-T-TK	TrkB truncated receptor with a partly functional tyrosine kinase domain
TSG101	Tumor susceptibility gene 101
U/mL	Unites per millilitre
Ub	Ubiquitin
UPS	Ubiquitin-Proteasome System
V5	14-amino acid tag
V-ATPases	Vacuolar H^+-ATPases
Veh	Vehicle
w/v	Weight per volume
WB	Western-blot

Y	Tyrosine
μM	Micromolar

1 Introduction

1.1 Neurotrophins and the Brain-derived Neurotrophic Factor

Within the realm of cellular communication, neurotrophins (NTs) are a family of growth factor peptides and proteins essential for the neurodevelopment and maintenance of both the central and peripheral nervous systems[1–3]. These soluble survival factors are a part of the Neurotrophic Factor superfamily (NTF), alongside other branches of signalling molecules, including the glial cell line-derived neurotrophic factor family ligands and the neuropoietic cytokines, both of which also exert a role in neuronal homeostasis[4–6]. NTs are one of the most well-studied family of NTFs, as they hold the first growth factor discovered, the Nerve Growth Factor (NGF); additionally, the remaining members of this family have also been highly studied as they are linked with the pathophysiology of several neurodevelopment, neuropsychiatric and neurodegenerative disorders, namely Alzheimer's disease (AD)[7–10].

NGF was first discovered in 1956 as a growth-enhancing agent capable of promoting morphological differentiation of sensory and sympathetic ganglia[7,11]. This was followed by the discovery of other ligands similar both in structure and sequence such as the Brain-derived neurotrophic factor (BDNF), Neurotrophin 3 (NT3), and Neurotrophin 4/5 (NT4/5), in mammals; additionally, Neurotrophin 6 (NT6) and Neurotrophin 7 (NT7) in fish[12–18].

Briefly, NTs are initially synthesized on the rough endoplasmic reticulum as precursor NTs (pre-pro-NTs), followed by the cleavage of their signal peptide. Similar to other secreted proteins, immature NTs (pro-NTs) are then directed towards the Golgi apparatus and later to the trans-Golgi network (TGN), where they are proteolytic processed and sorted into a vesicle-secretion pathway[19–21]. The fusion of these vesicles with the dendritic or axon terminal plasma membrane releases these pro- and/or mature homodimer NTs, capable of triggering the activation of two main receptors - the tropomyosin-related kinase (Trk) receptor and the p75 neurotrophin receptor (p75NTR, TNF-superfamily member) - that exert different effects[1,8,22] (Figure 1.1). In some instances, it is possible to occur the formation of NT heterodimers, also capable of inducing the activation of both receptors. However, these are not thermodynamically stable, nor is their dimer binding durable[23,24]. Depending on their maturation state, NTs have different binding affinities as to whether they bind to Trk

receptors or p75NTR receptors. While pro-NTs usually bind with higher affinity to the TNF-superfamily related receptor, they also are substrates, albeit with lower affinity, to Trk receptors. On the other hand, mature NTs bind strongly with Trk receptors, and poorly with p75NTR. Moreover, different NTs bind to different Trk receptors: NGF is the main ligand of TrkA, BDNF and NT4/5 bind to TrkB and NT3 to TrkC[1,10] (Figure 1.1). As referenced above, the activation of both receptors leads to signalling cascades with different effects. While triggering the activation of p75NTR receptor promotes cascades mainly related to neuronal death, Trk receptor activation promotes downstream pathways responsible for neuroprotection, including neuronal differentiation, plasticity and survival[1,22].

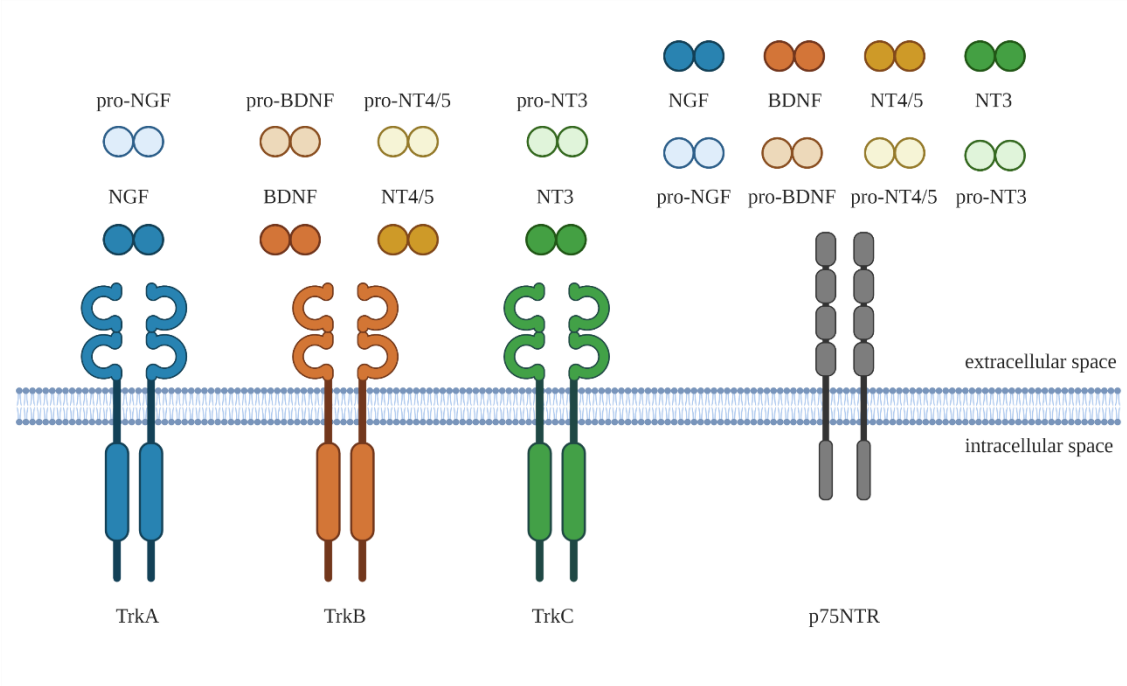

Figure 1. 1 - Ligand selectivty of pro-NTs and NTs to their Trk and p75NTR receptors.
While pro-neurotrophins bind with high-affinity to p75NTR receptors, neurotrophins have high ligand affinity with their Trk receptor counterparts. TrkA recognizes NGF, TrkB binds both BDNF and NT4/5 and TrkC recognizes NT3. BDNF – brain-derived neurotrophic factor; NGF – nerve growth factor; NT3/4/5 – neurotrophin 3,4,5; p75NTR – p75 neurotrophin receptor; TrkA/B/C – tropomyosin-related kinase A/B/C.

Considering that this work is mainly focused on the action of the BDNF/TrkB receptor system, more emphasis will be given to it hereinafter. BDNF was discovered almost two decades after NGF, when Barde and his team were able to purify, from a 1.5 kg pig brain, a new growth factor able to sustain the survival of embryonic chick sensory neurons[13]. Following studies have revealed that BDNF mRNA and protein levels are abundant in early postnatal and adult human and rodent brains, with high levels detected in the hippocampus, neocortex, cerebellum, and amygdala[19]. Its

regulation is controlled not only by multiple promoters in a tissue specific expression pattern, but also modulated by internal and external stimuli like neuronal activity, exercise, hormones and stress[25–27].

As described above, BDNF synthesis starts by translation of its mRNA, in the rough endoplasmic reticulum, to its pre-pro-BDNF precursor, followed by the cleavage of its pre-sequence. Pro-BDNF is then transported into the Golgi apparatus where its pro-domain is targeted by several post translation modifications, creating recognition moieties latter recognized by proteases. Subsequently, pro-BDNF is transported into the TGN, and sorted by two vesicle-trafficking pathways. In the constitutive pathway, prior to its encapsulation, pro-BDNF is converted into its mature form by action of the TGN-residing enzyme, furin. These small vesicles are transported by default to the cell periphery, fusing with the plasma membrane in a calcium (Ca^{2+})-independent mechanism; Conversely, in the regulated pathway, pro-BDNF can be packaged into larger convertase-containing vesicles, where its pro-domain is proteolytic cleaved. These vesicles fuse with the plasma membrane in a Ca^{2+}-dependent manner. Depending on the nature of the stimuli, both pathways may occur. Alternately, pro-BDNF can also be secreted unprocessed, and as a ligand for p75NTR and/or TrkB receptors, or be extracellularly processed by the action of tissue plasminogen activator and matrix-metalloproteinases [19,20,28–30].

1.1.1 BDNF receptors and signalling modulation

Following secretion of neuronal, astrocytic, or microglial pro- and mature BDNF, both NTs are capable of triggering autocrine and paracrine responses, by binding to TrkB or p75NTR receptors of neuronal cells[31–33]. Depending on which cell receptor and isoform they bind, different outcomes may result. As mentioned earlier, BDNF binds preferentially to TrkB receptors, and with lower affinity to p75NTR receptors. On the other hand, pro-BDNF binds preferentially to p75NTR, but also to TrkB, albeit with low affinity.

The role of p75NTR receptors has been bewildering scientists, as its mechanisms of action remain elusive. That said, this receptor is mainly known for promoting apoptosis; in addition, it seems that depending on its activation conditions, it can also promote cell survival and increase the synergy between BDNF and its receptor counterpart, TrkB[22,34,35]. In an attempt to demystify its regulation, this receptor has been in the spotlight of several studies since its first appearance. Briefly, pro-BDNF binds to the extracellular cysteine-rich domains of p75NTR, triggering its

receptor dimerization, death domain activation, and consequent recruitment of competitor adaptor proteins involved in the signalling of other TNFR. Among these, the recruitment of Rac1 and TRAF6 both activate the JNK pathway, promoting apoptosis, augmented also by the recruitment of NADE; RIP2 induces NF-κB pathway activation, thus promoting cell survival; and NRAGE, a cell cycle arrest promotor, which ultimately may also lead to cellular death[34,36]. Accordingly, studies using alternative splicing isoforms of p75NTR that lack their binding domain, or pathological-mediated cleaved p75NTR receptors seem to show a decrease in cellular apoptosis[22,34,36]. Interestingly, data also shows that p75NTR is capable of forming heterodimers with TrkB receptors, increasing BDNF affinity and its signal transduction[35].

Several studies have already described TrkB extensively, from its pathways, to its different isoforms and subsequent BDNF modulation. Aside from its full-length receptor (TrkB-FL), the predominant alternative splicing protein variants of *NTRK2* are tyrosine kinase negative (TrkB-TK-), reflecting their non-existing tyrosine kinase domains, in contrast with TrkB-FL (also described as TrkB-TK+). These C-terminal truncated forms are classified as TrkB-T1, TrkB-T2 and TrkB-T-Shc, depending on their length. Additionally, there is also an isoform containing a non-functional tyrosine domain, TrkB-T-TK[37–41] (Figure 1.2).

Briefly, when BDNF binds the extracellular domain of TrkB-FL, it induces receptor dimerization followed by a trans-autophosphorylation of opposite tyrosine kinase domains, in their tyrosine residues, thus triggering signal transduction intracellularly[1,36] **(Section 1.1.2)**. Interestingly, BDNF is able to bind TrkB-T1, -T2, -T-Shc and -T-TK, as their extracellular domains are conserved; however, their lack of a (functional) catalytic domain, prevents the transduction of the canonical TrkB-FL pathways. Moreover, unlike TrkB-T1 and -T2, both TrkB-T-Shc and TrkB-T-TK possess the Shr homologous and collagen-like adaptor (Shc) protein binding site, albeit TrkB-T-Shc dimerization does not induce the recruitment of this adaptor nor its downstream signalling (Figure 1.2). Curiously, although TrkB-T-TK homodimers do not promote downstream signalling, their dimerization with TrkB-FL can trigger Shc canonical pathways[40–43] **(Section 1.1.2)**.

As mentioned above, not only neurons but also glial cells contribute to the pool of secreted BDNF, and likewise, express different TrkB isoforms. Overall, these receptors portray roles in morphogenesis, evocation of calcium signalling, regulation of synaptic filopodia and bolstering of glia proliferation[43–45]. Interestingly, these isoforms are also known to completely or partly hinder BDNF/TrkB-FL signalling, due

to the formation of non-fully-functional heterodimers with TrkB-FL and their ability to bind and sequester extracellular BDNF[42,46–48] (Figure 1.2).

Understandably, not only the function but also the ratio expression of TrkB isoforms and p75NTR receptors helps maintaining neuronal homeostasis.

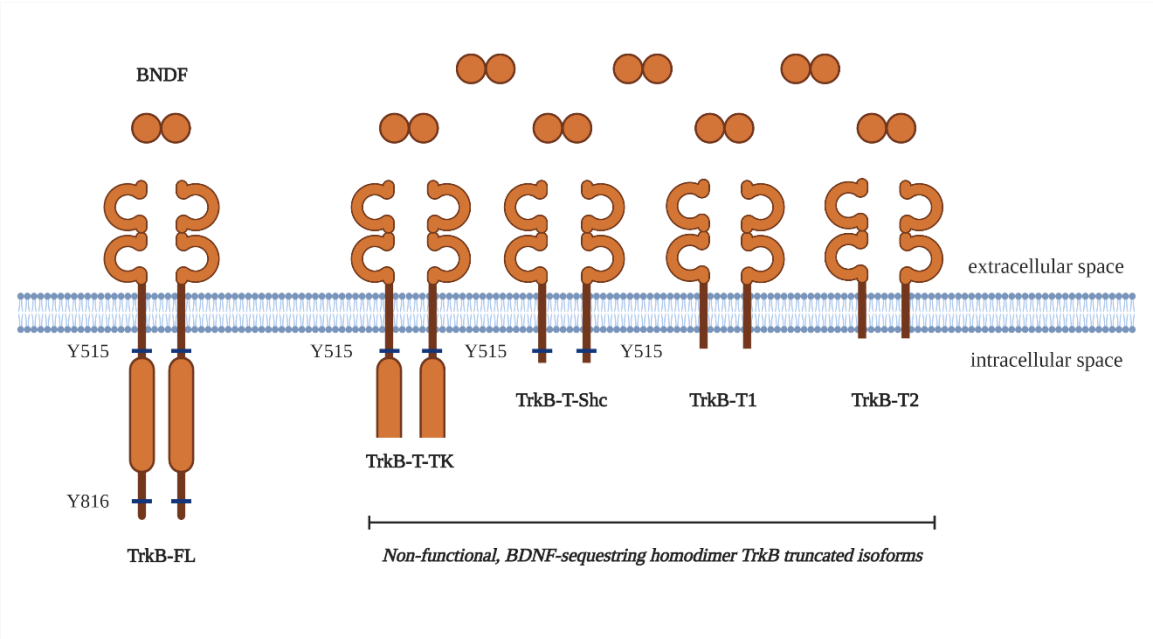

Figure 1. 2 - TrkB receptor homodimer isofoms.
BDNF binds to homodimers of TrkB-FL, triggering its cannonical signalling pathways. Conversely, alternative splicing of *NTRK2* gene leads to the lack of a functional tyrosine kinase domain in TrkB-T-TK or its absence in TrkB-T-Shc, TrkB-T1 and TrkB-T2. Moreover, these receptors are known to sequester free BDNF and form non-functional (aside from TrkB-T-TK) heterodimers with TrkB-FL. BDNF – brain-derived neurotrophic receptor; TrkB-FL – full-length tropomyosin-related kinase B; TrkB-T1/T2 - TrkB truncated receptor 1/2; TrkB-T-Shc - TrkB truncated receptor with a Shc binding site; TrkB-T-TK – TrkB truncated receptor with a partly functional tyrosine kinase domain; Y515/816 – tyrosine residues 515/816.

1.1.2 BDNF/TrkB-FL system

As seen in **Section 1.1.1,** BDNF homodimers bind to TrkB-FL receptors and trigger mechanisms of neuroprotection. Upon BDNF recognition by extracellular IgG domains, TrkB-FL receptors homodimerize and trans-autophosphorylate the adjacent TrkB-FL receptor in a triad of tyrosine residues (Y^{701}, Y^{705} and Y^{706}) present in the tyrosine catalytic domain. Consequently, this induces a new phosphorylation of two other Y residues located at the juxtamembrane and C-terminal regions, Y^{515} and Y^{816}, respectively[1,36,49]. Both of these tyrosine residues are docking sites for adaptor proteins that promote TrkB-FL downstream signalling. The former is the binding site of the Shc adaptor protein, responsible for promoting the activation of both the 1) Ras small GTPases-mitogen-activated protein kinase (MAPK) and extracellular signal-regulated kinase (Erk) pathway and also the 2) phosphatidylinositol 3-kinase (PI3K)-protein kinase B (Akt) pathway, through the recruitment of Ras and PI3K, respectively; the latter, which serves as the docking site for phospholipase Cγ (PLCγ), activates the 3) PLCγ-Ca^{2+} pathway[1,49] (Figure 1.3). Additionally, there are other adaptor proteins that can bind the phosphorylated residues in the tyrosine kinase domain of TrkB-FL, also enhancing its signalling[49,50].

Briefly, the phosphorylation of Y^{515} induces the docking of Shc adaptor protein, which in turn, depending on the selected route, recruits different sets of adaptor proteins. In the MAPK/Erk pathway, Shc induces activation of Ras with a subsequential increase in both MAPK and Erk proteins, responsible for promoting neuronal growth, differentiation, and survival through modulation of nuclear transcription factor CREB (cAMP response-element binding protein), capable of regulating expression of anti-apoptotic proteins, and modulation of BAD (Bcl-2 antagonist of cell death) and GSK-3β (Glycogen Synthase Kinase 3β), both proteins involved in neuronal apoptosis[1,36,49,51,52]. Additionally, Shc also induces the phosphorylation of intermediate adaptor proteins, leading to the activation of PI3K and thus increasing Akt levels (PI3K/Akt pathway). Similar to MAPK/Erk signalling, this pathway also promotes neuronal survival, as it modulates protein levels of NF-κB, mammalian target of rapamycin (mTOR), a protein involved in cell growth and survival, and transcription factors such as CREB. Interestingly, Akt protein is able to phosphorylate proteins capable of enhancing MAPK/Erk signalling, revealing the synergy between these two pathways[36,49,51]. Lastly, docking of PLCγ leads to the formation of inositol phosphates and diacylglycerol (DAG). The former triggers the release of intracellular Ca^{2+}, inducing the regulation of Ca^{2+}/Calmodulin (Ca^{2+}/CaM)-dependent kinases (CaMKII, CaMKK and CaMKIV), linked with synaptic plasticity behaviour, neuronal survival and neurite outgrowth

phenomena, through the regulation of CREB; on the other hand, DAG promotes de activation of protein kinase C (PKC), also known to modulate synaptic plasticity[36,49,53,54].

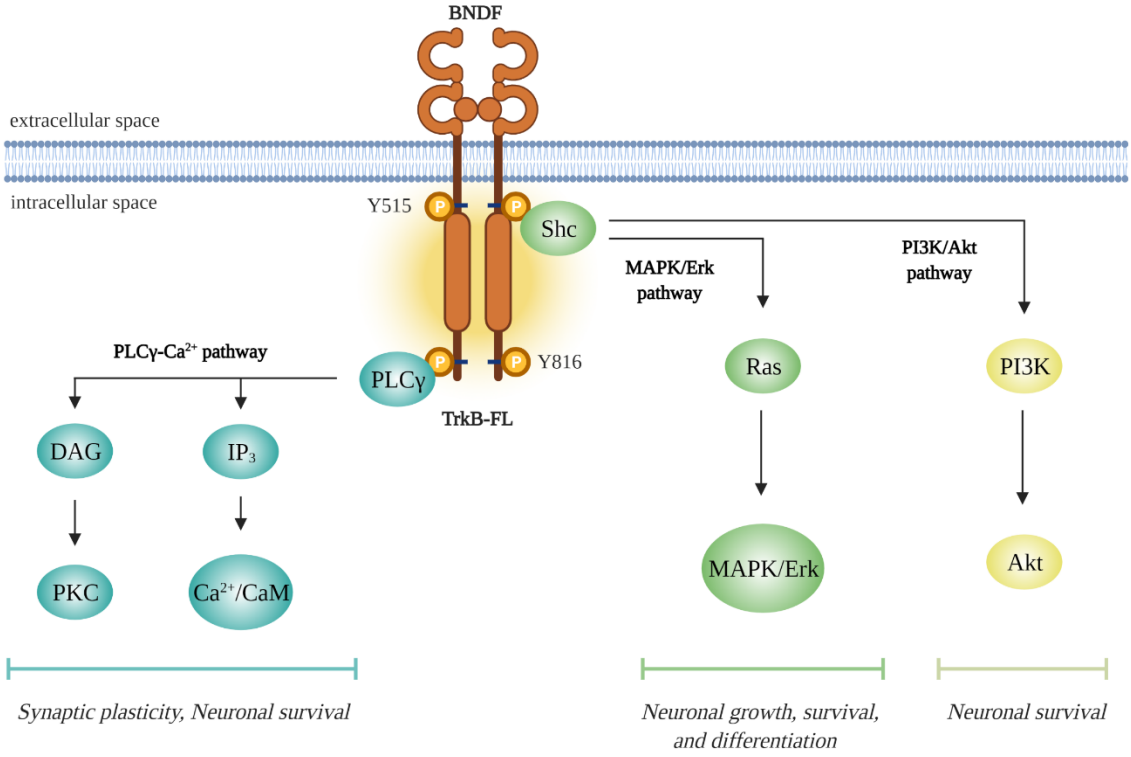

Figure 1. 3 - TrkB-FL canonical dowstream signalling pathways.
Upon BDNF binding to TrkB-FL, receptor dimerization is induced, phosphorylating (P) the tyrosine residues present in each catalytic domain together with tyrosine residues located at the juxtamembrane and C-terminal of the intracellular domain of TrkB-FL. As a consequence, the Y^{515} recruits the adaptor protein Shc, involved in both the MAPK/Erk and PI3K/Akt pathways, able to modulate neuronal growth, survival and differenitation. Adittionaly, the phosphorylated Y^{816} residue recruits the PLCγ adaptor protein, promoting and modulating synaptic plasticity together with neuronal survival. Akt - protein kinase B; BDNF – brain-derived neurotrophic factor; Ca^{2+}/CaM - calcium/calmodulin-dependent kinases; DAG – diacylglycerol; IP_3 – inositol triphosphate; MAPK/Erk - Ras-mitogen-activated protein kinase/extracellular signal-regulated kinase; PI3K - phosphatidylinositol 3-kinase; PKC – protein kinase C; PLCγ - phospholipase Cγ; Ras – small GTPase; Shc - Shr homologous and collagen-like adaptor; TrkB-FL – full-length tropomyosin-related kinase B; Y515/Y816 – tyrosine residue 515/816.

Ultimately, the correct function of all these pathways helps sustaining neuronal homeostasis. Understandably, any cellular or molecular process that uncontrollably alters either the physiology or any of its underlying players, can be seen as possible pathology mediator. Accordingly, reports have shown multiple pathologies where BDNF/TrkB-FL system is known to be dysfunctional, both in

chronic disorders, including AD, Parkinson's disease (PD) and schizophrenia, but also in acute conditions, such as strokes and other excitotoxic events[10,55–58].

Recent studies have described that when certain criteria are meet in AD, TrkB-FL receptors might be cleaved, thus compromising 1) the ratio of TrkB-FL/TrkB truncated receptors, alluded in **Section 1.1.1** as a risk for BDNF modulation, 2) its downstream signalling pathways and 3) the formation of intracellular toxic fragments known to dysregulate cellular processes[10,55,59]. Therefore, since this work is mainly focused on this system in AD, more emphasis will be given to this pathology and also to the required criteria for this dysfunctional signalling in **Section 1.2**.

1.2 Alzheimer's disease (AD)

Throughout the past decades, the rise in health care and cutting-edge biomedical research has allowed for an increase of population lifespan. Accordingly, the underlying cellular ageing process has brought forward a set of pathologies known as neurodegenerative diseases. These disorders are characterized by the progressive loss of specific groups of neurons alongside a potential accumulation of specific proteins that promote and disseminate both intra- and intercellular toxicity[60]. Importantly, neuron renewal is incredibly scarce, highlighting the impact that these diseases have in the lifestyle, diagnosis, and treatment of patients[61,62].

AD was first described in 1907 by the German psychiatrist Alois Alzheimer, and is currently the most prevalent neurodegenerative disorder worldwide as well as the most common form of dementia, affecting mainly the population over 65 years and accounting for 60-80% of dementia cases[63,64]. Importantly, AD research is paramount as studies predict that the number of patients will triple by 2050, as well as its associated socio-economic burden on patients, family members, healthcare systems and on society in general[62].

1.2.1 Clinical features and therapeutic strategies in AD

As a neurodegenerative disorder, AD is mainly characterized by the loss of pyramidal and cholinergic neurons in both the cortex and the CA1 (*cornu Ammonis*) region of the hippocampus, leading to its symptomology of progressive memory loss and impaired cognitive function. Moreover, AD patients can also suffer from behavioral changes, depression, apathy, and difficulties in speaking and walking. Actually, depending on the stage of this disorder, the whole brain can be affected, ultimately leading to its atrophy, enlarged ventricles and loss of neuronal processes[62,64,65]. In 2011, the National Institute on Ageing (NIA), together with the Alzheimer's Association proposed a new criteria for monitoring AD progression, subdividing it into three stages: 1) preclinical AD, thought as a stage where there are measurable changes in the brain, cerebrospinal fluid (CSF) and blood but with no direct correlation with the symptomatology; the patient has yet to develop symptoms, 2) mild cognitive impairments (MCI) due to AD or prodromal AD, indicating a stage where the individual has noticeable cognitive changes but can still carry out daily activities. Understandably, biomarker levels of misfolded proteins and other pathological mediators are presumably increased, and 3) dementia due to AD, where the individual loses the ability to function in its daily life without supervision, usually accompanied by the characteristic AD symptomatology[64,66].

As mentioned earlier, AD is molecularly characterized by the accumulation of two histopathological hallmarks: 1) extracellular senile plaques, which are misfolded aggregates of amyloid-β (Aβ) peptide and 2) intracellular neurofibrillary tangles, comprised of hyperphosphorylated tau protein[60,64,67]. More emphasis on Aβ peptide aggregation mechanism will be given in **Section 1.2.2**, as this will be the main toxic mediator involved in the dysfunction of BNDF/TrkB-FL signalling described in **Section 1.2.2 A1**. Accordingly, both histopathological features are the current golden standards in biomarker assessment, where Aβ42/Aβ40 ratio, total tau and phosphorylated tau, and the synaptic protein neurogranin are key elements of this pathophysiology present in the CSF of patients[68]. Additionally, topographical biomarkers obtained through brain imaging techniques, such as volumetric MRI and rate of metabolic reductions on FDG-PET (fluorodeoxyglucose-positron emission tomography), have also been a helping-hand in assessing neurodegeneration and AD progression[62,68].

Alarmingly, AD remains as a disorder having no effective treatments in stopping its unfolding. Throughout the last years, several studies, drug development programs and clinical trials have failed to provide an effective treatment capable of either halting or reversing its progression[62,69,70]. Nevertheless, the FDA (US Food and

Drug Administration) has currently four approved drugs on the market used to temporarily ameliorate its development: Rivastigmine, Donepezil and Galantamine, three cholinesterase inhibitors, that act by inhibiting acetylcholine-degrading enzymes and thus restoring levels of this neurotransmitter, essential for postsynaptic stimulation[71–77]. Apart from these, memantine, a *N*-methyl-$_D$-aspartate receptor (NMDAr) antagonist, has also been used, albeit in later phases of AD (in contrast with the previous inhibitors, which are used in a more initial stage of the disease). This agent is used to counteract glutamate-related excitotoxicity, which is known to accentuate AD progression[71,78,79]. Alongside these, there are also non-pharmacological interventions aiming to delay AD symptomatology. These involve cognitive training, emotional, physical, and social stimulation, music therapy and diet, helping in reducing behavioural symptoms, delay loss of cognitive function and increase quality of life[80].

The ongoing emergency on studying and developing new effective treatments for AD or any other neurodegenerative disease has been proven difficult due to the multifactorial aspect of these disorders. Nonetheless, as of February of last year, 121 pharmacological agents were being assessed for the treatment of AD; notably in the last four years, there has been an increase in different mediators other than Aβ- an tau-related drugs, showing emphasis on potential candidates for epigenetic, neurogenesis and neuroprotection modulators[81].

1.2.2 Etiopathogenesis of AD

AD is generally seen as disorder affecting older subgroups of the population. Indeed, according to the 2020 report issued by the Alzheimer's Association, an estimate of 5.8 million Americans over the age of 65 years were diagnosed with AD in 2020, with higher percentages projected to increasingly older age groups. Studies estimate that by 2025, these numbers will round 7.1 million, and that by 2050 will be projected to 13.8 million, once again reinforcing the emergency in developing new treatments[82].

Nonetheless, people under the age of 65 can develop AD, as genetics also plays a role in the appearance of this disorder. These cases are rare - up to 5% - compared to the sporadic cases of AD, thought to be enhanced by environmental and non-mendelian genetic susceptibility factors, clinical history, diet and ultimately ageing, as alluded earlier. The early-onset cases of AD are usually defined by mutations in genes expressing for AD-related proteins, such as *APP* but also both *PSEN1* and *PSEN2*,

transmitted in an autosomal dominant process[82,83]. Altogether, these genes share a pathway, by which are able to modulate the production of the Aβ peptide, eventually resulting in its misfolded aggregation and neuronal death[84–86].

Aβ peptides are originated from the aberrant proteolytic cleavage of amyloid precursor protein (APP), a membrane protein thought to be linked in neuronal development, trafficking and signal transduction[86–89]. Aside from its non-amyloidogenic degradation pathway, in which APP is sequentially proteolytically cleaved by α- and γ-secretases, originating a p3 fragment and an APP intracellular domain (AICD), APP can also be targeted by a sequential cleavage of β- and γ-secretases, resulting in the formation of AICD, but also Aβ monomers. The abundant secretion of these monomers into synapses favors their aggregation conditions in forming oligomer species, fibrils, and amyloid plaques. Curiously, both the p3 fragment and AICD also modulate neuronal homeostasis, as the former is also capable to aggregate, albeit not into oligomers, and alongside AICD, promote the activation of pathways involved in programmed neuronal death[86,87,90]. Several evidence have linked the accumulation of Aβ species, namely soluble Aβ oligomers, to synaptotoxic effects, capable of severing neuronal connections by the pruning of dendritic spines[86,91]. Accordingly, studies confirmed an increase in neuronal death associated with an increase in Aβ oligomer levels due to whether an overproduction of Aβ monomers or defective clearance mechanisms[84–86].

A) BDNF/TrkB-FL system modulation in AD

As alluded earlier, BDNF/TrkB-FL system signalling is an important modulator of neuronal survival in the mammalian nervous system. Hippocampal BDNF is also responsible for synaptic plasticity and maintenance of long-term potentiation (LTP), a prerequisite for memory formation. Accordingly, studies using BDNF antisense or BDNF heterozygous knockout mice have shown a deficit in LTP, accompanied by a reduction in dendritic spines and spatial and learning deficits[92–96]. Likewise, abolishment of TrkB isoforms holding a functional tyrosine kinase domain also result in learning impairments[97,98]. Accordingly, a link between the dysregulation of this system has been drawn with AD pathophysiology, as several studies have shown a decrease in both BDNF and TrkB mRNA and protein levels in the hippocampus and cerebral cortex[99]. Changes in BDNF expression are thought to be modulated via oligomeric Aβ-mediated downregulation of CREB phosphorylation, resulting in a reduction of gene expression, including BDNF transcripts[99,100]. Concomitantly, TrkB positive neurons were also found decreased in *post-mortem* tissue, explained by both

a downregulation in TrkB expression and neurodegeneration[101]. Interestingly, this raises a conundrum of whether the downregulation of BDNF/TrkB-FL signalling potentiates neurodegeneration, or if Aβ-mediated neuronal loss is a precursor in loss of neuroprotection. Intriguingly, it is known that BDNF dephosphorylates tau protein, acting as surveillance mediator and thus controlling the rate of neurofibrillary tangle formation. In that regard, BDNF decreased levels hinder this action and allows an aggravated mechanism of tau aggregation, contributing to trafficking impairments and ultimately, neurodegeneration[102,103]. Additionally, evidence show that despite the downregulation of TrkB-FL, other non-functional isoforms seem to be unaffected or even upregulated, creating an imbalance in TrkB-FL/TrkB-TK- ratio, allowing for an heterodimer-mediated impaired BDNF signalling[104–106]. Similarly, the prevalence of p75NTR receptors over TrkB-FL receptors also shifts downstream signalling of mature and pro-BDNF[107].

Despite TrkB-FL downregulation, BDNF administration in AD models has revealed promising results. Injection of BDNF-producing lentiviruses in APP transgenic (Tg) mice seem to show that, albeit unable to recover neuronal density nor decrease amyloid plaque density, it promotes the reestablishment of synapses with consequent mitigation of spatial memory impairments[108]. *In vitro* studies also described that BDNF signalling controls the amyloidogenic route of Aβ production, since its administration decreases the formation of this peptide and that BDNF deprivation allows Aβ oligomerization[109,110]. Additionally, the administration of memantine increases BDNF and TrkB levels in rats via a mechanism to be explained in the **Section 1.2.2 A1.**[111,112].

Altogether, these sets of data seem to correlate the modulation of the BDNF/TrkB-FL signalling with the pathophysiology of AD, showing that an alteration in these players leads to a loss of neuroprotection and consequent neurodegeneration. Moreover, albeit BDNF administration shows amelioration in certain aspects, its effects promote only a partial rescue of AD symptomatology.

A1. Aβ accumulation potentiates TrkB-FL calpain-mediated cleavage

Aside from previous Aβ-mediated modulations, this peptide is also able to promote the proteolytic cleavage of TrkB-FL, impairing this neuronal survival system. Indeed, when levels of toxic Aβ species increase (namely Aβ oligomers), this peptide triggers excitotoxic events promoting an exacerbated activation of the extrasynaptic NMDAr (eNMDAr), leading to a major influx of Ca^{2+} intracellularly[112]. In physiological

conditions, the activation of this receptor is linked with synaptic plasticity and memory formation, however in AD pathology, its aberrant signalling results in the overactivation of calpains, a group of Ca^{2+}-dependent cysteine proteases[55,113]. The role of calpains has been extensively reported, describing their functions in Ca^{2+} homeostasis, cell development, differentiation, proliferation, and cell death[113]. Nevertheless, a growing body of evidence suggests that in certain pathologies, AD included, the hyperactivation of these proteases leads to the cleavage of multiple intracellular substrates, including cytoskeleton, signal transduction and synaptic proteins, as well as transcription factors[113]. Studies have also revealed that the endogenous inhibitor that attenuates calpain activity, calpastatin, is depleted in AD, shifting calpain modulation to a more activated state[113,114]. In this regard, studies from our lab described a mechanism in which Aβ-mediated calpain overactivation proteolytically cleaves TrkB-FL receptors[55] (Figure 1.4).

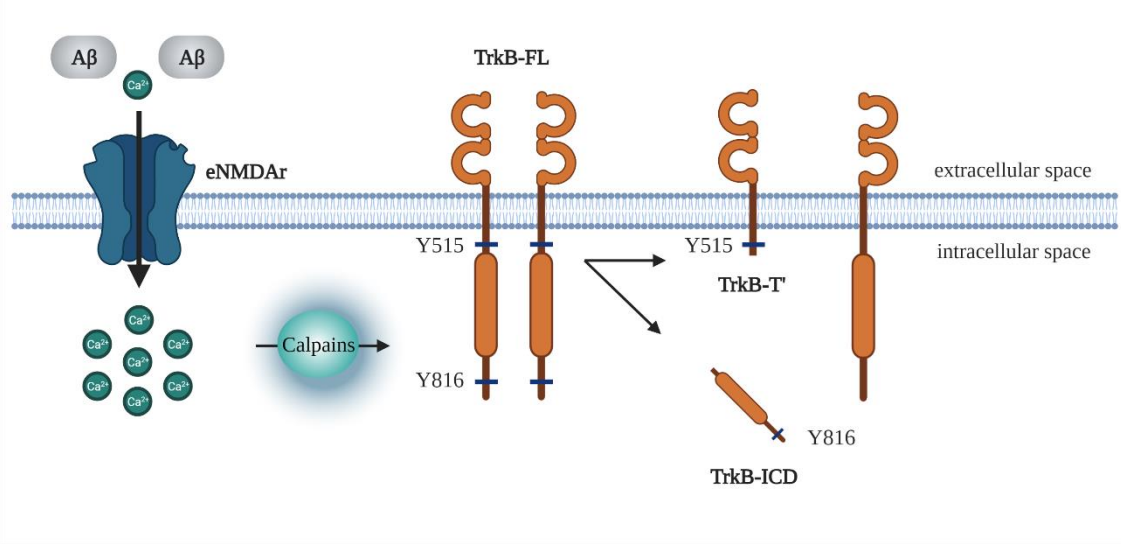

Figure 1. 4 – Amyloid-β accumulation impairs BDNF/TrkB-FL system.
In AD, the accumulation of Aβ species promotes the overactivation of eNMDAr, leading to a major influx of Ca^{2+} intracellularly. Consequently, this triggers and enhanced response by calpain proteases ultimately cleaving TrkB-FL. This results not only in a loss of neuroprotection, but also in a gain of toxic function, due to the formation of a non-functional membrane-bound TrkB truncated receptor – TrkB-T' – and a cytosolic fragment known to promote intracellular toxicity – TrkB-ICD. Aβ – amyloid-β; Ca^{2+} - calcium ion; TrkB-FL – full-length tropomyosin-related kinase B; TrkB-ICD - TrkB-intracellular domain (calpain-generated); TrkB-T' - TrkB Truncated (calpain-generated); Y515/816 - tyrosine residue 515/816.

Following cleavage on an asparagine residue beyond Y^{515}, two new mediators are originated: 1) a membrane-bound, tyrosine kinase domain negative truncated receptor, TrkB-T' and 2) an intracellular fragment withholding the tyrosine kinase

catalytic center as well as the PLCγ binding site, TrkB-ICD[55] (Figure 1.4). Accordingly, other studies from our group reported that the administration of memantine in primary neurons decreased TrkB-ICD levels with a recovery in TrkB-FL receptor[112]. This data aligns with what was described earlier, as the eNMDAr antagonist prevents an increase in intracellular Ca^{2+} levels and thus halting Aβ-mediated calpain overactivation.

Importantly, follow-up studies have been made to demystify the potential harmful effects that TrkB-ICD may have, as it is known that several fragments originated by calpain cleavage gain toxic function[115,116]. As for TrkB-T', further studies need to be made, but its lack of tyrosine kinase domain may hint for a possible TrkB-FL negative modulation, similar to those of other truncated TrkB isoforms. Following previous studies, researchers from our lab have reported that TrkB-ICD, albeit cleaved, is a stable fragment and maintains its kinase activity thus being able to promote the phosphorylation of axonal and nuclear proteins. Indeed, they have also described the presence of two nuclear localization sequences in this fragment, allowing for its translocation into the nucleus overtime[59]. Up until recently its nuclear activity remained unknown, but it has since been reported that TrkB-ICD is able to modulate gene expression, upregulating genes involved in neurotransmitter activity, brain diseases and neuronal development, including *NTRK2*[117]. Intriguingly, in light of other positive-feedback loop mechanisms, the increased expression of *NTRK2* may lead to increase levels of TrkB-FL protein, which will be systematically cleaved, thus producing more TrkB-ICD fragments. However, data is still missing as to whether this transcriptomic modulation correlates with its proteomic profile.

Finally, we also described that mice overexpressing lentiviral-induced TrkB-ICD in the hippocampus developed behavioural memory impairments[117]. Simultaneously, studies have revealed the detection of this fragment in CSF samples of AD patients, raising questions as to if this fragment can be used as a monitoring biomarker in AD and also opening a world of research in TrkB-ICD trafficking and secretion pathways[117,118].

A2. TAT-TrkB, a novel drug capable of preventing TrkB-FL cleavage

In light of the emerging studies surrounding calpain-mediated TrkB-FL cleavage and TrkB-ICD fragment formation, our lab proposed a peptide structure capable of preventing, to a degree, TrkB-FL cleavage. This peptide, TAT-TrkB, possesses the TAT protein transduction domain, a cell-penetrating peptide that

increases its diffusion capacity across cell membranes including the blood-brain barrier (BBB)[117,119]. Moreover, its structure has a sequence homologous to that of the cleavage site in TrkB-FL suggesting it being a substrate competitor of TrkB-FL. Up to date, this drug has shown promising results in preventing TrkB-FL cleavage in *in vitro* and *ex vivo* studies[117].

1.3 Cellular Clearance Mechanisms

The ability in keeping the integrity of the proteome is paramount in cellular function and survival. Proteostasis, commonly referred as protein homeostasis, alludes to the network of players that maintain protein regulation, assuring their concentration, folding, function, and cellular location, striving for proteome stability[120,121]. Amongst this network, there are systems specialized in protein quality control and degradation pathways triggered upon recognition of harmful misfolded proteins. Such degradation pathways will be mentioned ahead on **Section 1.3.2**. Additionally, molecular chaperones and co-chaperones are also involved in protein quality control, as they assist in protein folding and aggregation prevention[120,122]. Understandably, dysregulation events in the protein-regulation network, clearance mechanisms or in altered protein production may lead to accumulation and dissemination of intercellular toxicity[121].

Curiously, as mentioned earlier, within the world of cellular communication, secretion of mediators modulates autocrine and paracrine responses. Concomitantly, the release process of these intercellular modulators acts as a cellular clearance mechanism, as it is known that in several neurodegenerative diseases, AD included, misfolded proteins can be secreted. Interestingly, several studies have already linked the release of harmful mediators and their dissemination into neighbouring cells, thus propagating cellular pathology[123–128].

1.3.1 Secretome constitution

Originally described by Tjalsma in 2000, the concept of secretome has evolved from “both the components of machineries for protein secretion and the native secreted proteins” to being defined as the overall profile of 1) soluble factors, regardless of their biogenesis and composition, and 2) extracellular vesicles (EVs) carrying different signalling molecules, factors and mediators of health and disease (Figure 1.5). Similar to how proteome refers to the overall proteomic profile, secretome

comprises all cell- and tissue-secreted factors, mediators and by-products found in the extracellular space at a given time[129,130]. Understandably, depending on the cellular environment, different secretome signatures can be found[127]. Actually, secretome-based therapies have been gaining momentum, as studies show that both their soluble and vesicle fractions can potentiate both cellular protection and regeneration[131,132].

Congruently, a growing body of evidence has also described the possibility of using secretome as a potential reservoir of biomarkers, as pathological mediators have been detected in this medium. Indeed, studies have reported the transmission of EV-mediated misfolded and aggregated proteins, typically seen in proteinopathies such as AD and PD, leading to them exerting their putative toxicity in healthy neighbouring cells[123–127].

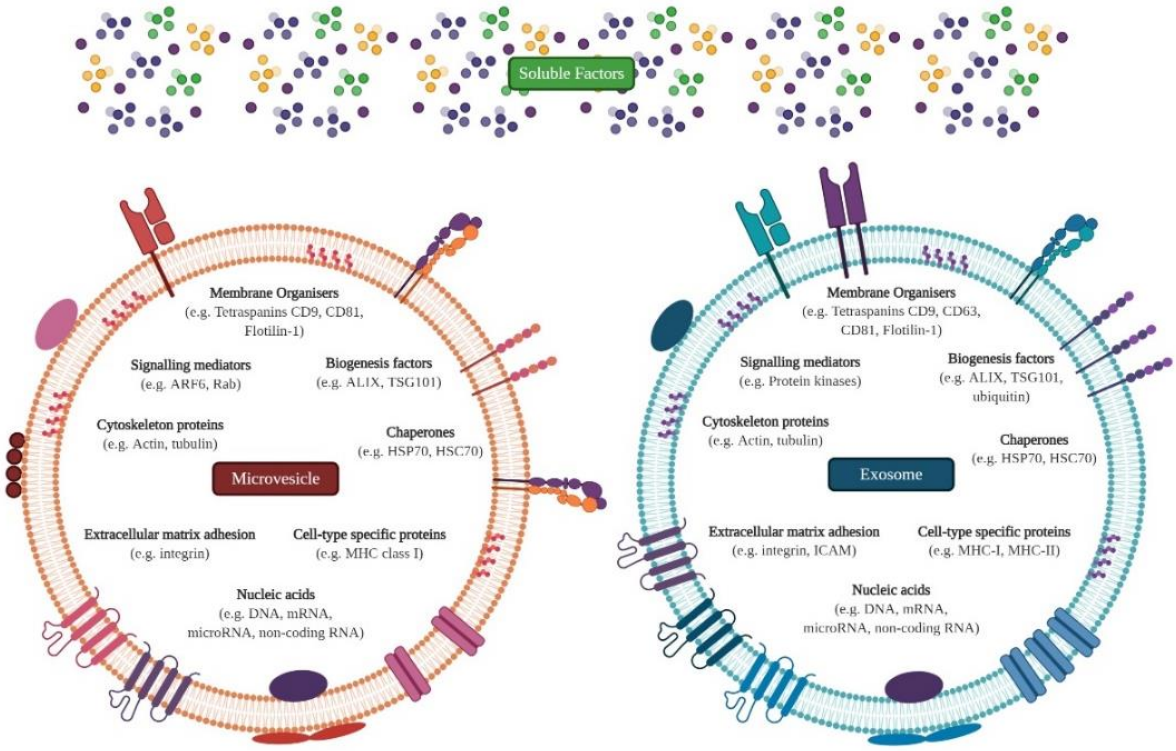

Figure 1. 5 - Secretome constitution.
Cells partake in cell-to-cell communication through the release of soluble factors and EVs, making up the secretome. Both microvesicles and exosomes are subtype of EVs with different origins, cargo, biogenesis, release pathways and sometimes functions. Their composition comprises multiple proteins, lipids, and nucleic acid species. ALIX – programmed cell death 6-interacting protein; ARF6 - ADP-ribosylation factor 6; CD9/63/81 – tetraspanin 9/63/81; TSG101 – tumor susceptibility gene 101; HSC70 – heat shock cognate 70 kDa protein; HSP70 –heat shock 70 kDa protein; ICAM – intracellular adhesion molecule; MHCI/II – major histocompatibility complex I/II; Rab - Ras-associated binding protein.

A) Secreted soluble fraction

Secretome soluble factors are non-encapsulated factors and mediators that promote autocrine and paracrine signalling. Several studies have reported the presence of a wide group of proteins, including growth factors – as mentioned above – and cytokines, that exert roles on neuronal survival, differentiation, angiogenesis, immunomodulation, and neurite outgrowth[133,134]. As expected, these signalling molecules are not only released by neurons, but also by astrocytes, microglia, and other neuronal cells in the CNS, highlighting the complexity of intercellular signalling communication[125].

B) Extracellular vesicles and intercellular communication

In the last few years, EV research has been gaining momentum, due to the unveiling of their biogenesis, function, and trafficking pathways. Initially thought as a cellular clearance mechanism, the concept of EV is now seen as vesicles partaking in cell-to-cell communication[127,128]. Indeed, in fact all cell types are able to release these lipid bound vesicles into the extracellular media, each containing an overall signature of their original cellular environment. Importantly, secretome-present EVs are not homogeneous as there are different types of vesicles, with distinct origins, cargoes, sizes, release pathways and functions, even when secreted by a single cell type[127,135]. Accordingly, there has been a particular interest in four main EV populations 1) apoptotic bodies, 2) microvesicles, interchangeably referred to as large EVs, 3) exosomes, also known as small EVs and 4) exomeres. More emphasis will be given to both microvesicles and exosomes hereinafter. Importantly, due to the overlapping size range, cargo content and morphology, new nomenclatures, characterization protocols and analysis methods are still being proposed to devise a more precise definition and distinction of all EV types[127,135,136].

B1. Extracellular vesicle biogenesis, composition, and cargo sorting

As mentioned above, EVs are small lipidic membranous vesicles released from all cells, able to provide important modulators and thus playing a role in intercellular communication. Despite having different origins, both microvesicles and exosomes are generated intracellularly with the involvement of membrane-trafficking mechanisms[127,136].

Briefly, biogenesis of microvesicles underlies the outward blebbing and fission of the plasma membrane, releasing newly formed vesicles into the extracellular space. The route of microvesicle formation still remains elusive, nevertheless studies explore the recruitment of cytoskeleton components such as microtubules, molecular motors, and fusion machinery proteins to promote its budding[135,137]. Additionally, Ca^{2+}-dependent lipid transporters such as flippases, floppases and scramblases play a role in membrane asymmetry, inducing its bending and thus helping in membrane budding[127,138]. Concomitantly, not only structural membrane proteins and membrane-associated lipidic components suffer temporary localized changes, modulating membrane curvature, but there is also a trafficking redistribution of specific cytosolic and membrane mediators, selectively enriched in microvesicles[127,135]. Accordingly, a growing body of evidence has shown that although mechanistically different from the formation of exosomes, as detailed below, microvesicle formation also recruits endosomal machinery, including the endosomal sorting complex required for transport (ESCRT) system[139].

Understandably, a diverse multitude of cytosolic and membrane proteins, lipids and nucleic acids are shuttled within these blebbing vesicles[127,136]. Protein content found within microvesicles ranges from membrane organisers such as tetraspanins, chaperones, heat shock proteins, biogenesis factors, cytoskeleton and signalling molecules, intracellular trafficking, and cell-type-specific proteins[127,136]. Similarly, nucleic acid content includes microRNAs (miRNAs), non-coding and messenger RNA and DNA (Figure 1.5).

Unlike exosome formation, microvesicle budding is not size-limited, allowing for the biogenesis of larger vesicles, generally ranging from 150 nm up to 1000 nm[125,127,135,136,140].

Conversely, exosomes are a subtype of EVs generated as intraluminal vesicles (ILVs) within the lumen of early endosomes, by inward budding of their membrane. Understandably, their size is limited by the outer membrane of the endosome, which after ILV budding, matures into multivesicular endosomes (MVEs), also known as late endosomes[127,135,141]. Following endosome maturation, MVEs can either fuse with lysosomes, promoting cargo degradation, fuse with the Golgi apparatus, and thus recycling their cargo, or fuse with the plasma membrane, releasing its components, including both soluble factors and exosomes[127,135]. Analogous to ILV formation, early endosomes derive from the inward budding of the plasma membrane, and together with MVEs, partake in both intracellular trafficking and endocytosis mechanisms[127,135,142]. Actually, as mentioned above, they are essential players in protein

trafficking, having functions involved in their sorting, recycling, transport, and release[127,135].

Exosome biogenesis involves tight-regulated mechanisms through the recruitment of sorting machineries. Initially, and similar to microvesicle formation, lipids, and membrane proteins form clusters in specific microdomains of the outer membrane of the MVE (or plasma membrane for microvesicles) through the transient recruitment of accessory proteins and ESCRT machinery, a known modulator of membrane rigidity and abscission[127,143]. Briefly, ESCRT-0 and ESCRT-I complexes promote clustering of ubiquitinated transmembrane proteins and, together with endosomal lipid rafts, promote a cytoplasmic sorting of other mediators. As a sequential mechanism, ESCRT-II recruits ESCRT-III complex, which is responsible for the invagination and abscission of the endosomal microdomain, resulting in the formation of ILVs withholding the previous sorted cargo[127,135,143].

Curiously, studies using interfering RNAs targeting ESCRT complex players have demonstrated that exosomes can also be formed through an ESCRT-independent mechanism, as ILVs enriched in CD63 tetraspanin were still originated[144,145]. Nevertheless, the usage of genetic modulators to deplete or downregulate either ESCRT complexes or its accessory proteins, lead to a deficiency in exosome secretion and its cargo[127,146]. In that regard, one of the drivers of ESCRT-independent mechanisms is the lipid ceramide, which helps generating membrane microdomains that induce membrane curvature[127,147]. Additionally, the metabolization of this lipid allows for the activation of the G_i-protein-coupled sphingosine 1-phosphate receptor, a key player in exosomal cargo sorting[127,148]. Apart from ceramide, tetraspanins, namely CD9, CD63 and CD81 are important transmembrane proteins that also help regulating endosomal sorting without the action of the ESCRT machinery, promoting membrane and cytosolic protein clustering[127,144,145].

Analogous to microvesicle cargo, exosomes also possess a wide range of proteins involved in cell adhesion, intracellular trafficking, chaperones and heat shock proteins, biogenesis factors, signal transduction and cell-type specific molecules and membrane organisers. Additionally, studies suggest that certain post-translation modifications, ubiquitination inclusive, promote protein incorporation in these shuttling vesicles[149]. Furthermore, exosomes are also enriched in lipids and lipid-associated proteins, with additional prevalence of the already mentioned nucleic acid species[127,136] (Figure 1.5). Despite the apparent indistinguishable cargo content, exosomes differ from microvesicle in their size range, varying from 50 nm to 200 nm, albeit there is still an overlapping size gap[125,127,135,136,140].

Furthermore, similar to microvesicle formation, the mechanisms of exosome biogenesis still present missing data, as some cell types do not abide by the explained biogenesis processes[127,150].

Altogether, this data reveals that EV research has only scratched the surface both in theoretical knowledge regarding vesicle biogenesis and trafficking but also in precise practical methods for EV isolation, characterization, and analysis.

B2. Extracellular vesicle release, dissemination, and uptake

Unlike exosomes, microvesicles are formed directly in the interphase of intracellular-extracellular environment, and thus, do not need to be intracellularly transported for their release. Upon membrane-induced curvature and budding, small GTPases, namely ARF6 and ARF1, induce the contraction of the plasma membrane through an ATP-dependent process, involving both cytoskeleton proteins and molecular motors[127,151–153]. As mentioned earlier, several studies have also linked microvesicle shedding to a Ca^{2+}-dependent process, as flippases, floppases and scramblases are Ca^{2+}-dependent lipid transporters that induced loss of membrane asymmetry, thus promoting membrane curvature[127,138]. Moreover, the generation of additional ceramide lipids through acidic sphingomyelinase also enhances microvesicle formation[154].

Contrarily to microvesicles, exosome precursors, ILVs, are originated inside endosomes, and thus require transportation to the plasma membrane, where upon fusion, release exosomes. This intracellular transport is mainly guided through the association of the MVE with cytoskeleton proteins, molecular motors, and molecular switches, namely Rab proteins[137,155]. As expected, the fusion of MVEs with the plasma membrane is also Ca^{2+}-modulated, as concentrations of this ion promote the recruitment of SNARE complex proteins, involved in vesicle-membrane fusion, proteins from the synaptotagmin family, known to be involved in vesicle docking, and tethering factors[137,156].

The release of both EV subtypes into the extracellular space allows for their uptake by either the original or by neighbouring cells, exerting autocrine and paracrine signalling, respectively. As alluded above, the resulting effects of EV internalization are determined by their vesicle type and cargo. The incorporation of EVs in recipient cells is a sequential process involving: 1) EV docking on the plasma membrane of the recipient cell; 2) recognition of EV proteins and lipidic cues, by receptors and mediators of the targeted cell, and finally 3) vesicle internalization.

Interactions between EVs and the cellular membrane are made through mediators such as tetraspanins, lipids, lipid-binding proteins, integrins and the extracellular matrix[127,157]. Importantly, EVs can also bind to specific cells according to their own cargo content and membrane signature. Indeed, studies show that vesicles enriched in CD63 are targeted to both neurons and glia, whereas EVs containing APP products are mainly targeted to neurons[158]. Nevertheless, other studies show that exosomes and microvesicles are generally cleared by cells with high-phagocytic activity such as microglia, once again highlighting the complexity of EV research[159,160].

Briefly, following vesicle docking, EVs may either remain on the surface of the cell or be internalized via a clathrin-mediated mechanism, micropinocytosis or phagocytosis, endocytosis via caveolae, internalisation by lipid rafts or by vesicular fusion[127,157,161–163]. Once internalized, EVs are incorporated into the endocytic pathway, and like in exosome biogenesis, directed towards MVEs. Once again, and depending on the trigger, MVEs can be allocated to lysosomes, thus promoting internalized cargo clearance[127]. That said, internalization by vesicular fusion promotes the release of EV intraluminal cargo, capable of modulating cellular pathways and/or alter gene expression. Importantly, this process is quickly susceptible to cellular clearance mechanisms, as it releases the cargo directly into the cytosol, whereas internalized cargo-containing EVs safeguard their content[164,165]. Interestingly, once vesicles are incorporated within MVEs, they can also fuse with their membrane, and release their content onto the cytosol, partaking in the same modulatory responses above described[166].

B3. Extracellular vesicle signalling in spread of disease and therapeutic usage

Intercellular EV-based communication is known to trigger beneficial responses involved in cell maintenance, promoting neurite growth, myelin formation, neuronal survival and an overall tissue repair and regeneration in neuronal cells[135,167–169]. However, a growing body of evidence demonstrates a harmful side to these shuttles, as they are able to carry misfolded proteins and toxic mediators, releasing them into targeting cells[123,125–127]. Indeed, recent studies in the field of neurodegenerative disorders have described the presence of Aβ and tau, alpha-synuclein and LRRK2 (major misfolded proteins in PD), SOD-1 and TDP-43 (in Amyotrophic Lateral Sclerosis) and PrP^{C} (in prion diseases), amongst others, specially within exosomes[170]. Importantly, these putative toxic proteins are not disease exclusive, as later stages of neurodegeneration usually impacts multiple brain areas.

In 2006, Rajendran described, for the first time, APP cleavage inside early endosomes with subsequent release of their content into the extracellular microenvironment, beneficial for Aβ extracellular aggregation[171]. Additionally, other APP fragments have been detected in exosomes in both *in vitro* and *in vivo* studies, suggesting again that these vesicles may have a role in generation of Aβ aggregates[172,173]. Furthermore, evidence show that during exosome biogenesis, ILVs may serve as nucleation hubs for Aβ aggregation, thus helping in oligomerization and fibrillization[174,175]. Altogether, these evidence seem to show one of two possibilities: either 1) exosomes have a neurotoxic role by being pathology mediators, releasing Aβ monomers and oligomers into the extracellular media, promoting their aggregation or 2) they have a neuroprotective function by clustering Aβ species within MVEs, that are later fused with lysosomes, promoting their clearance[170,174,175]. Interestingly, the former point can also be taken as a cellular neuroprotective mechanism, albeit allowing for EV-mediated insults to other cells. Moreover, it is known that EVs carry enzymes able to degrade Aβ, and miRNAs capable of triggering microglia-derived phagocytosis on neurodegeneration dendrites, once again alluding for their neuroprotective role[176–178]. Notwithstanding, depending on the lipid composition of the exosome, they may promote disassembly of stable Aβ species, giving rise to toxic oligomers[159,179].

In addition to Aβ, hyperphosphorylated tau proteins are also detected in exosomes present in CSF of AD patients[180]. *In vitro* reports with overexpressing tau models corroborate with these findings, proposing a means of spreading tauopathy in AD patients[181].

Interestingly, TrkB-FL protein levels have been detected in exosomes, which may suggest that TrkB-ICD may also be incorporated and disseminate its toxicity among other cells[123,182].

Still under investigation, exosome release is thought to be modulated by certain cellular events, including modulation of synaptic glutamatergic NMDAr and AMPA (α-amino-3-hydroxy-5-methyl-4-isoxazolepropionic acid) receptors in differentiated neurons, both systems known to be altered in AD[169].

Understandably, and for the reasons above mentioned, EVs can be seen as a disease progression source, as their presence in multiple bodily fluids – urine, blood, and CSF – facilitates their isolation and analysis[183–185]. Adding to that, these may constitute as biomarker carriers, as albeit pre-clinical AD does not show symptomology, it is characterized by molecular changes[64,66]. Nonetheless, quantification of both Aβ and tau in EVs has led to contradictory results, showing that both proteins are present in variable levels in EVs in multiple models and brain

areas[170]. Actually, miRNAs have also been emerging as potential exosome-cargo biomarkers in AD, as these mRNA-modulating single-stranded RNAs are known to be up- and down-regulated[125,186,187].

Finally, therapeutical strategies implementing EVs have also been sought out, as they have a variety of advantages: 1) ability to cross the BBB and 2) target specific cells according to their luminal and membrane content[125,127,170,187]. These, together with encapsulating pharmacological agents, miRNAs, and their ability to scavenge for misfolded proteins, allows for the development of highly specific engineered vesicles[125,170,187,188].

1.3.2 Ubiquitin-Proteasome System (UPS) and the Autophagy-Lysosomal Pathway (ALP)

As mentioned in **Section 1.3**, apart from EV-mediated clearance, there are also other mechanisms by which cells promote proteostasis. The occurrence of events that overwhelm the capabilities of the chaperone network, either by altering chaperone function, promote protein unfolding or increase production of prone-to-aggregate proteins, trigger the activation of proteolytic systems capable of degrading damaging and damaged components[121,189,190]. These systems are the Ubiquitin-Proteasome System (UPS) and the Autophagy-Lysosomal Pathway (ALP)[121,189,190]

The recruitment and action of both UPS and ALP underlies the tagging, recognition, and delivery of harmful misfolded proteins, to these cellular degrading machineries, promoting their proteolytic cleavage and consequent by-product recycling[121,189].

The UPS relies on the action of ubiquitin (Ub), a small molecule capable of binding not only to lysine (K) residues but also to serine, cysteine and threonine residues present in the N-terminal of specific proteins, in a process known as ubiquitination[190–193]. Actually, Ub binding serves as a tagging mechanism, distributing harmful proteins to either the UPS or the ALP[190]. These recognitions patterns involve different Ub chain conformations – polyubiquitination – formed upon the conjugation of the first Ub molecule or multi-monoubiquitination. Chain formation involves a sequential binding of Ub proteins to K or other residues of the previous Ub. Importantly and depending on the originated poly-Ub chain, different cellular responses may be triggered, including DNA repair, proteasome and/or lysosome degradation, mitophagy, kinase modification and mechanisms involved in cellular trafficking[121,189].

The conjugation of Ub to target proteins is promoted by the sequential action of three different classes of enzymes. Firstly, the ubiquitin-activating enzyme (E1) activates, through an ATP-dependent process, the glycine residue at the C-terminal of the Ub molecule, transferring it to the cysteine residue of the ubiquitin-conjugating enzyme (E2). Finally, a third enzyme, the ubiquitin ligase (E3), promotes the C-terminal linkage of the E2-transferred Ub molecule to a K residue of the target protein[189–191]. To counteract the formation of extensive Ub chains and possible errors, there is also a class of enzymes known as deubiquitinating enzymes that promote the cleavage of the protein-Ub peptide bond and the Ub-Ub linkage[190].

Upon Ub tagging, harmful proteins can be directed towards the 26S proteasome, a cylinder-like multi-subunit protease complex composed of multiple rings, creating an internal cavity where proteins are proteolytic cleaved[189,190]. Briefly, once ubiquitinated proteins arrive, recognition proteins on the base of the proteasome bind, unfold and translocate them into the proteolytic chamber, where through the action of other enzymes, Ub chain is cleaved[190]. Lastly, proteins are cleaved inside the chamber and their residues recycled.

Interestingly, this system is known to be modulated through post translational modifications, whereas phosphorylation, the most prevalent proteasomal modification, is known to increase proteasomal activity[190].

Apart from the UPS, certain misfolded and/or aggregated proteins, as well as damaged organelles can be engulfed by autophagosomes, a double lipid layer organelle involved in lysosome-mediated degradation[189,190,194]. Upon autophagosome maturation, this organelle fuses with lysosomes, originating the autolysosome, a hybrid organelle that mediates degradation of the selected engulfed cargo - macroautophagy[189,194,195]. The acidic pH of the lysosome allows to partly unfold protein structures, helping in the action of hydrolases present within this organelle[189,190]. Additionally, ALP can also degrade proteins through microautophagy or chaperone-mediated autophagy. Briefly, microautophagy is also able to clear proteins and organelles through lysosomal membrane invaginations[189,190,194]. Conversely, chaperone-mediated autophagy is only able to promote the clearance of deleterious proteins. Notwithstanding, this via considers the recognition of specific motifs by cytosolic chaperones that deliver the cargo to the lysosome. Upon cargo delivery, a luminal chaperone mediates its translocation to the lysosome lumen, promoting its degradation[189,195].

Studies described that both UPS and ALP systems are impaired in AD, as the accumulation of both Aβ and hyperphosphorylated tau block their activities and modulate intermediate players[190,194,195]. Alarmingly, AD enhances this loss of function,

leading to an over-accumulation of misfolded proteins not only due to their overproduction, but also due to the lack of their cellular clearance. The synergy between the UPS and ALP, together with the clearance driven by EVs, plays a paramount role in cellular proteostasis.

Understandably, cellular ageing as that associated to AD is known to promote loss of proteostasis through aberrant changes in translation, loss of protein function and gain in toxic function, downregulation of chaperones and dysfunctional protein degradation machineries[121,194]. At the proteasome level, dysfunction may happen by post translation modifications, decreased expression or aberrant replacement of its subunits, disassembly, or impairments in substrate recognition[121,195–198]. Similarly, lysosomal degradation is also hindered with ageing due to downregulation of Atg proteins, responsible for autophagy induction.

Once again, this highlights that AD is a multifactorial disease, targeting multiple systems within the cell, and that its research must continue to strive forward in search of new treatments.

2 Aims

The discovery of the novel TrkB-ICD fragment by our lab contributed to unveil a new mechanism that might portray a role in diseases with underlying calpain activation, in particular AD. The functional characterization of TrkB-ICD by Fonseca-Gomes and colleagues, brought up new insights on the modulatory capacity of this fragment highlighting some of its actions in the context of this neurodegenerative disease[59,117,199]. Importantly, and as previously mentioned, TrkB-ICD has been detected in the CSF of AD patients, leaving room to speculate on whether this fragment can or not be released by cells and if so, its respective secretion pathways. Accordingly, EV research has been gaining momentum in the field of cell-to-cell communication and dissemination of pathology mediators.

Moreover, up until now, the mechanisms by which this fragment is intracellularly cleared still remain elusive. Its stability and nuclear translocation pose a threat to cellular clearance, allowing for its prolonged cellular modulation. Understandably, unveiling its clearance mechanisms may help not only to understand additional crossing pathways of TrkB-ICD, but also to reveal possible important pharmacological targets that might be modulated to accelerate its clearance.

Additionally, a new pharmacological approach was developed by our lab through the production of TAT-TrkB peptide, a small peptide capable of preventing TrkB-FL receptor cleavage. Notwithstanding, albeit *in vitro* and *ex vivo* studies have already proven a remarkable action of this peptide, additional *in vivo* studies need to be made to confirm its pharmacological action in a close-related environment.

Accordingly, this thesis was developed to 1) give additional insight and elucidation on the study of TrkB-ICD fragment, but also 2) continue the study of the formulated TAT-TrkB peptide in an *in vivo* set. In conformity, this thesis specifically aimed at a) elucidating TrkB-ICD cellular clearance mechanisms, both ALP- and UPS-mediated clearance intracellular pathways and its extracellular secretome release through the isolation and characterization of EV-enriched and EV-depleted fractions and b) studying the efficacy of TAT-TrkB in 5xFAD mice, an AD mouse model that develops severe amyloid pathology.

3 Materials and Methods

3.1 Animal Handling and TAT-TrkB administration

5xFAD mice, and respective controls (C57BL/6J) were purchased from Charles River (Barcelona, Spain) and Jackson Laboratory (#34840, Maine, USA). All animals were housed at Instituto de Medicina Molecular João Lobo Antunes, Portugal in a temperature (22-24^{0}C) and humidity-controlled (55±10%) room with a 14-hour light-dark cycle and fed with food and water *ad libitum*. Animals were handled according to the current Portuguese Laws (DL 113/2013) for Animal Care for Research Purposes and with the European Community Directive (Directive, 2010/63/EU). This project was also approved by the internal committee (ORBEA) of Instituto de Medicina Molecular João Lobo Antunes and the Portuguese Animal Ethics Committee (DGAV - Direção Geral de Alimentação e Veterinária).

For experimental design, all animals were carefully identified and distributed into groups of 4 to 5 animals per housing cage. The number of mice was minimized, and all efforts were made to reduce animal suffering. Importantly, all animal procedures were performed by João Fonseca-Gomes and Rita Belo, both certified with Animal Handling courses and/or by researchers supervised by qualified personnel.

The behavioural and molecular tests withdraw from these animals were part of a wider project involving a full behavioural and molecular characterization of 5xFAD mice upon chronic administration of an in-lab designed drug, TAT-TrkB. Accordingly, only a small portion of the behavioural tests were incorporated in this document, whereas the remaining tests were analyzed by fellow colleagues.

Briefly, after 5xFAD mice genotyping, intraperitoneal (i.p.) injections of TAT-TrkB (25 or 50 mg/kg, TAT25 and TAT50, respectively) or saline solution [NaCl 0.9% – in Vehicle (Veh) animals] were administrated daily (except weekends) at 4 months old (m.o.) for a period of 2 months. At 6 m.o., mice were sacrificed, and the brain collected for molecular studies, amongst them, protein analysis. Upon 1.5 months of daily administration (at 5.5 m.o.), all animals performed a battery of behavioural tests evaluating for locomotion, anxiety, spatial memory, and memory impairments and recovery. Amongst all 36 studied animals there were: 11 Veh wild type (WT), 7 Veh transgenic (Tg), 8 TAT-TrkB 25 mg/kg WT, 3 TAT-TrkB 25 mg/kg Tg, 3 TAT-TrkB 50 mg/kg WT and 4 TAT-TrkB 50 mg/kg Tg animals.

3.2 Behavioural assessment tests

As soon as mice completed 5.5 m.o., behavioural assessment tests started to be performed, in order to evaluate not only whether TAT-TrkB could rescue 5xFAD mice memory impairments, but also if it had any impact on their anxiety levels by either increasing it – anxiogenic – or decrease it - anxiolytic effect.

All behavioural tests were performed during the light phase between 8 am and 6 pm in a sound-attenuated room.

3.2.1 Morris Water Maze test

Hippocampal-dependent spatial memory and learning performances were evaluated through a Morris Water Maze (MWM) test, as previously performed, and described by our lab[117]. MWM is capable of giving insight on spatial memory deviations caused either by drug-induced changes and/or genetic manipulations[200–202]. The assay was performed in a circular pool (100 cm in diameter, 60 cm deep) filled with opaque, non-toxic, white-colored water to create contrast with the animals, thus allowing an easy recording, and to ensure that animals could not see through it. The temperature of the water was kept at a constant 23-25ºC to avoid hyper- or hypothermia. The pool was virtually divided into four quadrants: target quadrant, where the platform was placed/hidden, opposite quadrant (diametrically opposite to the target quadrant) and left and right quadrant (to the target quadrant). Outside the tank, there were four stationary visible distal landmarks to be used as spatial navigation cues in line with each one of the quadrants.

The test was performed over the course of 6 days, divided into three sequentially phases: 1-day platform habituation training, a 4-day acquisition phase and a 1-day probe test. After completing the trials of each day, animals were deposit back in their respective home cages under heat lamps to prevent temperature loss.

For the platform habituation training day, an 8 cm circular escape platform was placed in the center of the pool, 1 cm above water level, and each animal was put on top of it for 20 seconds (sec). When an animal fell from the platform, it, was manually guided towards it again. Each animal had a total of 2 minutes (min) to succeed in this task. After completing the task, the same procedure was performed, but this time with the platform 1 cm beneath water level.

During the acquisition phase, animals were released at water-level in a pre-determined randomized starting point other than the target quadrant, facing the

outer edge of the pool. They were allowed to freely explore the pool for 60 sec in search of the platform, now hidden in a randomized fixed position, for each animal, 1 cm beneath the water surface. If animals reach the platform within 60 sec, they were allowed to remain there for an additional 10 sec; if not, they were manually guided towards it and allowed to remain there for 20 sec. During this phase, each animal was submitted to four trials per day, with a minimum of 30 min interval in-between trials. Data regarding the latency of the animals to find the platform throughout this period was recorded, giving insight on their learning curves.

Lastly, during the probe test, animals were given 60 sec to swim freely and try to find the platform, now removed from its previous fixed position. In this stage, it was measured the percentage of time that each animal spent in the target quadrant and the number of platform crossings at 60 sec.

All tracings and recordings were made and analyzed using the SMART software (PanLab, Barcelona), using the center of the animal dorsum as the default tracking point.

3.2.2 Elevated Plus Maze test

Anxiety levels were assessed by performing an Elevated Plus Maze (EPM) test, as routinely done by our lab[117,203]. The assay was performed in a plus sign-shaped platform, 50 cm above the floor. This platform is composed of two open (5x29 cm) and two closed arms (5x29x15 cm), the later enclosed by 3 walls. Animals were initially placed in the center of the maze, facing an open arm, and were allowed to freely explore for 5 min.

The number of entries between open and closed arms and the time spent in each one was used to measure their anxiety. In this regard, the center of the maze was considered as an open arm and therefore any transition from a closed arm to the middle of the maze is considered as an open arm entry and vice-versa. Importantly, an entry was only considered valid if all four limbs were within the arm area.

3.3 Cell Cultures

3.3.1 SH-SY5Y Cell line – Neuroblastoma cells

Human SH-SY5Y neuroblastoma cells (Figure 3.1A) were kindly gifted by Prof. Dora Brites from Faculdade de Farmácia da Universidade de Lisboa, Portugal. This cell line was originally obtained by successive subcloning of the neuroblastoma line SK-N-SH, established in culture from a bone-marrow biopsy[204,205].

SH-SY5Y neuroblastoma cells were cultured in Opti-MEM® reduced serum media supplemented with 10% fetal bovine serum (FBS), 2 mM L-Glutamine, 100 U/mL penicillin/streptomycin, at 37°C in a humified 5% CO_2 atmosphere. Cellular maintenance was kept by splitting every two to four days with ratios of 1:5 or 1:10, respectively, being washed with Ca^{2+}- and Mg^{2+}-free Hank's Balanced Salt Solution (HBSS) followed by the addition of trypsin-EDTA solution 0.05% (w/v). Subculture allowed for an ongoing exponential growth upkeep while ensuring cellular viability and preserving the characteristic phenotype. Also, for these reasons, cells were kept under passage 35. Every two passages, cryovials were prepared, keeping a stock of SH-SY5Y cells at different growth stages.

For immunofluorescence, neuroblastoma cells were plated in sterile glass coverslips, previously coated with a mixture of 10 µg/mL poly-D-lysine (PDL) and 4 µg/mL laminin and subsequentially washed twice.

For cell counting and cell viability analysis, cells were diluted in a 0.4% trypan blue solution (T8154, Sigma-Aldrich, MO, USA) and counted using a hemacytometer.

3.3.2 Primary neuronal cultures

Primary cultures of cortical neurons (Figure 3.1B) were prepared from E17-E18 embryos from previous anesthetized pregnant Sprague Dawley females. Brains were then dissected in ice cold HBSS, followed by the removal of meninges to avoid contamination with non-neuronal cells[206]. Next, cerebral cortices were isolated, mechanically fragmented and digested with 0.025% (w/v) trypsin solution in HBSS for 15 min at 37°C. Following tissue digestion, cells were centrifuged at 200g and washed three times with a 30% FBS solution in HBSS. Disassociated cells were resuspended in Neurobasal medium supplemented with 0.5 mM L-Glutamine, 25 µM glutamic acid, 2% B-27, 25 U/mL penicillin/streptomycin. This suspension was then filtered using a nylon filter (BD Falcon™ Cell Strainer 70 µM, Thermo Fisher Scientific, MA, USA) to

avoid cellular clusters and tissue residues, followed by cell density calculation using a 0.4% trypan blue solution (T8154, Sigma-Aldrich, MO, USA) and a hemocytometer. Finally, cortical neurons were plated on pos-coating washed 10 ug/mL PDL-coated dishes at a density of $5x10^5$ cells/cm^2 for Western-blot (WB) at 37°C in a humified 5% CO_2 atmosphere.

For immunofluorescence, primary cortical neuronal cultures were plated in sterile glass coverslips, previously coated with 10 µg/mL of PDL at a density of $1.5x10^5$cells/cm^2 and subsequentially washed twice.

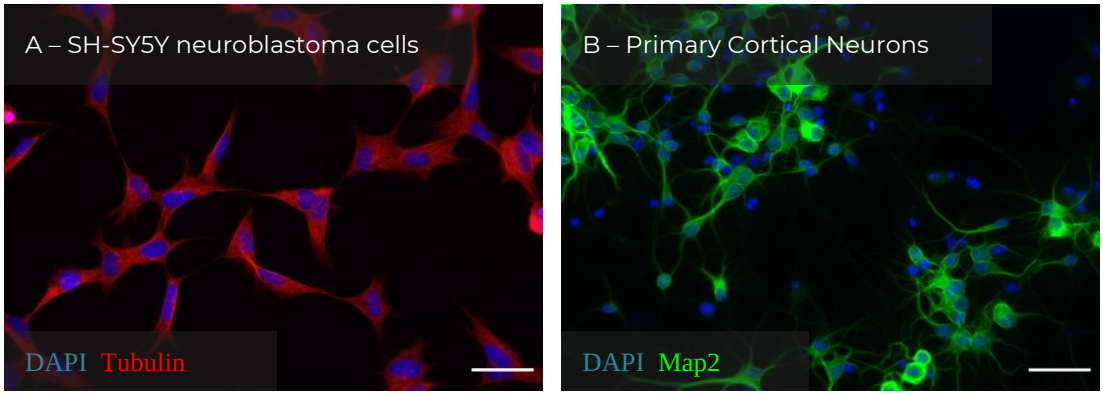

Figure 3. 1 – Representative fluorescent micrographs of SH-SY5Y neuroblastoma cells and primary cortical neurons.

A. Representative immunofluorescence image of SH-SY5Y neuroblastoma cells. In red it is probed tubulin, a cytoskeleton protein present in the cytosol and in blue the cell nuclei (DAPI staining). **B.** Representative immunofluorescence image of primary cortical neurons. In green it is probed Map2, a neuron-specific microtubule-associated protein, and in blue it the cell nuclei (DAPI straining). Both micrographs were acquired using an Axiovert microscope (Carl Zeiss Inc., Oberkochen, Germany), 10x magnification (scale bar: 25µm).

3.4 SH-SY5Y neuronal-like differentiation

SH-SY5Y cells are a heterogeneous population of both non-neuronal substrate adherent (S-type) and neuroblastic (N-type) cells, able to undergo transdifferentiation upon treatment with retinoic acid (RA) and BDNF[207,208].

As a prerequisite to study TrkB-ICD EV-presence (**Section 3.5)**, SH-SY5Y cells were differentiated, from a neuroblast-like state into mature human neuron-like cells. Accordingly, SH-SY5Y cells were cultured in washed plates containing a mixture of 10 µg/mL PDL/4 µg/mL Laminin. Both extracellular matrices are known to enhance neurite outgrowth and differentiation[209]. Initially, cells were cultured in their previous established medium, 0 days *in vitro* (DIV0) followed by a change into media supplemented with 5% FBS and 10 µM of *all-trans* RA (Sigma-Aldrich, MO, USA) at DIV1. At DIV3, a new media change was performed, now to 2% FBS-supplemented media alongside the same concentration of RA for 3 days. Two more media changes were performed at the 6th and 9th day, replacing it with Neurobasal medium supplemented with 0.5 mM L-Glutamine, 2% B-27, 27 U/mL penicillin/streptomycin and 50 ng/mL of BDNF (Regeneron, NY, USA). Afterwards, at the 12th day, SH-SY5Y neuronal-like cells were ready to be used.

3.5 Lentiviral transduction

In order to stably assess TrkB-ICD intra- and extracellular trafficking, SH-SY5Y cells were transduced with lentiviral particles capable of expressing GFP or TrkB-ICD-V5 proteins. These lentiviruses were previously prepared by a colleague from our lab and purified using a transformation protocol on HEK293T cells, in Helsinki[117]. The volume of lentiviral particles for the transduction took into account its viral titer (Table 3.1), being optimized to approximately 150 000 cells and a multiplicity of infection (MOI) of 1.75, meaning that each cell incorporated an average of 1.75 lentiviral particles. The required volume of virus was diluted into Opti-MEM medium and added to DIV2 SH-SY5Y cells. The following day, new medium was added, to renewal not only the nutrients but also to remove non-incorporated lentiviral particles. Once cells reached confluency, cells were split and frozen or used for subsequent molecular analysis: live imaging (**Section 3.11**) was performed to confirm the correct expression of GFP protein alongside sample collection for WB analysis (**Section 3.10**)

Table 3. 1 - List and titers of lentiviral particles used in this work

Lentivirus	Titer (pg/µL)	Molecular Weight (kDa)	Specific antibody
pCaMKIIa-eGFP	68600	-	-
pCaMKIIa.ICD.IRES.V5	68600	37	anti-Trk C-terminal (C-14) anti-V5-Probe (G-14)

3.6 Lipofectamine-based transfection

For experiments regarding cellular degradation pathways and protein stability, undifferentiated SH-SY5Y cells and primary cortical neurons were transiently transfected with an empty vector and a TrkB-ICD-stop vector[199] (Table 3.2). Isolation of both vectors was performed by growing previously transformed *E.coli* in LB agar, overnight at 220 rpm and 37°C, followed by plasmid DNA isolation using the NZYMaxiprep kit (MB051, NZYTech genes & enzymes, Lisbon, Portugal) according to the manufacture instructions.

Table 3. 2 . List of plasmid vectors used in this work

Vector	Molecular Weight (kDa)	Specific antibody
Empty vector (EV)	-	-
TrkB-ICD-stop (TrkB-ICD)	32	Anti-Trk C-terminal (C-14)

The transfection was performed using Lipofectamine® 2000 reagent (Invitrogen, CA, USA), a lipid-based transfection reagent known as the gold-standard for its transfection efficiency in a wide range of cells, including difficult-to-transfect cells[210], such as SH-SY5Y[211]. Lipofectamine® 2000 was used according to the manufacturer instructions. Briefly, first both lipofectamine and vector DNA were separately diluted and incubated for 5 min at room temperature (RT) in Opti-MEM® reduced serum media, as serum tends to interfere with the formation of DNA-Lipofectamine® complexes. Thereafter, both solutions were gently mixed at RT for 20 min and added to DIV4 undifferentiated SH-SY5Y cells or DIV7 primary cortical neurons, timepoint corresponding to 80-90% confluency. Several amounts of Lipofectamine® and DNA vectors were used in the optimization always keeping a 1:1 (w/v) ratio. After optimization, a total of 1.5 µg of vector DNA and 1.5 µL of Lipofectamine® was used. After a 16-hour (h) transfection, cells were ready for the experiments.

3.7 Characterization and isolation of EVs by differential ultracentrifugation

Microvesicles and exosomes were isolated and collected from the secretome of Control (non-transduced, CTR), GFP-transduced (GFP) and TrkB-ICD-V5-transduced (ICD-V5) differentiated SH-SY5Y cells 48h after incubation with FBS-free conditioned medium. Initially, cell secretome was centrifuged at 1000g for 10 min to remove cell debris, and its supernatant was transferred into an ultracentrifuge tube and centrifuged at 16 000g for 1 h using an Avanti J-25I high-speed Centrifuge (Beckman Coulter, IN, USA) with a JA-25.50 rotor (Beckman Coulter Life Sciences, IN, USA) to pellet microvesicles with a diameter size of 200 nm-1000 nm (Figure 3.2). The microvesicle-enriched fraction was then washed in phosphate-buffered saline (PBS) (137 mM NaCl, 2.7 mM KCl, 8 mM $Na_2HPO_4.2H_2O$ and 1.5 mM KH_2PO_4, pH 7.4), centrifuged again at 16 000g for 1 h and resuspended in the appropriate buffer for the analysis. Samples were kept at -20°C until further analysis.

The supernatant resulting from the first 16 000g centrifugation, was then filtered using a 0.22 µm pore size filter to remove microvesicles and other particles larger than 220 nm. The supernatant was then transferred into another tube and ultracentrifuged at 120 000g for 2 h to pellet exosomes, using a Beckman Optima XL-90 ultracentrifuge (Beckman Coulter, IN, USA), with a Type 70 Ti Fixed Titanium Rotor (Beckman Coulter Life Sciences, IN, USA) (Figure 3.2). The resulting pellet was washed in PBS and once again ultracentrifuged at 120 000g for 2 h and the EV-depleted fraction kept for protein analysis (Figure 3.2). The final exosome-enriched fraction was then resuspended in appropriate buffer and kept at -20°C until further analysis. All centrifugations and ultracentrifugations were performed at 4°C.

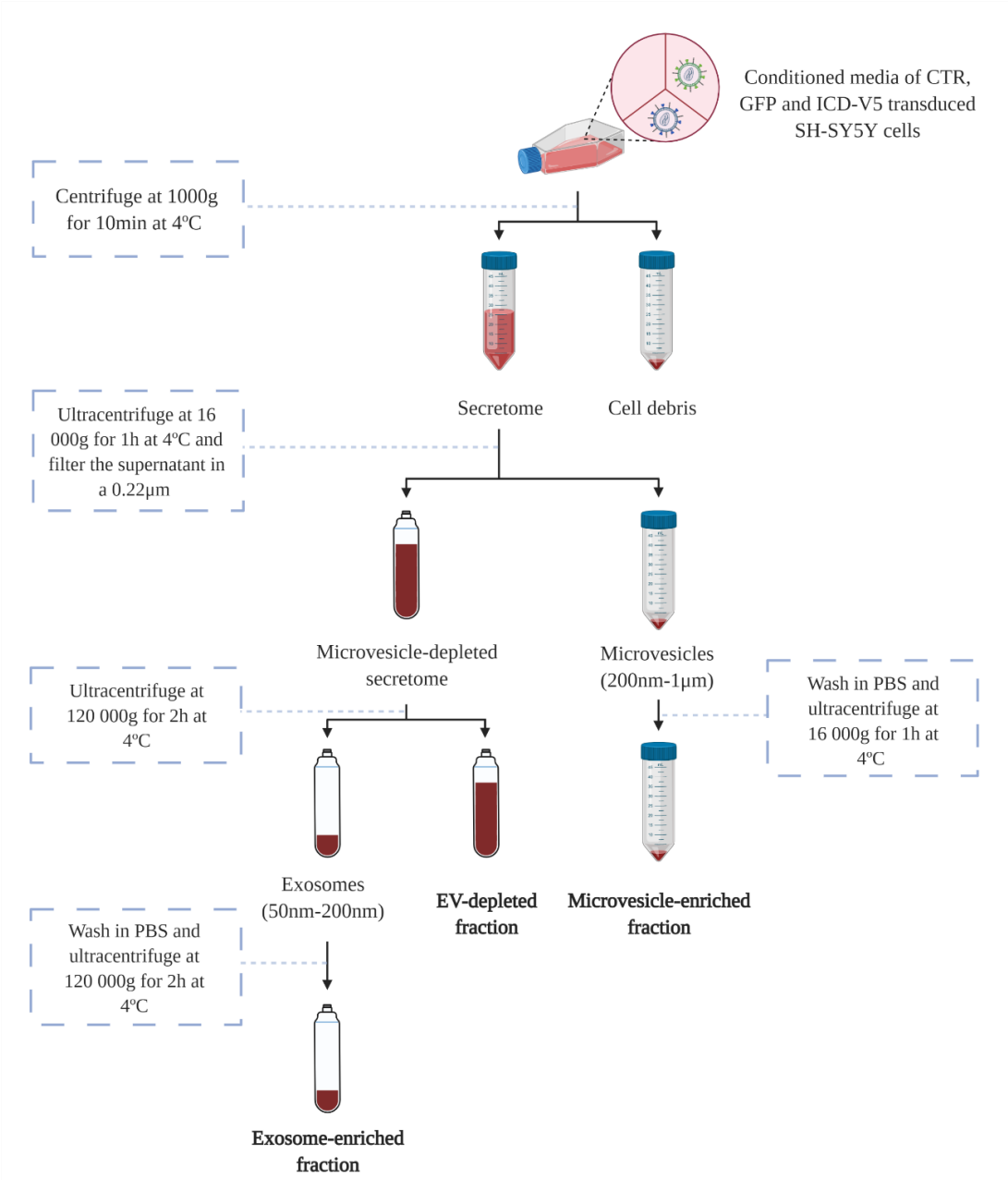

Figure 3. 2 - Scheme of differential ultracentrifugation to obtain EV-enriched fractions

Conditioned medium from CTR and transduced SH-SY5Y cells was initially centrifugated at 1000g to remove cell debris, following by an ultracentrifugation at 16 000g using an Avanti J-25I high-speed Centrifuge (Beckman Coulter, IN, USA) with a JA-25.50 rotor (Beckman Coulter Life Sciences, IN, USA) to obtain a microvesicle-enriched pellet. This pellet is then washed and ultracentrifuged at the same speed. The supernatant of the first ultracentrifugation is filtered and ultracentrifuged at 120 000g using a Beckman Optima XL-90 ultracentrifuge (Beckman Coulter, IN, USA), with a Type 70 Ti Fixed Titanium Rotor (Beckman Coulter Life Sciences, IN, USA) to obtain an EV-depleted fraction and an exosome-enriched pellet. Afterwards, this pellet is washed similarly as before. Both EV-enriched and EV-depleted fractions are stored until analysis.

To characterize the isolated microvesicles and exosomes, both EV types were resuspended in HEPES buffer (10 mM HEPES, 150 mM NaCl) and submitted to Transmission Electron Microscopy (TEM) using a Tecnai™ G² Spirit BioTWIN (FEI Company, OR USA) with an Olympus-SIS Veleta CCD Camera to assess vesicle diameter and shape. This analysis was made by the Electron Microscopy Unit at Instituto Gulbenkian de Ciência in Oeiras, Portugal. Briefly, a negative staining protocol was applied where a drop of each sample was placed on a grid and let adsorb for 20 min before being incubated and fixed in 2% formaldehyde in HEPES. After washing, all samples were stained in 2% uranyl acetate for 5 min. Dynamic Light Scattering (DLS) technique was performed to assess overall vesicle population size distribution, using the Zetasizer Nano ZS (Malvern Instruments, Malvern, UK). Finally, to evaluate the expression of typical EV markers, vesicle pellets were resuspended in Radio-Immunoprecipitation Assay (RIPA) buffer containing: 50 mM Tris-HCl (pH 7.5), 150 nM NaCl, 5 mM EDTA, 0.1% SDS, 1% Triton X-100 and protease inhibitors [10 mM NaF, 5 mM Na_3VO_4 and cOmplete Mini, EDTA-free protease inhibitor cocktail (Roche Diagnostics, Mannheim, Germany)] WB analysis was performed, as described below.

3.8 Secretome protein precipitation

Protein content released by differentiated, transduced SH-SY5Y cells into the media, was collected 48 h after switching to conditioned medium. After being processed by differential ultracentrifugation, EV-depleted fraction was used for protein precipitation. Total protein extraction for immunoblotting was performed by adding 10% Trichloroacetic acid (TCA) in acetone to the fraction in 1:10 ratio. The mix was vortexed and frozen overnight at -20°C followed by a 10 min 15 000g centrifugation and supernatant removal. The pellet was washed twice by being resuspended in acetone containing 20 mM of dithiothreitol (DTT) and centrifuged at 15 000g for 10 min to pellet protein content. Pellets were left to dry for 1 h in ice, prior to being dissolved in RIPA buffer and resuspended by sonication. All centrifugations were performed at 4°C.

3.9 Drug Treatment

In order to evaluate TrkB-ICD stability and estimate its half-life ($T_{1/2}$) in SH-SY5Y cells, the protocol previously used by Fonseca-Gomes in H4 neuroglioma cells was performed[59]. After 16 h of TrkB-ICD transfection at DIV4, SH-SY5Y neuroblastoma cells were incubated with 10 µg/mL cycloheximide (CHX), an eukaryotic *de novo* protein biosynthesis inhibitor[212]. Similar incubation periods were assessed – 0 h, 4 h and 8 h. Following drug incubation, protein content was collected and analysed by WB (**Section 3.10**). The strategy implemented by Belle and colleagues was used to determine mathematically the $T_{1/2}$ of TrkB-ICD, assuming that the degradation rate of the protein followed a first-order decay kinetics[213]. Therefore, TrkB-ICD levels (corresponding to *N* in the equation) were initially Ln-transformed, later used for a linear regression, obtaining the decay rate constant (*k*), and then applied to the equation, calculating for $T_{1/2}$.

$$\mathrm{Ln}(N) - \mathrm{Ln}(N_0) = -kt \Leftrightarrow T_{1/2} = \frac{\mathrm{Ln}\,(2)}{k}$$

To evaluate protein degradation mechanisms, specific pathway inhibitors were used. For assessing protein degradation via the ALP, transfected DIV5 undifferentiated SH-SY5Y cells and transfected DIV8 primary cortical neurons were incubated with 10 nM bafilomycin A_1, a specific inhibitor of vacuolar-type H^+-ATPase (V-ATPases), that halts lysosome acidification and thus protein degradation[214,215]; via UPS, cells were treated with 10 µM MG132, a peptide capable of blocking the proteolytic activity of the 26S proteasome complex, thus increasing ubiquitinated intracellular protein levels[191]. Similarly, different incubations times – 0 h, 4 h, 8 h and 24 h - were tested and the resulting protein content analysed by WB.

3.10 Protein quantification and Western blot

Similar to EV-depleted fraction protein extraction, SH-SY5Y cells and primary cortical neurons were washed with ice-cold PBS and lysed with RIPA buffer for 10 min in ice. Cell lysates were then sonicated and centrifuged at 4°C at 15 000g and the amount of protein determined using the Bio-Rad *DC* reagent kit according to the manufacturer protocol and measuring the absorbance using a microplate reader TECAN Infinite M200 (TECAN, Switzerland). Similarly, mice cortex tissue samples were digested using RIPA, sonicated and quantified using the same kit. All samples were

chemical and physically denatured by adding protein sample buffer 5x (350 mM Tris pH 6.8, 10% SDS, 30% glycerol, 600 mM DTT, 0.06% bromophenol blue) and by heating at 95°C for 10 min, respectively.

Afterwards, 20-40 µg of each sample, alongside a NZYColour Protein Marker II (MB090, NZYTech genes & enzymes, Lisbon, Portugal), were loaded and separated on a 10-15% sodium dodecyl sulfate polyacrylamide gel (SDS-PAGE), using a standard migration buffer (25 mM Tris-base (pH 8.3), 192 mM Glycine, 10% SDS) at a constant voltage between 80 and 120 mV in a Bio-Rad electrophoresis system (Hercules, CA, USA). The proteins were then transferred onto polyvinylidene difluoride (PVDF) membranes (GE Healthcare, Buckinghamshire, United Kingdom), previously activated in methanol, using a standard migration buffer [25 mM Tris (pH 8.3), 192 mM Glycine, 15% methanol] at 350 mA and subsequentially stained with Ponceau S to confirm the electrotransference efficacy. After washing the Ponceau S solution, membranes were blocked with 3% Bovine Serum Albumin (BSA) in Tris-Buffered Saline Tween 20 (TBS-T) (20 mM Tris base, 137 mM NaCl and 0.1% Tween-20) for 1 h at RT, washed three times with TBS-T and incubated with the primary antibody, also diluted in 3% BSA, overnight at 4°C with constant agitation. The membranes were again washed three times with TBS-T prior to being incubated with the respective horseradish peroxidase-conjugated secondary antibody, once again prepared in 3% BSA, for 1 h at RT, shaking. Afterwards, membranes were washed for 30 min in TBS-T and immunoreactivity assessed using the Blotting detection reagent ECL chemiluminescence system (Amersham-ECL Western Blotting Detection Reagents from GE Healthcare, Buckinghamshire, UK) on Chemidoc XRS+ (Bio-Rad, California, USA) or Amersham 680 systems (GE Healthcare, Buckinghamshire, UK). Band intensities were quantified by digital densitometry using *ImageJ* 1.45 software (Maryland, USA), normalizing to GAPDH or Ponceau S staining bands and lane, respectively, quantification as a loading control.

Membranes that required a re-incubation with different antibodies were incubated with a stripping buffer (200 mM glycine, 0.1% SDS, 1% Tween® 20, 50% acetic acid glacial, pH 2.2) up to 30 min at RT, followed by three washes with TBS-T and re-blocked with 3% BSA for 1 h at RT. The remaining procedure follows the same previously mentioned steps.

3.11 Cell Imaging and Immunofluorescence

Brightfield micrographs of undifferentiated and differentiated SH-SY5Y neuroblastoma cells were obtained using an Axiovert 135 TV fluorescence microscope (Carl Zeiss, Thornwood, NY, USA).

As previously mentioned in **Section 3.3.1** and **3.3.2**, prior to immunofluorescence assays, neuroblastoma cells and primary neuronal cultures were plated in washed PDL/laminin and PDL coated glass coverslips, respectively. Both of these extracellular matrices help in the adhesion and growth of cultured cells, promoting for a better neurite growth and cell plasticity[209]. Cells were rinsed in PBS and then fixed and permeabilized in methanol for 15 min at RT. Afterwards, cells were blocked with 3% BSA solution for 1 h and then incubated with the primary antibody overnight at 4°C. In the following day, the fluorophore-tagged secondary antibody was added after two washes. Finally, glass coverslips were mount on microscope slides using Mowiol. Fluorescence imaging was acquired using an Axiovert 135 TV (Carl Zeiss, Thornwood, NY, USA).

3.12 *In silico* ubiquitination sites prediction

Since ubiquitination stands as a post translational modification capable in directing proteins to specific clearance mechanisms, TrkB-ICD and TrkB-ICD-V5 mouse sequences were ran in an *in silico* prediction tool - BDM-PUB: Prediction of Ubiquitination sites with Bayesian Discriminant Method. For this prediction, a balanced cut between high specificity and high sensitivity was chosen with a threshold of 0.3.

3.13 Statistical analysis

All data, graphing and statistical comparisons, were made using the *GraphPad Prism 8* software (La Jolla, California, USA). Statistical results are expressed as mean ± standard error of mean (SEM) for an *n* number of independent experiments, where *n* is at least 3. Preliminary results include experiments with an *n* inferior to 3. Statistical significance between two conditions was calculated by paired/unpaired *t*-student tests. Multiple comparisons were evaluated by One/Two-Way ANOVA tests, with

Dunnett's or Tukey's post-test. Differences were considered significant if the *p*-value was inferior to 0.05.

3.14 Reagents, drugs, and antibodies

3.14.1 Culture reagents

Table 3. 3 - List and purpose of each reagent used in SH-SY5Y and primary cortical neuron cultures

Reagent	Description/Purpose	Supplier
Opti-MEM Medium	Reduced-serum medium ideal to lipofectamine transfection reagents. Medium used to grow SH-SY5Y cells.	Gibco
Fetal Bovine Serum (FBS)	Medium supplement which provides nutrients, growth, and attachment factors.	Merck
L-Glutamine	Unstable amino acid required for the formation of other building blocks.	Gibco
Pen-Strep solution	Solution composed of both penicillin and streptomycin; antibiotics used to keep cell cultures bacteria-free	Gibco
Trypsin-EDTA	The enzymatic proteolytic action of trypsin cleaves adhesion peptides and promotes the detachment of cells from the plate. EDTA acts as a metal chelator, removing Ca^{2+} and Mg^{2+} ions from adhesion proteins, weakening the adhesion strength in-between cells.	Gibco
Hanks' Balanced Salt Solution (HBSS)	Used for washing cells before dissociation while maintaining the pH and osmotic balance. Also, a source of essential inorganic ions.	Gibco
B-27 supplement	Serum-free supplement used in neuronal cultures.	Gibco
Neurobasal medium	Basal medium ideal for maintaining neuronal cell populations. Used in neuronal differentiation.	Gibco
Glutamic Acid	Growth and development of neuronal cultures.	Sigma
Lipofectamine® 2000	Drug used for transfection of a wide range of cell types, SH-SY5Y neuroblastoma cells inclusive.	Invitrogen

3.14.2 Drugs

Table 3. 4 - List of drugs used in this work

Drugs	Description/Purpose	Concentration	Supplier
Cycloheximide (CHX)	Inhibitor of *de novo* protein biosynthesis. Used in protein half-life determination.	10 µg/mL	Tocris Bioscience
MG132	Reversible inhibitor of proteolytic activity of 26S proteasome.	10 µM	Sigma
Bafilomycin A_1	Reversible inhibitor of autophagy.	10 nM	Sigma Life Sciences
Retinoic Acid (RA)	Induces expression of TrkB-FL receptors. Used in neuronal differentiation.	10 µM	Sigma
BDNF	Induces neuronal plasticity when bound to TrkB-FL receptors. Used in neuronal differentiation.	50 ng/mL	Regeneron (gifted)

3.14.3 Antibodies and Dyes

Table 3. 5 - List of primary and secondary antibodies used in this work

Antibody/Dye	Reference	Technique and Dilution	Supplier
anti-Trk C-terminal tail (C-14)	sc-11	WB – 1:500	Santa Cruz Biotechnology, Inc
anti-V5-Probe (G-14)	sc-83849	WB – 1:500	
anti-Alix (1A12)	sc-53540	WB – 1:500	
anti-TSG101 (C-2)	sc-7964	WB – 1:1000	
anti-CD9 (C-4)	sc-13118	WB – 1:1000	
anti-HSC70 (B-6)	sc-7298	WB – 1:1000	
anti-Ubiquitin (A-5)	sc-166553	WB – 1:1000	

anti-Flotillin-1	610820	WB – 1:1000	BD Transduction Laboratories™
anti-Syntaxin1a	AB5820-50UL	WB – 1:2000	Millipore Corporation
anti-βIII-Tubulin (TU-20)	#4466	WB – 1:500	Cell Signaling Technology®
anti-Map2 (clone HM-2)	M4403	IF – 1:100	Sigma-Aldrich®
anti-alpha Tubulin	ab4074	IF – 1:100	Abcam®
anti-GAPDH	6C5	WB – 1:5000	Thermo Fisher Scientific
DAPI	D9564-10MG	IF – 1:1000	Sigma-Aldrich®
anti-rabbit IgG-HRP	sc-2004	WB – 1:5000	Santa Cruz Biotechnology, Inc
anti-mouse IgG-HRP	sc-2005	WB – 1:5000	

4 Results and Discussion

4.1 Elucidation on TrkB-ICD cellular clearance mechanisms

4.1.1 Evaluation of TrkB-ICD release into the secretome

A) Optimization and validation of SH-SY5Y protocols

A1. Validation of TrkB-ICD-V5 lentiviral transduction

Setting our goal in studying the possible incorporation of TrkB-ICD in secreted EVs, we decided to use the SH-SY5Y neuroblastoma cell line model. Accordingly, and to increase its possible cargo selection, these cells were either non-transduced (CTR) or transduced at DIV2 with pCaMKIIa-eGFP or pCaMKIIa.ICD.IRES.V5, different lentiviral particles expressing for GFP, serving as a transduction positive control, and TrkB-ICD-V5 (ICD-V5, hereinafter), respectively. ICD-V5 is a modified version of the endogenous fragment TrkB-ICD, with an added V5-tag on the C-terminus that should not compromise TrkB-ICD intrinsic characteristics.

After 3 days of expression, at DIV5, we proceeded to cell imaging or protein extraction (Figure 4.1A).

Through fluorescent micrographs we were able to assess transduction efficiency to a yield of 61.2%±4.89% (n=4) in GFP-transduced cells (Figure 4.1C,D). Presumably, the same transduction efficiency can be withdrawn for ICD-V5, as the same MOI and titer were taken into consideration when transducing cells with both lentiviruses. Additionally, through WB analysis, we observed a marked synthesis of the new engineered TrkB-ICD fragment, at a molecular weight of 37 kDa (in contrast with the 32kDa endogenous TrkB-ICD) (Figure 4.1B). Moreover, we performed immunocytochemistry experiments in CTR, GFP- and ICD-V5-transduced cells, probing them with an anti-V5-tag (G-14) antibody. Nonetheless, due to its fairly common sequence in the proteome, multiple non-specific bindings were found in all conditions, masking the expressed ICD-V5 protein in its overexpressed condition (data not shown).

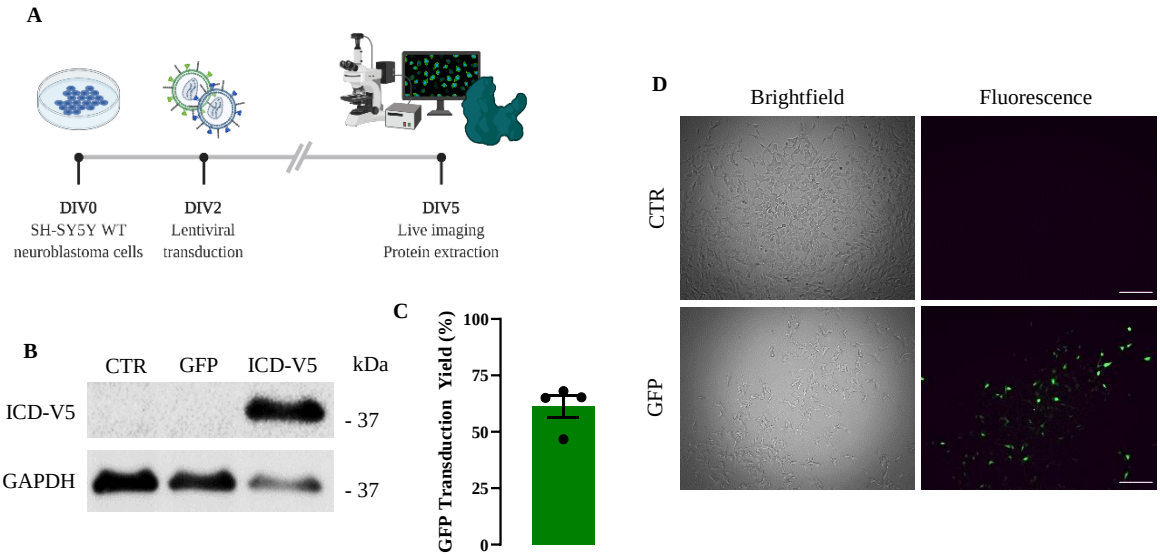

Figure 4. 1 - Lentiviral GFP- and ICD-V5-transduction in SH-SY5Y cells.

A. Timeline of the experimental design. After 3 days of expression, cell imaging or protein extraction were performed. **B.** Representative western-blot of the different conditions at DIV5: CTR, pCamKIIa-eGFP-transduced and pCaMKIIa.ICD.IRES.V5.ICD-V5-transduced SH-SY5Y neuroblastoma cells probed with anti-V5-tag (G-14) antibody. A marked expression of ICD-V5 can be observed at 37 kDa. GAPDH was used as the internal control. **C**. Transduction yield - 61.2%±4.89% (n=4) - obtained through counting of 4 independent micrographs of GFP-expressing cells. **D.** Brightfield and eGFP fluorescent cell imaging micrographs of non-transduced and transduced SH-SY5Y cells was performed to confirm transduction efficiency. Micrographs were obtained using an Axiovert microscope (Carl Zeiss Inc., Oberkochen, Germany), 10x magnification (scale bar: 200µm). All data represented as mean±SEM. CTR – control; GAPDH – Glyceraldehyde 3-phosphate dehydrogenase; GFP – Green Fluorescent Protein; ICD-V5 – TrkB-ICD fragment (calpain-generated) with a V5-tag; WT – wild type

A2. Optimization of RA-BDNF SH-SY5Y neuronal differentiation

Before assessing TrkB-ICD secretion though EVs, a neuronal differentiation protocol was performed to mimic as close as possible their release in neuronal physiological conditions. Non-transduced SH-SY5Y cells were submitted to a neuron-like differentiation protocol using all-trans RA alongside BDNF[207,216]. Moreover, a successive serum-deprivation protocol was also applied. Supporting both added supplements, cells were plated in a mix of PDL and laminin to enhance neurite growth[209].

After 12 days of RA-BDNF based-differentiation, cell imaging or protein extraction analysis were performed (Figure 4.2A).

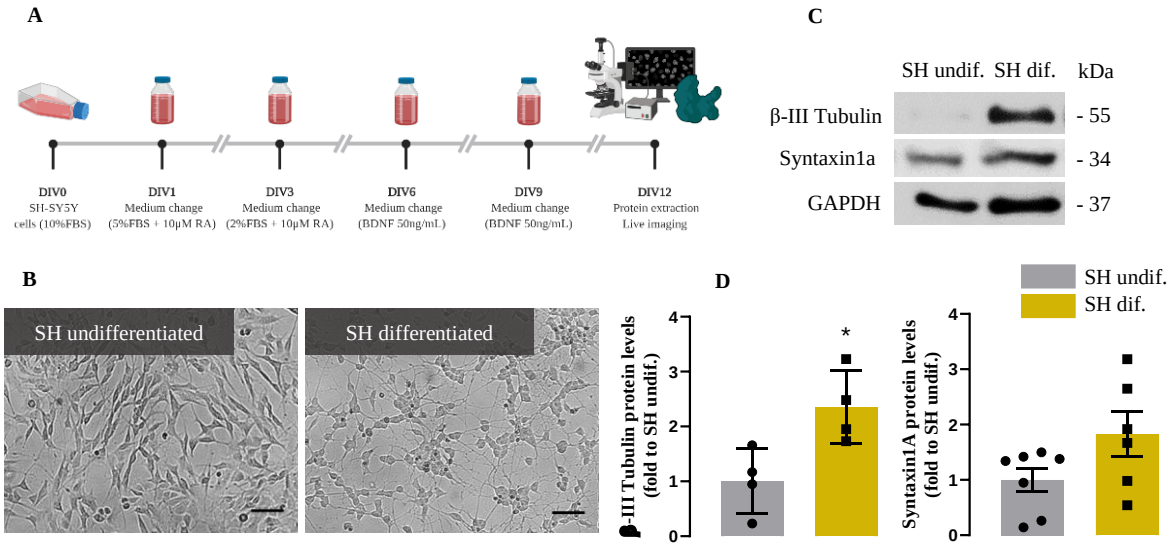

Figure 4. 2 - Morphological and biochemical changes upon SH-SY5Y neuroblastoma cell RA-BDNF differentiation.

A. Timeline of the experimental design. Sucessive medium changes were performed, changing FBS percentage, RA and BDNF incorporation. Non-differentiated cells were supplmented in the standard 10% FBS supplemented medium and protein extraction or cell imaging were performed at DIV4; at DIV12 for differentiated cells. **B.** Representative sections of brightfield cell imaging micrographs of undifferentiated and differentiated SH-SY5Y cells obtained using an Axiovert microscope (Carl Zeiss Inc., Oberkochen, Germany), 10x magnification (scale bar: 25μm). **C.** Representative western-blot of two different neuronal markers in both undifferentiated (DIV4) and differentiated (DIV12) SH-SY5Y cells. A higher expression of both syntaxin 1a and β-III Tubulin was observed in differentiated cells. GAPDH was used as the internal control. **D.** Analysis of band intensity represented in **C.** Data normalized to SH undif. (SH undif: n=4 for β-III Tubulin and n=7 for syntaxin 1a; SH dif: n=4 for β-III Tubulin and n=6 for syntaxin1a7, *p-value<0.05, unpaired t-student test). All data represented as mean±SEM. BDNF – Brain-derived neurotrophic factor; FBS – Fetal Bovine Serum; GAPDH – Glyceraldehyde 3-phosphate dehydrogenase; RA – retinoic acid; SH undif – SH-SY5Y undifferentiated cells; SH dif – SH-SY5Y differentiated cells.

As observed in Figure 4.2, upon differentiation, SH-SY5Y cells presented a slower rate of proliferation and an overall higher number of neurites per cell. In addition, neurite length also increased (Figure 4.2B).

Moreover, we tested for two common neuronal markers: i) syntaxin 1a, a nervous system-specific protein involved in synaptic vesicle docking in the presynaptic plasma membrane and ii) β-III Tubulin, a microtubule element exclusively found in mature neurons. As reported in the literature[207,209,217,218], we detected an enhanced expression of β-III Tubulin (p-value<0.05, unpaired t-student test, n=4) and an increase in syntaxin 1a protein levels, albeit not statistically significant (p-value>0.05, unpaired t-student test, n=6-7) (Figure 4.2C,D).

A3. Characterization of SH-SY5Y-derived extracellular vesicles

Given that TrkB-ICD fragment was recently found in CSF samples of AD patients, we hypothesized for its ability to be released in the secretome of cells, either within EVs or in its soluble fraction[117]. To test it, we first needed to validate a stable overexpression system in SH-SY5Y cells through lentiviral transduction, as well as the optimization of their neuron-like differentiation, to mimic the events in physiological conditions. With both optimizations completed, we started by isolating and characterizing SH-SY5Y-derived EVs. Hence, DIV0 neuroblastoma cells (CTR) were submitted to the previously described differentiation protocol and, at DIV12, new FBS-free medium was added for 48 h – conditioned medium - to collect the secretome of cells. As described extensively in the literature, FBS-enriched medium is known to contain EVs, reason why we chose to have it serum-depleted, as it otherwise would interfere with our analysis. Afterwards, the enriched medium was submitted to a differential ultracentrifugation protocol to isolate both microvesicles and exosomes (interchangeably referred to as MVs and EXOs in figures hereinafter, respectively) and also its soluble EV-depleted fraction (Figure 4.3A).

Initially, an EV characterization was performed to confirm pellet enrichment in either microvesicles or exosomes. Accordingly, the EV pellets obtained after 16 000g and 120 000g ultracentrifugations were submitted to TEM, DLS and WB analysis. TEM allowed the characterization of vesicles in terms of morphology and size (diameter), DLS was employed to assess the overall size distribution of both EV populations and WB technique enabled to evaluate the presence of typical EV markers in the isolated EV-enriched pellets (Figure 4.3).

Negative staining micrographs showed a correct cup-shaped morphology of both microvesicles and exosomes, as described in the literature[219,220] (Figure 4.3B, C). Moreover, the diameter of each vesicle matched their correct size. Accordingly, overall size distribution results obtained by DLS also showed that both vesicle populations matched within the previously mentioned size ranges [microvesicles (150 nm-1000 nm) – CTR: 215 nm±1.34 nm; exosomes (50 nm-200 nm) – CTR: 165 nm±2.85 nm] (Figure 4.3D, E). Curiously, control exosomes presented a profile with particles above 200 nm, hinting for the possible presence of larger particles.

To further confirm that both pellets were enriched in microvesicles and exosomes, both samples were probed with EV markers - HSC70, Flotillin-1, TSG101 and CD9 (Figure 4.3F).

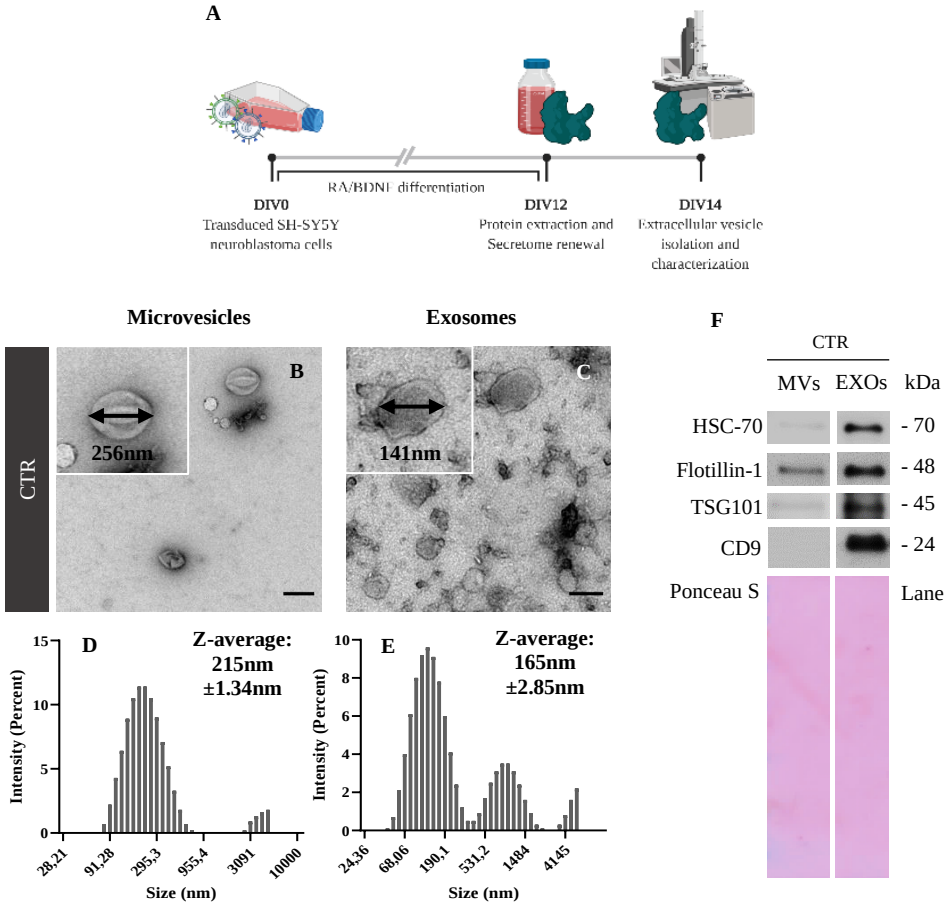

Figure 4. 3 - Characterization of SH-SY5Y-derived control microvesicles and exosomes via TEM, DLS and WB

A. Timeline of the experimental design. Following cell differentiation, non-transduced and transduced SH-SY5Y cells were incubated in fresh media to collect their secretome for 48 h. The enriched media was then submitted to protein analysis by western-blot, EV morphology and diameter through TEM and overall population size distribution by DLS. **B, C.** Representative transmission electron microscopy negative staining micrographs of non-transduced SH-SY5Y-derived microvesicles and exosomes, respectively. Ampliation of a small section with a representative vesicle and its diameter. Micrographs were acquired using a TecnaiTM G2 Spirit BioTWIN (FEI Company, OR USA), magnitude 5000x-26000x for microvesicles and 60000x for exosomes. (Scale bar: microvesicles – 200 nm; exosomes – 100 nm (n=1). **D, E.** Representative dynamic light scattering population size distribution plotted as a function of scattered light intensity percentage of non-transduced SH-SY5Y-derived microvesicles and exosomes, respectively. Data acquired using a Zetasizer Nano ZS (Malvern Instruments, Malvern, UK). Z-average was calculated from the mean of 3 independent reads. **F.** Representative western-blot of EV protein markers (HSC-70, Flotillin-1, TSG101 and CD9). The same amount of protein was loaded in each well and ponceau S used as the internal control. Data represented as mean±SEM for DLS. CD9 – tetraspanin 9; CTR- control; DLS – Dynamic Light Scattering; EXOs – exosomes;

As referenced earlier, none of the probed EV markers are exclusively present in one population over the other, nonetheless studies have shown that high ultracentrifugations (>100 000g) pellets tend to be more enriched in tetraspanins, namely CD9, as shown in Figure 4.3F[221].

B) TrkB-ICD-V5 and the endogenous TrkB-ICD fragments are released into the secretome

After all the optimizations and confirmation of the overall correct EV population isolation in control conditions, the same procedure was applied to the secretome of transduced cells. We observed a correct EV morphology and expected size for both microvesicle and exosome samples (microvesicles – CTR: 215 nm±1.34 nm; GFP: 277 nm±0.546 nm; ICD-V5: 274 nm±7.62 nm; exosomes – CTR: 165 nm±2.85 nm; GFP: 105 nm±1.19 nm and ICD-V5: 124 nm±1.10 nm) (Figure 4.4A-C, G-I). Nevertheless, in both microvesicle samples prepared from GFP or ICD-V5 transduced cells, there was a distinct separation of two populations, in contrast with their control condition (Figure 4.4E, F). WB analysis also detected the previously assessed EV markers (Figure 4.5A).

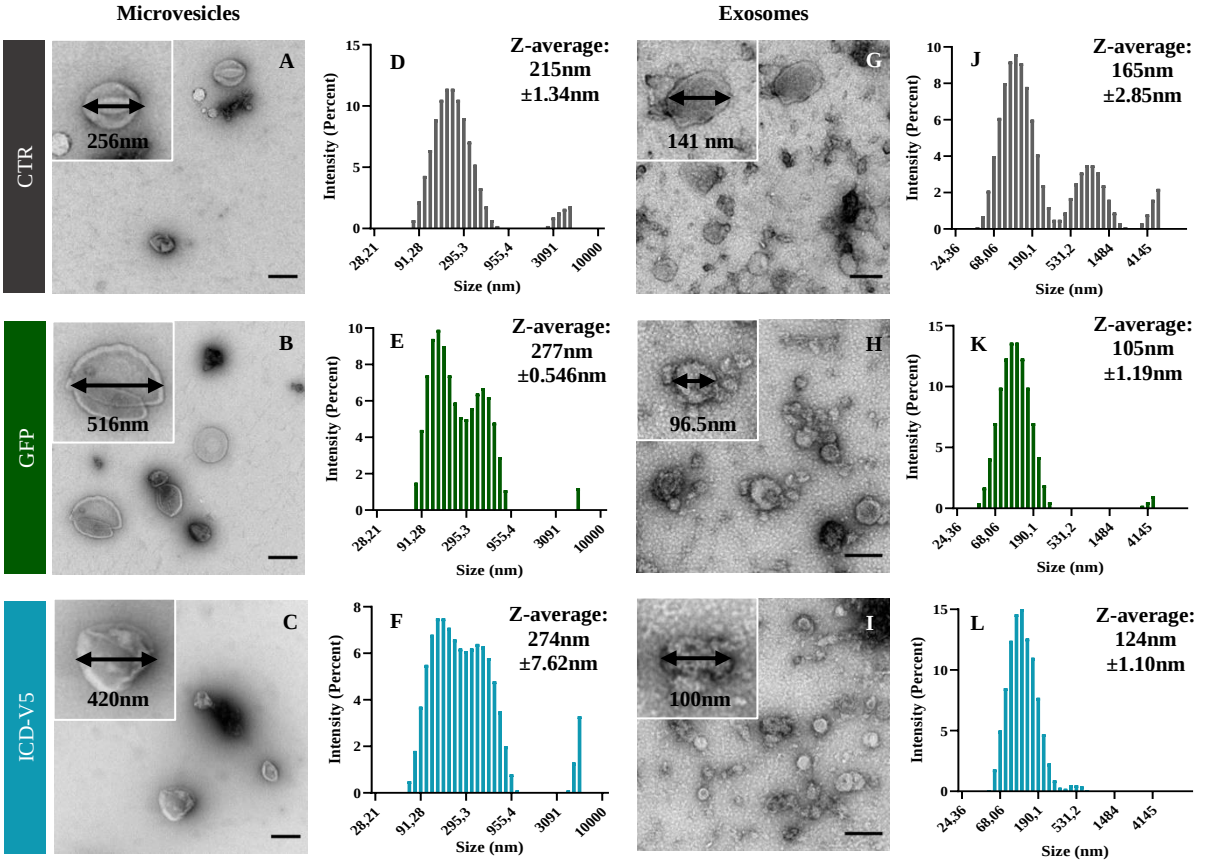

Figure 4. 4 - Characterization of SH-SY5Y-derived microvesicles and exosomes via TEM and DLS

A-C, G-I. Representative transmission electron microscopy negative staining micrographs of SH-SY5Y-derived microvesicles and exosomes, respectively. Magnification of a small section with a representative vesicle and its diameter. Micrographs were acquired using a TecnaiTM G2 Spirit BioTWIN (FEI Company, OR USA), magnitude 5000x-26000x for microvesicles and 60000x for exosomes. (Scale bar: microvesicles – 200 nm; exosomes – 100 nm (n=1). **D-F, J-L.** Representative dynamic light scattering population size distribution plotted as a function of scattered light intensity percentage of SH-SY5Y-derived microvesicles and exosomes, respectively. Data acquired using a Zetasizer Nano ZS (Malvern Instruments, Malvern, UK). Z-average calculated from the mean of 3 independent reads. Data represented as mean±SEM for DLS. CTR – control; DLS – Dynamic Light Scattering; GFP – Green Fluorescent Protein; ICD-V5 - TrkB-ICD fragment (calpain-generated) with a V5-tag; TEM – Transmission Electron Microscopy

Expectedly, we found once again an increase in the presence of CD9 tetraspanin in transduced exosome samples, similar to control conditions, when compared to microvesicle-enriched pellets.

Following the characterization of transduced SH-SY5Y-derived EVs, WB studies were made to assess the presence of ICD-V5 in both microvesicle and exosome pellets (Figure 4.5A).

We detected the presence of the overexpressed intracellular fragment, ICD-V5, in both EV populations, microvesicles and exosomes (Figure 4.5A, B). Both vesicle types were also confirmed by the EV probing markers - HSC70, Flotillin-1, TSG101 and CD9. Curiously, data suggests that ICD-V5 fragment is equally incorporated by both vesicle types as no statistical difference was seen between both groups (microvesicles: 1.0±0.20 and exosomes: 0.97±0.47, *p*-value>0.05, paired *t*-student test, n=3). Surprisingly, we also observed the presence of the endogenous TrkB-ICD in both EVs (Figure 4.5A, C, D, E). Similarly, there was no preferable route of secretion for the endogenous fragment, being released by both populations equally (*p*-value>0.05 for CTR, GFP and ICD-V5 groups, paired *t*-student test, n=3). Additionally, within the same population of vesicles, endogenous TrkB-ICD levels were not altered by transduction (*p*-value>0.05 for CTR, GFP and ICD-V5 groups, One-way ANOVA followed by Dunnett's post-test, n=3 Figure 4.5F, G).

Moreover, the full-length receptor of TrkB-ICD, TrkB-FL, was also found in EVs, albeit only present in exosomes (Figure 4.5A).

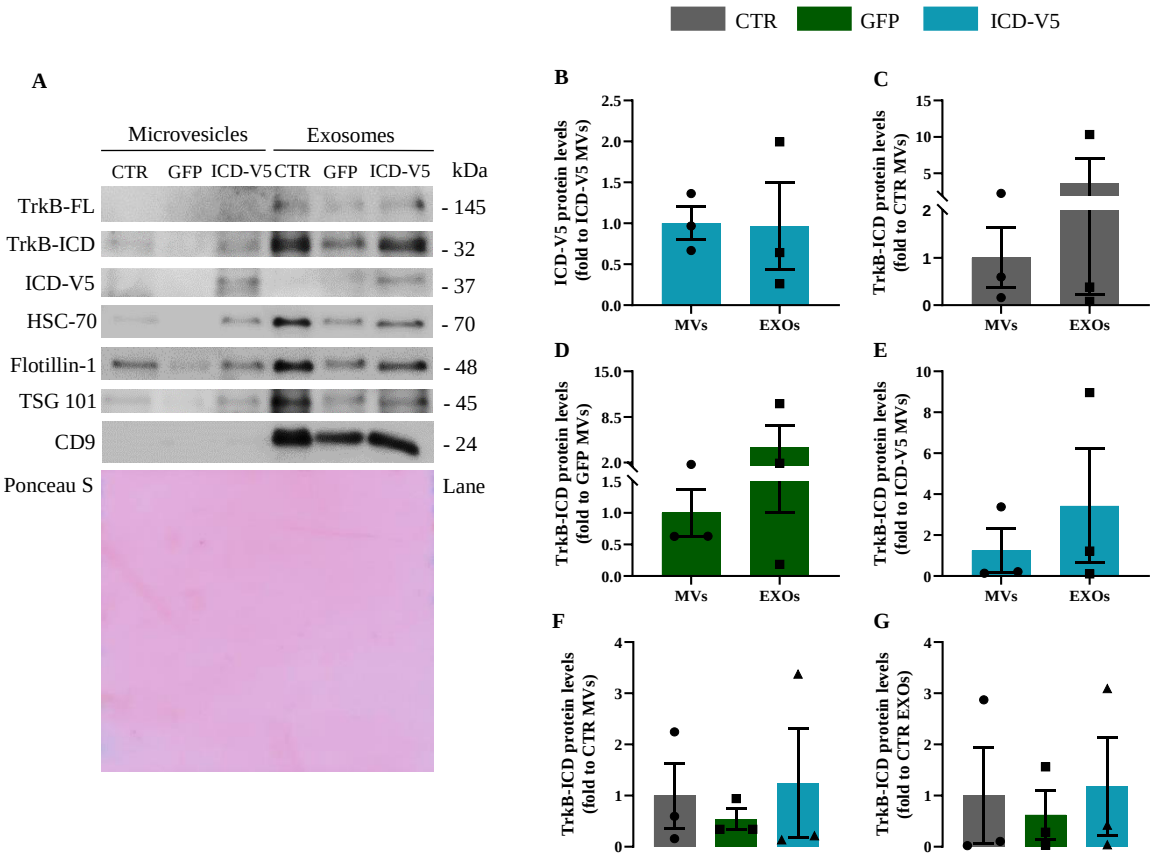

Figure 4. 5 – Detection of both ICD-V5 and its endogenous counterpart, TrkB-ICD, in both EV populations

A. Representative western-blot of both ICD-V5, probed with anti-V5-tag antibody (G-14), and TrkB-ICD, probed with anti-Trk C-terminal tail antibody (C-14). Presence of other known EV protein markers (HSC-70, Flotillin-1, TSG101 and CD9). The same amout of protein was loaded in each well and ponceau S used as the internal control. **B.** Analysis of ICD-V5 band intensity represented in **A**. Data normalized to ICD-V5 MVs, no statistical difference between groups (*p*-value>0.05, paired *t*-student test, n=3). **C-E:** TrkB-ICD is incorporated equally in both EV subpopulations, independent of transduction. **C.** Analysis of TrkB-ICD band intensity represented in **A**. Data normalized to CTR MVs, no statistical difference between groups (*p*-value>0.05, paired *t*-student test, n=3). **D.** Analysis of TrkB-ICD band intensity represented in **A**. Data normalized to GFP MVs, no statistical difference between groups (p>0.05, paired *t*-student test, n=3). **E.** Analysis of TrkB-ICD band intensity represented in **A**. Data normalized to ICD-V5 MVs, no statistical difference between groups (*p*-value>0.05, paired *t*-student test, n=3). **F, G**: TrkB-ICD EV protein levels are independent of transduction. **F.** Analysis of TrkB-ICD band intensity represented in **A**. Data normalized to CTR MVs, no statistical difference between groups (*p*-value>0.05, One-way ANOVA, followed by Dunnett's post-test, n=3). **G.** Analysis of TrkB-ICD band intensity represented in **A**. Data normalized to CTR EXOs, no statistical difference between groups (*p*-value>0.05, One-way ANOVA, followed by Dunnett's post-test, n=3). All data represented as mean±SEM. CD9 – tetraspanin 9; CTR – control; GFP – Green Fluorescent Protein; EXOs – exosomes; HSC-70 - heat shock cognate 70 kDa protein; ICD-V5 - TrkB-ICD fragment (calpain-generated) with a V5-tag; MVs – microvesicles; TrkB-FL – full-length tropomyosin-related kinase B; TrkB-ICD - TrkB-intracellular domain (calpain-generated); TSG101 - tumor susceptibility gene 101.

Given that ICD-V5 and the endogenous TrkB-ICD fragments were found in both EV populations, we also decided to perform some preliminary experiments to understand whether this fragment could be released in the soluble fraction of the secretome. For that, after ultracentrifugation and collection of the exosomal pellet supernatant (the EV-depleted secretome) a precipitation protocol and WB analysis were performed. In one experiment it was possible to detect TrkB-ICD in the soluble fraction of secretome (n=1) (Figure 4.6A). Unexpectedly, a higher level of the endogenous TrkB-ICD was found in the ICD-V5 condition (n=1). Conversely, ICD-V5 was not detected in this fraction (Figure 4.6A).

Simultaneously to all EV and secretome analysis, cell counting was performed after secretome removal to guarantee that cell number was not decreasing nor increasing between conditions (*p*-value>0.05, One-way ANOVA, followed by Dunnett's post-test, n=3, Figure 4.6B), A trypan-blue exclusion assay was used for cell viability (n=1) (Figure 4.6C).

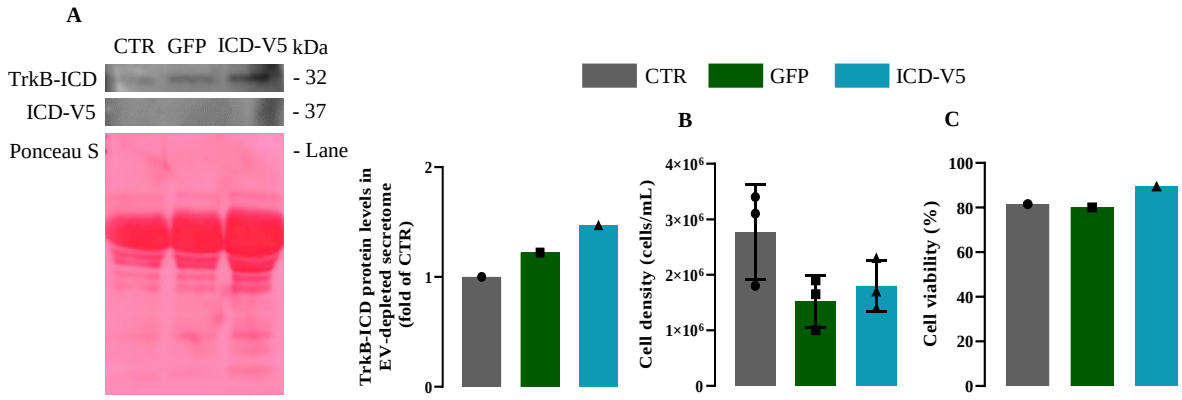

Figure 4. 6 – TrkB-ICD fragment is released in the soluble fraction of the secretome.
A. Preliminary representative western-blot analysis showing the presence of TrkB-ICD in the soluble fraction of the secretome (n=1), probed with anti-Trk C-terminal tail antibody (C-14) (n=1). The same amount of protein was loaded in each well and ponceau S was used as the internal control. **B.** SH-SY5Y cell density upon the removal of conditioned medium, no statistical difference between groups (*p*-value>0.05, One-way ANOVA, followed by Dunnett's post-test, n=3). **C.** Trypan-Blue cell viability assay hinting for a maintenance of cell viability upon cell transduction (n=1). All data represented as mean±SEM. CTR – control; GFP – Green Fluorescent Protein; ICD-V5 - TrkB-ICD fragment (calpain-generated) with a V5-tag; TrkB-ICD - TrkB-intracellular domain (calpain-generated).

4.1.2 Study of TrkB-ICD intracellular stability and degradation

Considering the previous data, we were able to demonstrate for the first time, that TrkB-ICD fragment is capable of being cleared from cells through its incorporation into EVs. This is an important information which may underlie a dissemination mechanism, where TrkB-ICD-containing EVs could spread its putative toxicity. Aside from its secreted fraction, which in of itself acts as a cellular clearance mechanism, there is still the presence of TrkB-ICD fragment intracellularly. Indeed, and as studied in our lab, cytosolic TrkB-ICD can alter the overall cellular phosphorylation profile and modulate gene expression. Therefore, studying other intracellular clearance mechanisms by which this fragment gets degraded is also of great importance to not only gain knowledge on its cellular interactions but also to develop possible pharmacological strategies to accelerate its elimination.

For this, a different overexpression system was used by applying a lipofectamine-transfection protocol as previously performed in our lab, albeit this time in undifferentiated SH-SY5Y neuroblastoma cells. This alternative overexpression system was used to ensure the continuation of previous studies, where we assessed TrkB-ICD function using this plasmid vector. Understandably, we first validated the transfection protocol since this particular neuroblastoma cell line is amongst the hardest cell lines to transfect, whereas before we had performed it in H4 neuroglioma cells[59,117,211,222].

Accordingly, cells were either non-transfected (CTR) or transfected for 16 hours at DIV4 with an empty vector (EV) or TrkB-ICD-stop plasmids, the later expressing for the endogenous TrkB-ICD fragment (Figure 4.7A,B).

Afterwards, we tested for TrkB-ICD stability and half-life with a CHX-chase assay, as previously performed by our lab[59]. As such, transfected SH-SY5Y cells were incubated with 10 µg/mL of CHX with protein extraction at 0 h, 4 h and 8 h. It can be observed that at the 8-hour timepoint, TrkB-ICD levels were already below 50%, implying that its half-life is between 4 h and 8 h (Figure 4.7C,D). In light of this, and as explained in **Section 3.8**, we applied an initial Ln-transformation to the obtained percentages followed by a linear regression to obtain its decay rate constant (Figure 4.7E). Consequently, we calculated the half-life of TrkB-ICD through the previous presented formula, rounding up to 6 h (Figure 4.7E).

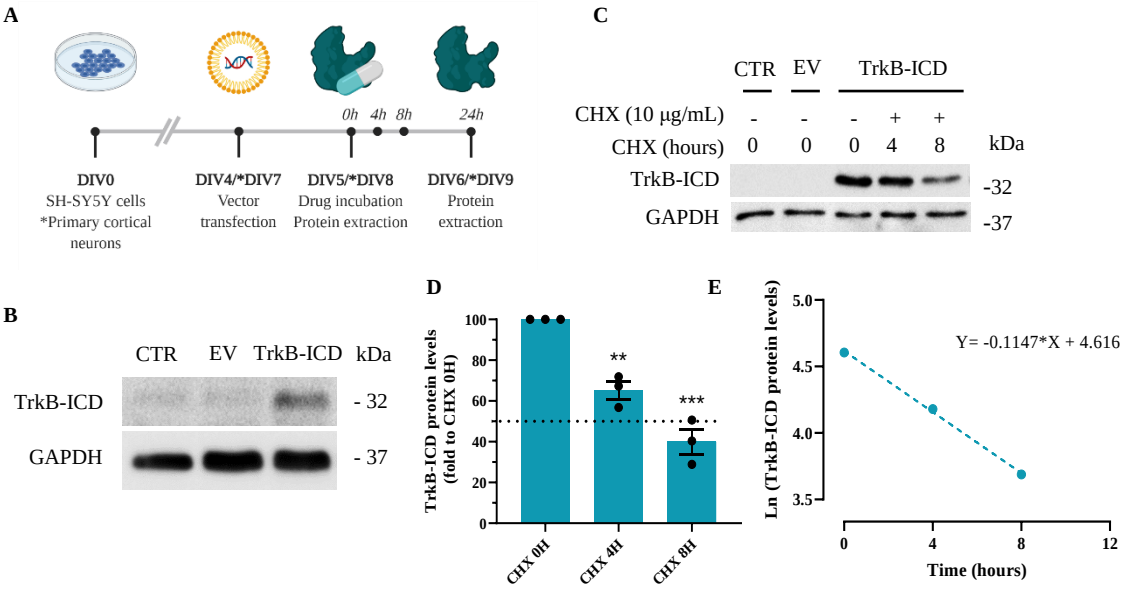

Figure 4. 7 - Determination of TrkB-ICD half-life by a CHX-chase assay.

A. Timeline of the experimental design. DIV4 SH-SY5Y cells and DIV7 primary cortical neurons were transfected, or not (CTR), with EV and TrkB-ICD plasmids. Protein was collected at DIV5/6 and DIV8/9, respectively, at different timepoints. **B.** Representative western-blot of the different DIV4 conditions: non-transfected (CTR), EV- and TrkB-ICD-transfected SH-SY5Y neuroblastoma cells probed with anti-Trk C-terminal tail antibody (C-14). A marked overexpression of TrkB-ICD can be observed at 32 kDa. Basal levels of TrkB-ICD can also be observed at both CTR and EV conditions. GAPDH was used as the internal control. **C.** Representative western-blot of a 10 µg/mL CHX-chase assay in 16 h-transfected SH-SY5Y cells probed with anti-Trk C-terminal tail antibody (C-14). Different incubations timepoints at 4 h, 8 h and 24 h. GAPDH was used as the internal control. **D.** Analysis of band intensities represented in **C** from densitometry quantification of TrkB-ICD immunoreactivity of three independent cultures. Data normalized at CHX 0 h (**p-value<0.01 and ***p-value<0.001, One-way ANOVA, followed by Tukey's post-test, n=3). **E.** Ln-transformation and linear regression of TrkB-ICD percentages. Its slope represents the decay rate constant of the fragment, k = 0.1147.All data represented as mean±SEM. CHX – cycloheximide; CTR – control; EV – empty vector; GAPDH - Glyceraldehyde 3-phosphate dehydrogenase; TrkB-ICD - TrkB-intracellular domain (calpain-generated).

Afterwards, we followed this protein degradation study by monitoring TrkB-ICD protein levels upon inhibition of cellular clearance mechanisms. As such, we mainly focused on the two most described degradation pathways, the UPS and ALP.

Accordingly, after a 16-hour transfection, DIV5 undifferentiated SH-SY5Y neuroblastoma cells and DIV8 primary cortical neurons were incubated with 10 µM MG132 or 10 nM bafilomycin A1, the former a typical inhibitor of proteasome activity and the latter, a selective inhibitor of the ALP[191,214,215] (Figure 4.8A,B and Figure 4.9A,B). Similarly, protein extraction was performed at 0 h, 4 h, 8 h and 24 h after treatment (Figure 4.7A left and right).

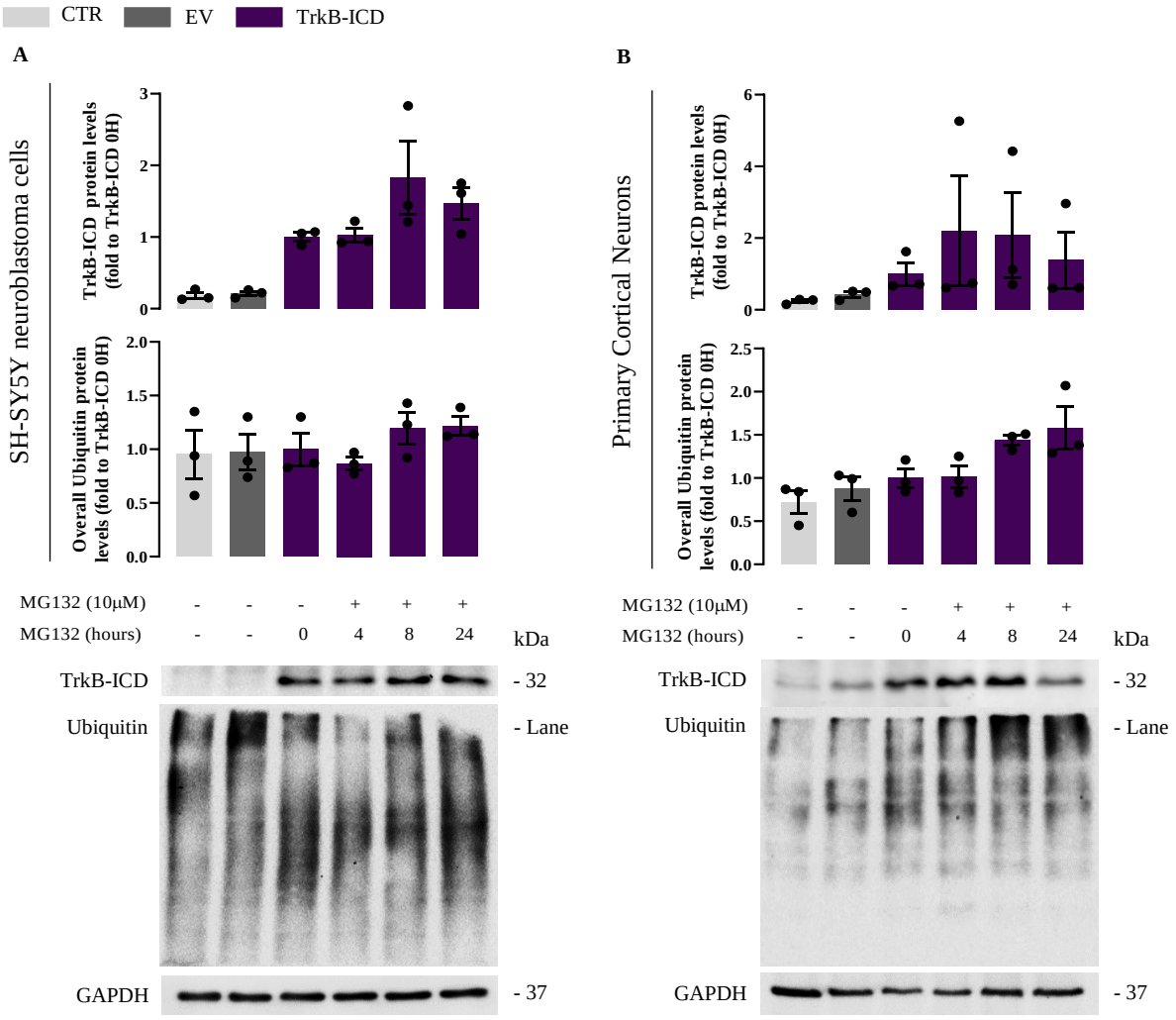

Figure 4. 8 - Evaluation of TrkB-ICD protein levels upon MG132-mediated proteasome inhibtion.

A. Representative western-blots of MG132-pharmacological treated undifferentiated CTR, EV- and TrkB-ICD-transfected SH-SY5Y cells probed with anti-Trk C-terminal tail (C-14) and anti-Ubiquitin (A-5) antibodies. GAPDH was used as the internal control. (**bottom**). Ubiquitin probes the overall ubiquitination profile including monoubiquitin, multi-monoubiquitinated and polyubiquitinated residues. Analysis of band intensities represented in **A** from densitometry quantification of TrkB-ICD and Ubiquitin immunoreactivity of three independent cultures (**top** and **middle**, respectively). Data normalized at TrkB-ICD 0 h (*p*-value>0.05, One-way ANOVA, followed by Tukey's post-test, n=3). **B.** Representative western-blots of MG132-pharmacological treated CTR, EV- and TrkB-ICD-transfected primary cortical neurons probed with anti-Trk C-terminal tail (C-14) and anti-Ubiquitin (A-5) antibodies. GAPDH was used as the internal control. (**bottom**). Analysis of band intensities represented in **B** from densitometry quantification of TrkB-ICD and Ubiquitin immunoreactivity of three independent cultures (**top** and **middle**, respectively). Data normalized at TrkB-ICD 0H (*p*-value>0.05, One-way ANOVA, followed by Tukey's post-test, n=3). All data represented as mean±SEM. CTR – control; EV – empty vector; GAPDH - Glyceraldehyde 3-phosphate dehydrogenase; TrkB-ICD - TrkB-intracellular domain (calpain-generated).

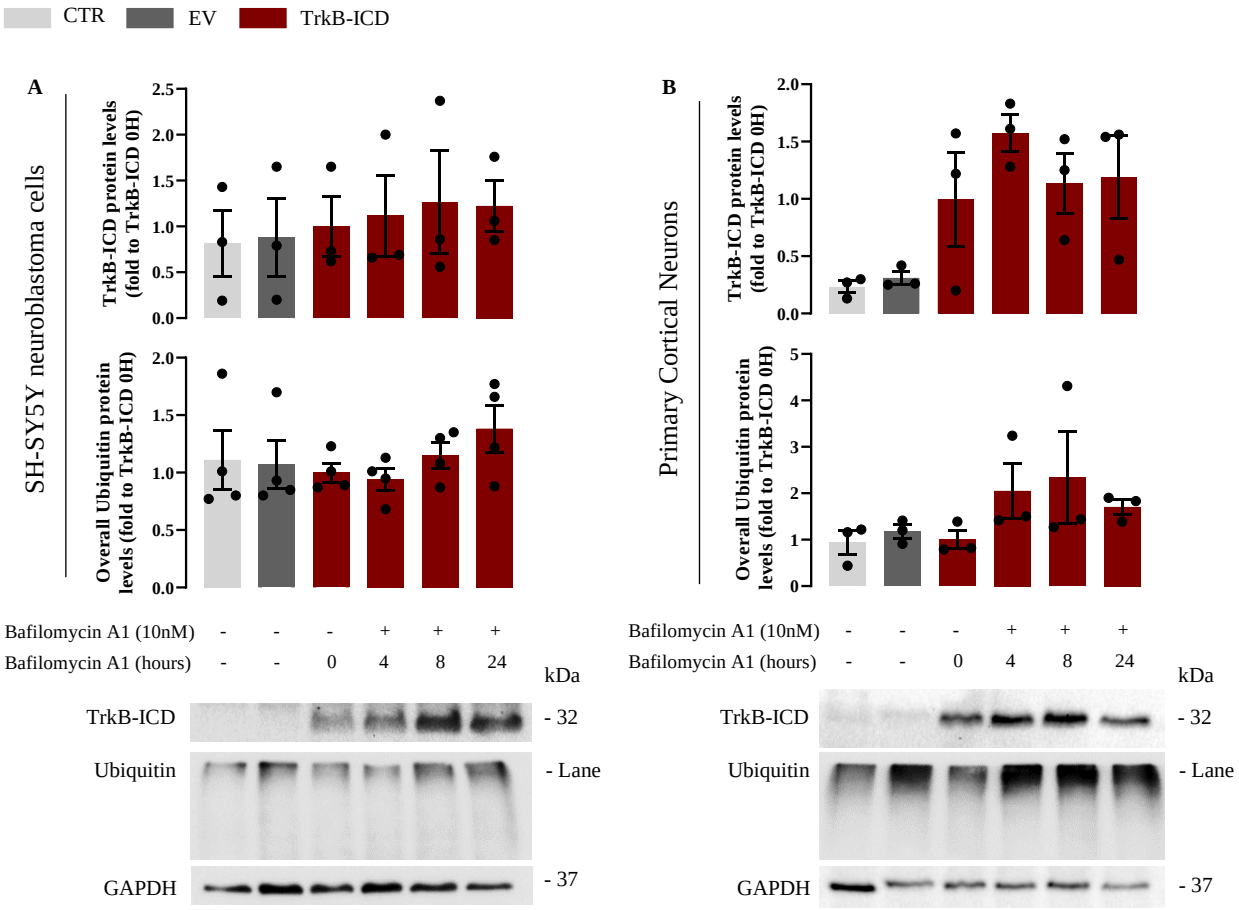

Figure 4. 9 - Evaluation of TrkB-ICD protein levels upon bafilomycin A1-mediated autophagy inhibition.

A. Representative western-blots of bafilomycin A1-pharmacological treated undifferentiated CTR, EV- and TrkB-ICD-transfected SH-SY5Y cells probed with anti-Trk C-terminal tail (C-14) and anti-Ubiquitin (A-5) antibodies. GAPDH was used as the internal control. (**bottom**). Ubiquitin probes the overall ubiquitination profile including monoubiquitin, multi-monoubiquitinated and polyubiquitinated residues. Analysis of band intensities represented in **A** from densitometry quantification of TrkB-ICD and Ubiquitin immunoreactivity (**top** and **middle**, respectively). Data normalized at TrkB-ICD 0H (*p*-value>0.05, One-way ANOVA, followed by Tukey's post-test, n=3-4). **B.** Representative western-blots of bafilomycin A1-pharmacological treated CTR, EV- and TrkB-ICD-transfected primary cortical neurons probed with anti-Trk C-terminal tail (C-14) and anti-Ubiquitin (A-5) antibodies. GAPDH was used as the internal control. (**bottom**). Analysis of band intensities represented in **B** from densitometry quantification of TrkB-ICD and Ubiquitin immunoreactivity of three independent cultures (**top** and **middle**, respectively). Data normalized at TrkB-ICD 0H (*p*-value>0.05, One-way ANOVA, followed by Tukey's post-test, n=3-4). All data represented as mean±SEM. CTR – control; EV – empty vector; GAPDH - Glyceraldehyde 3-phosphate dehydrogenase; TrkB-ICD - TrkB-intracellular domain (calpain-generated).

As it can be observed in Figure 4.8A and B (top), TrkB-ICD protein levels did not show a significant increase upon incubation with MG132 (*p*-value>0.05, One-way

ANOVA, followed by Tukey's post-test, n=3) in neither SH-SY5Y neuroblastoma cells nor primary cortical neurons.

Moreover, it also seems that proteasomal inhibition did not alter the cellular ubiquitin profile (*p*-value>0.05, One-way ANOVA, followed by Tukey's post-test, n=3), which raised questions as to whether or not MG132 was exerting its activity [Figure 4.8A,B (middle)].

Aside from proteasome degradation, incubation with bafilomycin A1 and thus, inhibition of autophagy, suggest no results in increasing TrkB-ICD fragment protein levels in neither neuroblastoma cells (*p*-value>0.05, One-way ANOVA, followed by Tukey's post-test, n=3) nor primary cortical neurons (*p*-value>0.05, One-way ANOVA, followed by Tukey's post-test, n=3). Additionally, and similarly to MG132 incubation, bafilomycin A1 was also insufficient to promote ubiquitin species accumulation in either model (*p*-value>0.05, One-way ANOVA, followed by Tukey's post-test, n=3-4), as observed by Figure 4.9A,B (middle).

Concomitantly, we observed that TrkB-ICD overexpression by itself is unable to alter the ubiquitination cellular profile, as no changes were seen in overall ubiquitinated protein levels in both SH-SY5Y cells and primary cortical neurons (*p*-value>0.05, One-way ANOVA, followed by Tukey's post-test, n=6-7) (Figure 4.9A, B).

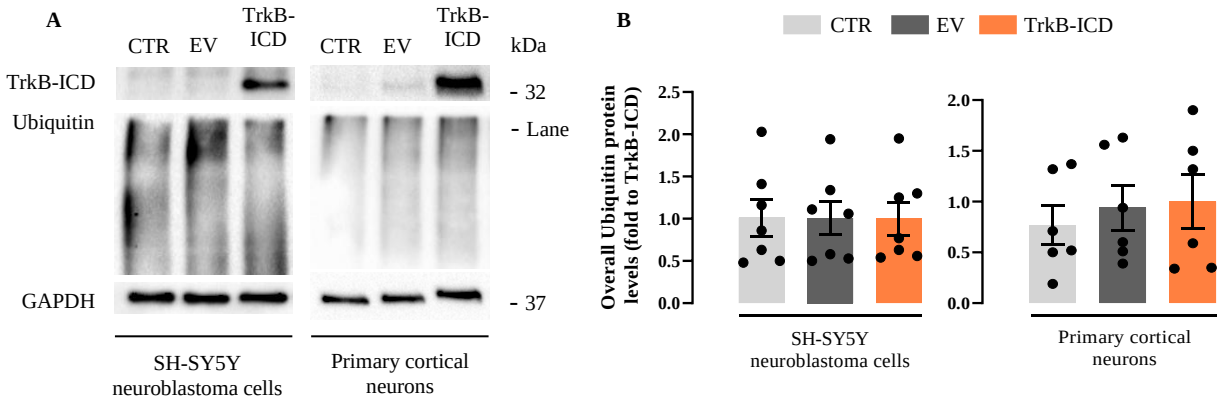

Figure 4. 10 - TrkB-ICD overexpression does not alter cellular ubiquitin levels.
A. Representative western-blots of TrkB-ICD overexpression in SH-SY5Y cells (**left**) and primary cortical neurons (**right**). Probing with anti-Trk C-terminal tail (C-14) and anti-Ubiquitin (A-5) antibodies. Ubiquitin probes the overall ubiquitination profile including monoubiquitin, multi-monoubiquitinated and polyubiquitinated residues. GAPDH was used as the internal control. **B.** Analysis of band intensities represented in A from densitometry quantification of TrkB-ICD and Ubiquitin immunoreactivity in SH-SY5Y cells (**left**) and primary cortical neurons (**right**). Data normalized at TrkB-ICD 0H (p-value>0.05, One-way ANOVA, followed by Tukey's post-test, n=6-7). All data represented as mean±SEM. CTR – control; EV – empty vector; GAPDH - Glyceraldehyde 3-phosphate dehydrogenase; TrkB-ICD - TrkB-intracellular domain (calpain-generated).

Although TrkB-ICD overexpression did not promote an increase in the cellular ubiquitination profile, an *in silico* prediction of possible ubiquitination sites in both TrkB-ICD and ICD-V5 was performed, as it is known that this protein modification is able to modulate protein trafficking, including protein encapsulation in EVs [as seen in **Section 4.1.1 B)**] and protein degradation. Accordingly, BDM-PUB: Prediction of Ubiquitination sites with Bayesian Discriminant Method was used to predict ubiquitination sites in TrkB-ICD and in ICD-V5. For its prediction, a balanced cut between high specificity and high sensitivity was chosen. As it can be seen in Table 4.1, a total of 8 lysine residues were predicted as being capable of suffer ubiquitination in both TrkB-ICD and ICD-V5[223] (Table 4.1).

Table 4. 1 - *In silico* prediction of TrkB-ICD and ICD-V5 ubiquitinated residues. Display of each residue alongside its flanking sequences, position, score, and threshold.

TrkB-ICD and ICD-V5 Residue Position	Position	Score	Threshold
****SQL**K**PDTFVQH	4	1.88	0.30
KRHNIVL**K**RELGEGA	20	0.45	0.30
LGEGAFG**K**VFLAECY	30	1.85	0.30
NLCPEQD**K**ILVAVKT	45	0.87	0.30
DKILVAV**K**TLKDASD	51	2.28	0.30
LVAVKTL**K**DASDNAR	54	2.31	0.30
DASDNAR**K**DFHREAE	62	0.51	0.30
TLLQNLA**K**ASPVYLD	291	0.36	0.30

4.1.3 Discussion

The presented data demonstrates, for the first time, the presence of TrkB-ICD in the secretome, in both microvesicles and exosomes. Additionally, preliminary results have also hinted for its presence as a soluble factor in the secretome. Moreover, this work corroborates previous experiments regarding TrkB-ICD protein half-life, while trying to assess possible intracellular clearance mechanisms, apart from EV release.

Previously, we have reported that TrkB-ICD fragment, resulting from BDNF-receptor cleavage, was detected in the CSF of AD patients, and remarkably an ongoing study in our lab has already shown a significant increase of this fragment in these samples when compared to CSF from non-AD patients[117]. Notwithstanding, the mechanisms by which this secretion occur are yet to be disclosed. Plasma membrane permeabilization upon neurodegeneration was a potential candidate for TrkB-ICD detection in the CSF, as the release of their luminal content could underlie its presence in these samples[224]. Therefore, to tackle our hypothesis that TrkB-ICD detection in the CSF was partly due to its release in EVs, we first started to validate an overexpression system that allowed for a prolonged expression of a similar fragment, ICD-V5. Using a lentiviral transduction system, we not only promoted an increased protein expression but also benefitted from a decreased associated toxicity, when compared to other overexpression systems, namely plasmid transfection[117]. The ICD-V5 fragment withholds the same sequence as TrkB-ICD with an added V5-tag on its C-terminal, allowing for its accurate pinpoint with multiple antibodies. Moreover, the absence of this fragment in physiological conditions allows to study its cellular presence without being masked by the endogenous TrkB-ICD. Importantly, due to the unknown presence of this fragment in secreted vesicles, we decided to use a neuroblastoma cell line instead of primary neuronal cultures, as with the former we are capable in producing an exponential number of cells but also, able in keeping a supply of transduced cells with successive passages. In addition, this approach avoided animal sacrifice, following the desirable replacement, reduction, and refinement policy in animal welfare.

Afterwards, a neuron-like differentiation protocol was optimized in this cell line. SH-SY5Y cells are a known cell model in the field of neurodegenerative diseases, as they can differentiate into a neuronal-like phenotype. Originated from successive subcloning of a cell line derived from a neuroblastoma tumor biopsy, and as previously mentioned in **Section 3.5**, this cell line is known to possess two distinct phenotypes: a non-neuronal substrate adherent (S-type) and a neuroblastic (N-type) type, able to

undergo transdifferentiation upon treatment with RA and/or BDNF[204,205,207,225]. Albeit this differentiation mechanism is still not fully understood, data shows that RA is able to enhance the expression of TrkB-FL, which, in synergy with the supplemented BDNF, allows for its downstream signalling, including neuronal differentiation and growth[207,216,225,226]. Additionally, and in synergy with both supplemented factors, a successive serum deprivation protocol was also implemented. According to the literature, serum deprivation helps select against epithelial cells (S-type in SH-SY5Y cells), allowing for a more homogenous neuronal culture[207,216,227]. Both the use of RA and serum deprivation are also known to slow the growth rate of cells, providing a better differentiation[228]. Understandably, the introduction of extracellular components such as PDL and laminin also contributed to cellular branching[209]. Altogether, the procedure resulted in an increased number of neurites per cell, neurite length as well as an increase production of neuron-specific proteins, such as β-III Tubulin[207,209,229]. Importantly, syntaxin 1a protein levels were also detected in both undifferentiated and differentiated states, as a subpopulation of the former SH-SY5Y cells are of neuroblastic origin. Interestingly, albeit this cell model has been extensively used in PD research, its characteristics allowed us to obtain an *in vitro* model capable of mimicking, to a degree, the environment of a neuronal-like cell and thus allowing us to study ICD-V5 in a more reliable source[207].

With the optimization of both prerequisites, we proceeded to establish a differential ultracentrifugation protocol. Once this procedure was also rounded up, EV pellets started to be collected for protein, imaging, and size distribution analysis. Initially, samples were sent to Instituto Gulbenkian de Ciência, Oeiras, Portugal, and negative staining micrographs were taken by TEM to assess vesicle morphology and diameter. Moreover, to further confirm the overall vesicle population size profile, EVs were also submitted to DLS spectroscopy. From the obtained data, there are no alterations in vesicle morphology, preserving their typical cup-shaped profile[219,220]. Their diameter also corresponded to the descriptions for each vesicle population. Upon DLS analysis, it can be observed that each enriched-vesicle pellet matched the expected dimensions, since microvesicles presented a range of 100-1000 nm in size and exosomes sizing roughly from 50 to 200 nm. Once again, it is important to highlight that these pellets are enriched in their specific EV type, which does not exclude the possibility of having exosomes present in the pellet of microvesicles and vice versa. Accordingly, lower sizes in microvesicle pellets may be due to exosome presence. Actually, by analyzing the distribution pattern of the control condition of exosomes, it can be seen a shift towards higher dimensions, which might be explained due to the presence of said microvesicles, but also, the presence of dust

particles and exosome aggregates[230,231]. Moreover, it is also known that exosomes might fuse with each other, forming vesicles with a larger diameter[232]. This data shows that ICD-V5 does not alter vesicle morphology nor their size. Moreover, we were able to detect the presence of typical EV markers in both pellets, with higher levels of tetraspanin CD9 in exosome pellets, which go in line with the literature, as higher ultracentrifugation pellets tend to me more enriched in tetraspanins[136,221].

Once characterized, we were able to confirm the presence of the transduced fragment as part of both microvesicles and exosomes. Moreover, its incorporation is vesicle-independent, as no statistical difference was found in its protein level between both EVs. Strikingly, we were also able to detect the presence of the endogenous fragment, TrkB-ICD, in both vesicles. Similarly to ICD-V5, no difference was found in its protein levels inside EVs, implying for an equal cargo selection and lack of specific secretion mechanisms. Nevertheless, it is important to highlight that our results show a high SEM, implying that we may achieve significance once we increase our sample size. Additionally, its protein levels are also transduction-independent, in both microvesicles and exosomes, with no difference for its secreted levels in each vesicle population.

In this regard, past studies already demonstrated the presence of the full-length receptor, TrkB-FL, in Rab7- and Rab9-positive endosomes, proteins known to be enriched in MVEs[233,234]. Indeed, in certain conditions, Trk receptors, including TrkB-FL, are internalized after ubiquitination mediated by ligand binding[235,236]. Sequentially, these vesicles eventually form endosomes and MVEs, from which TrkB-FL can be targeted for recycle and degradation. As seen earlier, these late endosomes can also fuse with the membrane thus releasing their luminal content. Accordingly, Pinet and her team have already described the presence of this full-length receptor in exosomes, reinforcing its anterior presence in MVEs[123]. Our data reinforced this observation, since we also detected TrkB-FL receptors on such EVs.

As mentioned earlier in **Section 1.3.1 B)**, ubiquitination is known to be a post-translational modification capable of modulation intracellular trafficking and protein encapsulation, as endosomal and exosomal cargo selection are modulated by this modification[149]. Adding to these, and as briefly mentioned above, TrkB-FL can undergo mono- and poly-ubiquitination in several of its residues upon BDNF recognition in primary cortical neurons[236,237]. This data corroborated ubiquitination patterns in several other tyrosine kinase receptors, usually monoubiquitinated within their intracellular domain[238]

Importantly, TrkB ubiquitination is described as being dependent on its tyrosine kinase activity, as studies show that both phosphorylation and ubiquitination

in primary cultures are severely attenuated upon incubation with both BDNF and K252A, an inhibitor of Trk kinases[236,239]. Accordingly, these data suggest that, similar to other ubiquitinated intracellular domains of tyrosine kinase receptors, TrkB-ICD could also be ubiquitinated. Moreover, despite cleaved from its full receptor, previous data obtained by our lab clearly demonstrated that TrkB-ICD and ICD-V5 maintain their tyrosine kinase activity and thus, if ubiquitination is dependent on the catalytic domain activity, both fragments would maintain their capability of being ubiquitinated[59]. To confirm this hypothesis, an *in silico* ubiquitination tool was used, predicting a total of 8 lysine residues capable of suffering ubiquitination in both fragment sequences.

Additionally, recent studies also suggest the presence of high levels of tyrosine phosphorylated sites within exosomes, suggesting that phosphorylation of exosomal proteins, in their tyrosine residues, may contribute to exosome secretion[240,241].

Altogether, these data suggest that TrkB-ICD and ICD-V5 can indeed be ubiquitinated, which in turn may explain their internalization in MVEs and consequently, their presence in released exosomes, now confirmed by the presented work. Concomitantly, since microvesicle cargo selection can also involve the same ESCRT machinery as exosomes, ubiquitination would also be able to modulate protein incorporation. Accordingly, TrkB-ICD and ICD-V5 were also detected in microvesicles.

Finally, preliminary results obtained through western blotting of EV-depleted secretome, allowed us to detect the presence of TrkB-ICD in the secreted soluble fraction. Conversely, ICD-V5 was not detected. Although this data still needs to be further corroborated, the presence of the V5-tag may 1) hinder its secretion in the soluble fraction, 2) be cleaved extracellularly, masking its presence, and detecting the transduced fragment as the endogenous TrkB-ICD or 3) alter trafficking signalling for ICD-V5. Moreover, ICD-V5 transduction yield together with a dilution factor of the total amount of proteins present in the medium may contribute to mask its presence.

Concomitantly, a preliminary cell viability assay showed no difference between cell viability in transduced and non-transduced cells, refuting the secretome presence of ICD-V5 and TrkB-ICD due to exacerbated cellular death. Nonetheless, further determinations are required. After secretome removal, cellular density data also shows no differences between conditions.

Altogether, the obtained data suggest a possible dissemination of TrkB-ICD and ICD-V5 through EVs, probably potentiating and serving as pathology mediators in the progression of AD.

Previously, we have reported that TrkB-ICD fragment has a half-life of 8 h in both transfected H4 neuroglioma cells and primary cortical neurons[59,117]. Given that in

the present work SH-SY5Y cells were used to study TrkB-ICD clearance mechanisms, the same cell model was used to corroborate the half-life of this fragment.

Understandably, and conversely to H4 neuroglioma cells, which are portrayed as a suitable model for cell transfection, SH-SY5Y neuroblastoma cells are described as one of the hardest cell lines to transfect. Vector transfection was carried out with Lipofectamine® 2000, a reagent known to promote a good transfection yield, albeit preferentially used in easy-to-transfect cells and primary neurons[211,222].

Moreover, contrary to methodology used in **Section 4.1.1 B)**, we decided to perform this battery of experiments using previously prepared plasmid vectors containing the endogenous sequence of TrkB-ICD, refraining from spending, and thus saving lentiviral particles. Moreover, TrkB-ICD protein half-life experiments were previously carried out in our lab with this overexpression system, reason why this strategy was implemented. The use of these vectors also came with the added benefit of mimicking the action of the endogenous fragment, as no V5-tag was added. Nonetheless, this transfection procedure also carried its own disadvantages when compared to cell transduction, highlighting an increased associated lipofectamine toxicity, but also a decrease in transfection and consequently, overexpression yield[117,211].

As such, we first validated TrkB-ICD transfection in this undifferentiated cell model. Once optimized, we performed the same assay previously done by Fonseca-Gomes, incubating DIV5 transfected SH-SY5Y cells with 10 µg/mL of CHX, an eukaryotic *de novo* protein biosynthesis inhibitor, known to prevent translational elongation[212,242]. Accordingly, this inhibition allowed us to acquire a profile of TrkB-ICD abundance in a steady state, disregarding contributions from protein synthesis. By performing this assay at multiple timepoints – 0h, 4h and 8h – we were able to pinpoint, through western blotting and linear regression analysis, its half-life.

Surprisingly, a slight shift of this parameter was observed when compared to previous data, reducing from a mean of 8h to a 6h-half-life. Notwithstanding, it must be highlighted that a different plasmid concentration was used in these difficult-to-transfect cells, with the added necessity of increasing the quantity of lipofectamine to keep the 1:1 ratio of plasmid to transfection agent. As such, the increase in lipofectamine may have driven a higher time-dependent toxicity, possibly promoting a decrease in cell viability with consequent depletion of TrkB-ICD-expressing cells alongside its protein levels. Importantly, and as mentioned above, this assay was already performed in primary cortical neurons, mimicking a better physiological environment than this *in vitro* model. As such, TrkB-ICD fragment maintains its stable presence with a half-life around 6-8h. This range of TrkB-ICD half-life may be explained

due to the cellular environment of different cellular typologies, however the time scale of its half-life time remained similar.

When compared to the literature, and specifically to other secreted proteins, TrkB-ICD has a relatively high half-life time, posing a threat to both intra- and intercellular communication, as an increased protein lifespan would imply a longer presence of this fragment and thus a dissemination of its toxic effects[243]. Actually, when compared to is activated receptor, TrkB-ICD shows a 3 to 4-fold of its half-life[59,117,244,245]. However, it is still unknown if this parameter would translate itself in TrkB-ICD present in EVs or in the soluble fraction of the secretome, as both routes differ from its original environment. Additionally, it is important to refer that its incorporation in EVs leads to a decrease in its cytosolic concentration, which is used to calculate TrkB-ICD half-life. As such, its secretion may alter this cytosolic parameter.

Taking its half-life in consideration, we sought out to study other two cytosolic degradation mechanisms, the UPS and ALP. As seen in **Section 1.3**, clearance pathways are key players in cellular proteostasis, as they can maintain protein concentrations within boundaries, avoiding their overaccumulation. Moreover, and as alluded earlier, TrkB-ICD cytosolic and nuclear presence lead to dysfunctions in both cellular compartments, reason why studying its clearance stands as an important mechanism to avoid its putative toxicity.

Initially, DIV5 transfected and undifferentiated SH-SY5Y cells and DIV8 transfected primary cortical neurons were incubated with 10 μM of MG132, an inhibitor of the 26S proteasome subunit[246,247]. The mindset behind this methodology was to observe if the inhibition of proteasomal activity would lead to an accumulation of TrkB-ICD, implying that this fragment would be targeted by ubiquitination and consequently degraded by the UPS. No significant changes were seen in neither SH-SY5Y cells nor primary cortical neurons. However, a small increase in TrkB-ICD protein levels was detected in higher timepoints, which may indicate the possible contribution of the UPS in its clearance. Notwithstanding, this increase may also be explained due to a longer transfection period of the fragment. To evaluate this hypothesis, we could either: 1) incubate both cultures with CHX and MG132, halting not only protein degradation by the proteasome, but also the *de novo* protein biosynthesis; or 2) extract protein samples of each selected timepoint without pharmacological treatment, drawing a linear regression in TrkB-ICD production overtime.

Additionally, we also quantified the overall ubiquitination cellular pattern upon MG132 treatment. According to the literature, the inhibition of the proteasome leads to an accumulation of ubiquitinated proteins since this post-translational

modification underlies the targeting and re-directing of cytosolic misfolded and toxic proteins to their degradation[246]. Strangely, the results did not show differences in ubiquitin immunoreactivity. These unexpected results may be due to a reversible action of the proteasomal inhibitor but also due to the administration of a non-functional dosage of MG132, compromising also the obtained TrkB-ICD data. The lack of an increase in ubiquitin species hints for a possible compromised proteasomal inhibition. Posterior tests will be necessary to re-evaluate this degradation mechanism, as with our current data we are unable to draw a conclusion. The treatment dosage might need to be checked, alongside its effective timepoints to ensure a non-reversible pharmacological action. Moreover, incorporating known positive control substrates of proteasome degradation, such as p53 and p21 proteins, would also help to clarify UPS inhibition[246].

Concomitantly to UPS studies, we also applied the same methodology using bafilomycin A1, a specific and reversible inhibitor of the ALP[215,248,249]. Bafilomycin A1 acts by inhibiting the fusion of the autophagosome with the lysosome, promoting and increase in autophagosomes carrying cargo for degradation. Curiously, we were also unable to observe differences in TrkB-ICD immunoreactivity, implying that this fragment is not degraded via autophagy, or at least via macroautophagy. Similarly to the UPS experiment, we also evaluated their ubiquitin profile, as different poly-ubiquitin chain conformations also shift ubiquitinated cargo to the ALP. Once again, no significant differences were observed. Although this preliminary study shows no indications of a possible autophagy-mediated action, we will also re-assess these experiments evaluating the immunoreactivity of LC3B-II, a protein present in the membrane of autophagosomes, alongside the LC3B-II/LC3B-I ratio. LC3B is known to be converted from LC3B-I to LC3B-II upon autophagosome formation, and thus a higher presence of its converted state would imply an inhibition of autophagosome-lysosome fusion[214,215].

Additionally, overexpression of TrkB-ICD does not promote changes in the ubiquitination profile when compared to CTR conditions, implying that this fragment alone is unable to promote the dysfunction of these clearance systems.

Altogether, our date shows an ambiguity in pinpointing if the UPS has a role in TrkB-ICD clearance, while hinting from a possible refrain of the ALP regarding its degradation.

Interestingly, considering its full-length receptor, and as previously mentioned, reports have described that TrkB-FL receptors are detected in MVEs upon BDNF-driven receptor ubiquitination[10,233,234]. Its internalization and incorporation in the cellular cytosolic trafficking system allow for its possible re-direction towards cellular

clearance mechanisms. Indeed, studies have demonstrated that Trk-containing MVEs fuse with lysosomes, thus promoting their clearance[250]. Specifically, reports on TrkA described not only its ubiquitination and consequent internalization, but also its degradation by both the proteasome and the lysosome[251,252]. Likewise, TrkB-FL is also known to suffer down-regulation upon BDNF ligation in cultured cerebellar granule neurons[244,253]. Interestingly, Sommerfeld and collaborators have suggested that BDNF-induced TrkB degradation is proteasome-dependent, as cells incubated with different proteasome inhibitors presented a decrease in TrkB-FL degradation[244]. Curiously, proteasomal phosphorylation is known to modulate its catalytic activity, and in particular, nearly a third of its phosphorylation residues are phosphor-tyrosine sites[254]. Proteasomal phosphorylation has been shown to both enhance and halt its proteolytic capability[190,254]. Since TrkB-ICD maintains it tyrosine kinase activity, this prompted us to speculate on whether this fragment can promote, or not, its phosphorylation, and if so, whether it would accelerate or decrease protein degradation.

Alternatively, recent studies also point to a TrkB-FL lysosome-mediated degradation. Proenca and her team observed a decrease in TrkB-FL degradation in cortical neurons upon incubation with BDNF and leupeptin, a lysosome inhibitor, when compared to basal degradation upon BDNF treatment[245]. This same study also suggested the possibility of an alternative degradation pathway of TrkB-FL depending on the binding neurotrophin. As referenced earlier, both BDNF and NT4 are able to bind TrkB-FL, and in this study, the use of NT4 alongside leupeptin resulted in a lesser efficient degradation blocking when compared to BDNF and leupeptin. As such, this may suggest not only a sustained signalling by NT4, but also an alternative pathway by which NT4-mediated signalling may drive TrkB-FL degradation [245]. Moreover, they observed different degradation kinetics upon treatment with each individual NT, hinting for a differential sorting not only to the lysosome, but also to the proteasome and to protein recycling, corroborating the data described by Sommerfeld[244,245]. Interestingly, it must also be taken into consideration that both degradation pathways are able to communicate, as several proteins make up an interplay crosstalk between both systems. It has already been reported that when the UPS is impaired, p62, a multidomain autophagy receptor protein, re-directs and promotes the clearance of ubiquitinated proteins through the ALP instead[190,255]. Curiously, autophagy studies have likewise revealed that certain Atg-knockout mice show an accumulation of UPS substrates, but also increased levels of aggregates, which in turn have been shown to block the UPS[190,256–259]. Together, this information suggests and intrinsic interplay between both the ALP and the UPS, where a

dysregulation in one may cause a mutual compensation mechanism and proteolytic hindrance.

As mentioned earlier, tyrosine kinase receptors are highly ubiquitinated in their intracellular domain, which in turn lead to their endocytic incorporation. Moreover, a TrkB-ICD *in silico* simulation was performed, obtaining a total of 8 lysine residues capable of being ubiquitinated. Altogether, this data suggests a similar degradation process for TrkB-ICD, disregarding our obtained data. As such, new experiments will be performed to re-assess TrkB-ICD-mediated clearance. Notwithstanding, our remarkable finding that TrkB-ICD is secreted in EVs, not only helps unveiling one of its possible cellular clearance mechanisms, but also may hint for a role in intercellular toxicity and dissemination at short and long distances.

4.2 Effect of TAT-TrkB peptide on learning and memory

4.2.1 TAT-TrkB hints for a restoration of spatial memory and does not alter anxiety levels in 6 months old 5xFAD mice

Considering the previous work done in our lab about the mechanism behind TrkB-ICD formation, Fonseca-Gomes designed and developed a compound capable of preventing, to a certain degree, TrkB-FL calpain-mediated cleavage, the TAT-TrkB peptide. This small peptide has already shown promising results in both *in vitro* and *ex vivo*, with current *in vivo* studies being performed[117].

Accordingly, preliminary efficacy studies of TAT-TrkB were performed in 5xFAD, an AD mouse model previously described. At 4 m.o., 5xFAD mice started to be i.p. injected five times a week for two months with two different dosages of the peptide – 25 mg/kg and 50 mg/kg, TAT25 and TAT50, respectively – or with Veh (Figure 4.11A). At 5.5 m.o., mice were submitted to a battery of behavioural tests, assessing their spatial and cognitive memory, as well as their anxiety levels (Figure 4.11A, B). During the acquisition phase of the MWM test, the latency of each mice to reach the platform was registered to assess their learning. As expected, Veh-injected mice presented significant differences depending on their phenotype, as WT animals quickly learned the position of the platform, outperforming Tg animals (**p-value<0.01, Two-way ANOVA, followed by Tukey's post-test, n=3-19 animals per group) (Figure 4.11C).

Moreover, WT mice injected with TAT-TrkB did not show differences in spatial learning when compared to WT Veh mice, as observed in the latency test of the MWM

test (*p*-value>0.05, Two-way ANOVA, followed by Tukey's post-test, n=4-19) (Figure 4.11D). Similarly, Tg mice administrated with the peptide also did not show differences when compared to the control condition (*p*-value>0.05, Two-way ANOVA, followed by Tukey's post-test, n=3-17 animals per group) (Figure 4.11E). It is however important to point out that data obtained by TAT25-treated Tg mice suggest a potential learning restoration. Additionally, no differences were observed in other probe test memory-assessing parameters, such as number of platform crossings and time spent in the correct quadrant, among all experimental groups (*p*-value>0.05, Two-way ANOVA, followed by Tukey's post-test, n=3-19 animals per group) (Figure 4.11F-K).

Mice were also assessed for their anxiety-like behaviour through an EPM test. Data shows that no differences were observed in both the time spent on the open arm and its number of entries, between Veh-treated WT and Tg mice (*p*-value>0.05, Two-way ANOVA, followed by Tukey's post-test, n=17-19 animals per group) (Figure 4.11L, O), nor among WT and Tg TAT25- or TAT50-treated animals (*p*-value>0.05, Two-way ANOVA, followed by Tukey's post-test, n=3-19 animals per group) (Figure 4.11M, N, P and Q).

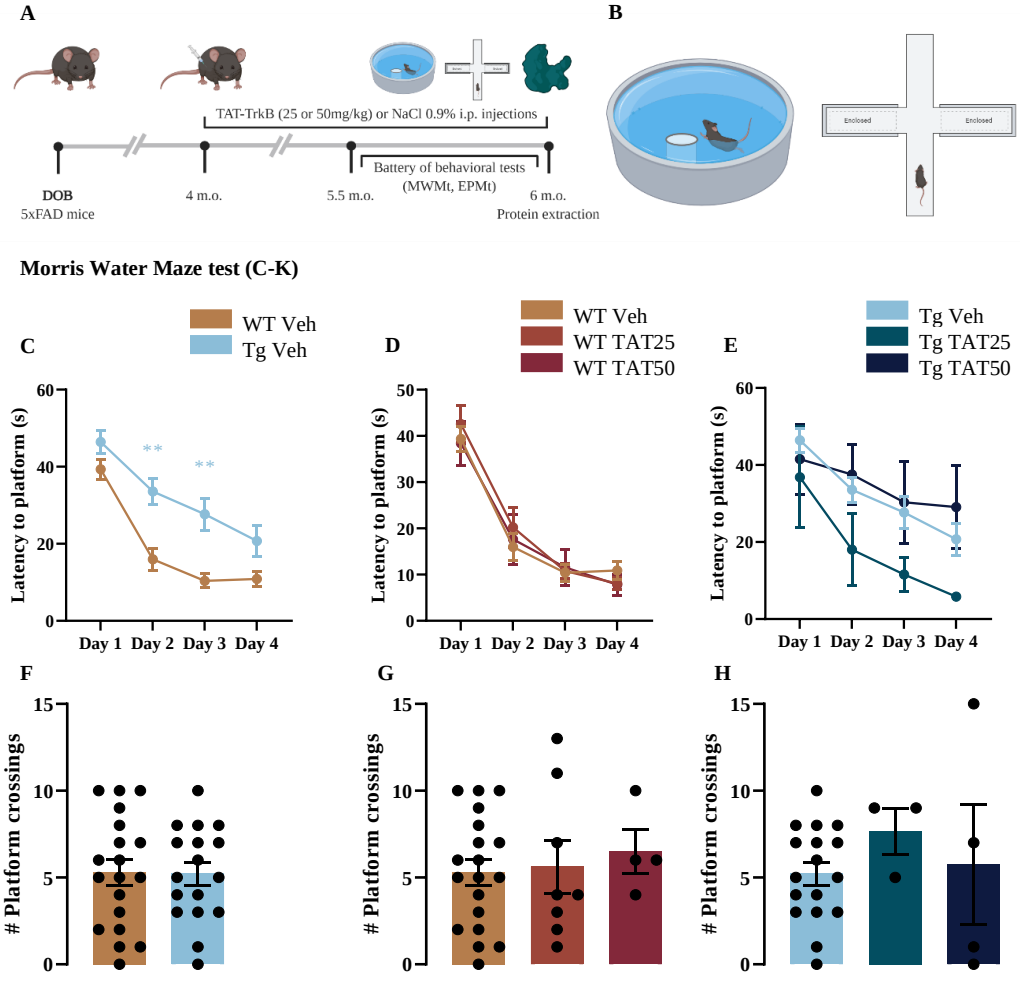

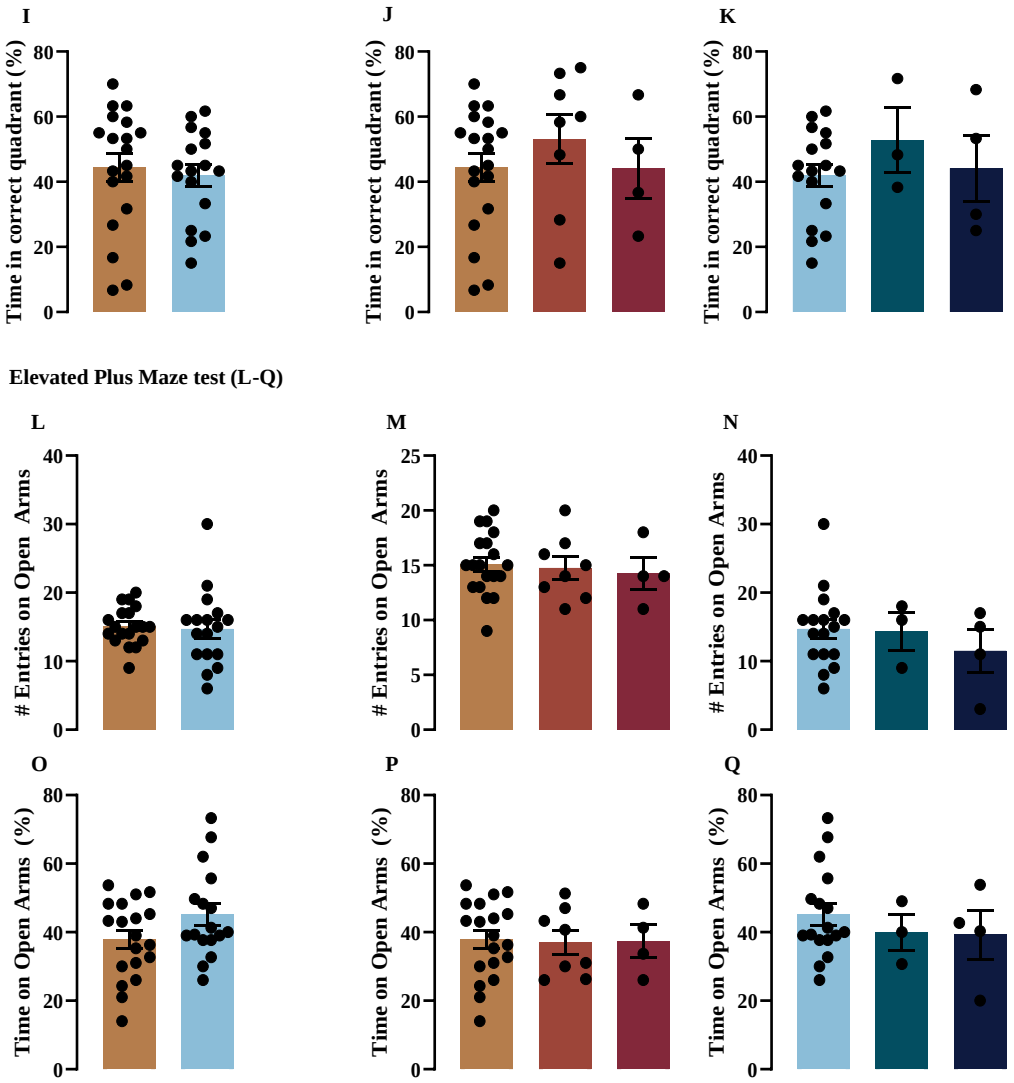

Figure 4. 11 - Effect of TAT-TrkB in memory and anxiety of 6 m.o. 5xFAD mice.

A. Timeline of the experimental design. After 1.5 months of being i.p. injected with TAT-TrkB or saline solution, both WT and Tg mice were submitted to a battery of behavioural tests. **B.** Representative scheme of MWM test (**left**) and EPM test (**right**). **C-E.** Acquisition phase of MWM test - during the four days of training, mice were trained to reach the platform, and their latency recorded. **C.** Tg Veh mice showed an impaired spatial memory when compared to their WT counterparts (**p-value<0.01, Two-way ANOVA, followed by Tukey's post-test, n=17-19 per animal group). **D, E.** No significant changes were seen when comparing the administration of TAT-TrkB in WT no Tg mice (p-value>0.05, Two-way ANOVA, followed by Tukey's post-test, n=3-19 per animal group). **F-K.** Probe test of MWM test – to assess their spatial memory, both the number of platform crossings and time spent on the correct quadrant were registered, having observed no significant changes among experimental groups (p-value>0.05, Two-way ANOVA, followed by Tukey's post-test, n=3-19 per animal group). **L-Q.** The EPM test, performed to assess anxiety-like behavior indicated no significant changes between experimental groups (p-value>0.05, Two-way ANOVA, followed by Tukey's post-test, n=3-19 per animal group). All data represented as means±SEM. DOB – days of birth; EPMt – Elevated-Plus Maze test; i.p. – intraperitoneal injection; MWMt – Morris Water Maze test; TAT25 - TAT-TrkB 25 mg/kg ; TAT50 – TAT-TrkB 50 mg/kg; TAT-TrkB – peptide capable in preventing TrkB-FL cleavage; WT – wild-type; Tg – transgenic; Veh – sodium chloride (NaCl) injection;

4.2.2 Administration of TAT-TrkB showed no alteration in TrkB-FL and TrkB-ICD levels in 6 months old 5xFAD mice

Upon two months of i.p. injections and finished the behavioural assessment tests, mice were sacrificed for molecular analysis (Figure 4.11A). Hippocampal (Figure 4.12) and cortical (Figure 4.13) brain areas were digested, and immunoreactivity WB assays performed.

To study if the phenotype had any impact in TrkB-FL and TrkB-ICD protein levels, WB analysis of both hippocampal and cortical samples from WT and Tg Veh-treated mice was performed. Accordingly, no differences were observed in TrkB-FL and TrkB-ICD levels in neither hippocampal (p-value>0.05, unpaired t-student test, n=7-11 per animal group) (Figure 4.12B, E) nor cortical samples (p-value>0.05, unpaired t-student test, n=6-7 per animal group) (Figure 4.13B, E). Moreover, TrkB-ICD/TrkB-FL ratio was also calculated for both sample types, albeit no statistical differences were observed (p-value>0.05, unpaired t-student test, n=6-11 per animal group) (Figures 4.12H and 4.13H).

Additionally, studies to assess a possible toxicity from this peptide were also conducted, where again, both types of samples were analyzed. As a result, WT TAT-TrkB-treated animals also did not present significant changes in TrkB-FL and TrkB-ICD levels, with the exception of a rise in TrkB-ICD in cortical samples of TAT25-treated WT mice, when compared to WT Veh animals (p-value>0.05, *p-value<0.05, One-way ANOVA, followed by Tukey's post-test, n=3-11 per animal group) (Figure 4.12C, F and 4.13C, F). Similarly, their ratio was also assessed, showing no observable differences between treatments (p-value>0.05, One-way ANOVA, followed by Tukey's post-test, n=3-11 per animal group) (Figure 4.12I and 4.13I).

Finally, we did immunoreactivity analysis to assess if this fragment had an impact in restoring TrkB-FL levels in both the hippocampus and cortex of Tg mice. As observed in Figure 4.12D, G and 4.13D, G, no measurable changes were observed in neither TrkB-FL nor TrkB-ICD protein levels (p-value>0.05, One-way ANOVA, followed by Tukey's post-test, n=3-7 per animal group). Once again, their ratio was calculated and no significant differences were found among conditions (p-value>0.05, One-way ANOVA, followed by Tukey's post-test, n=3-7 per animal group) (Figure 4.12J and 4.13J).

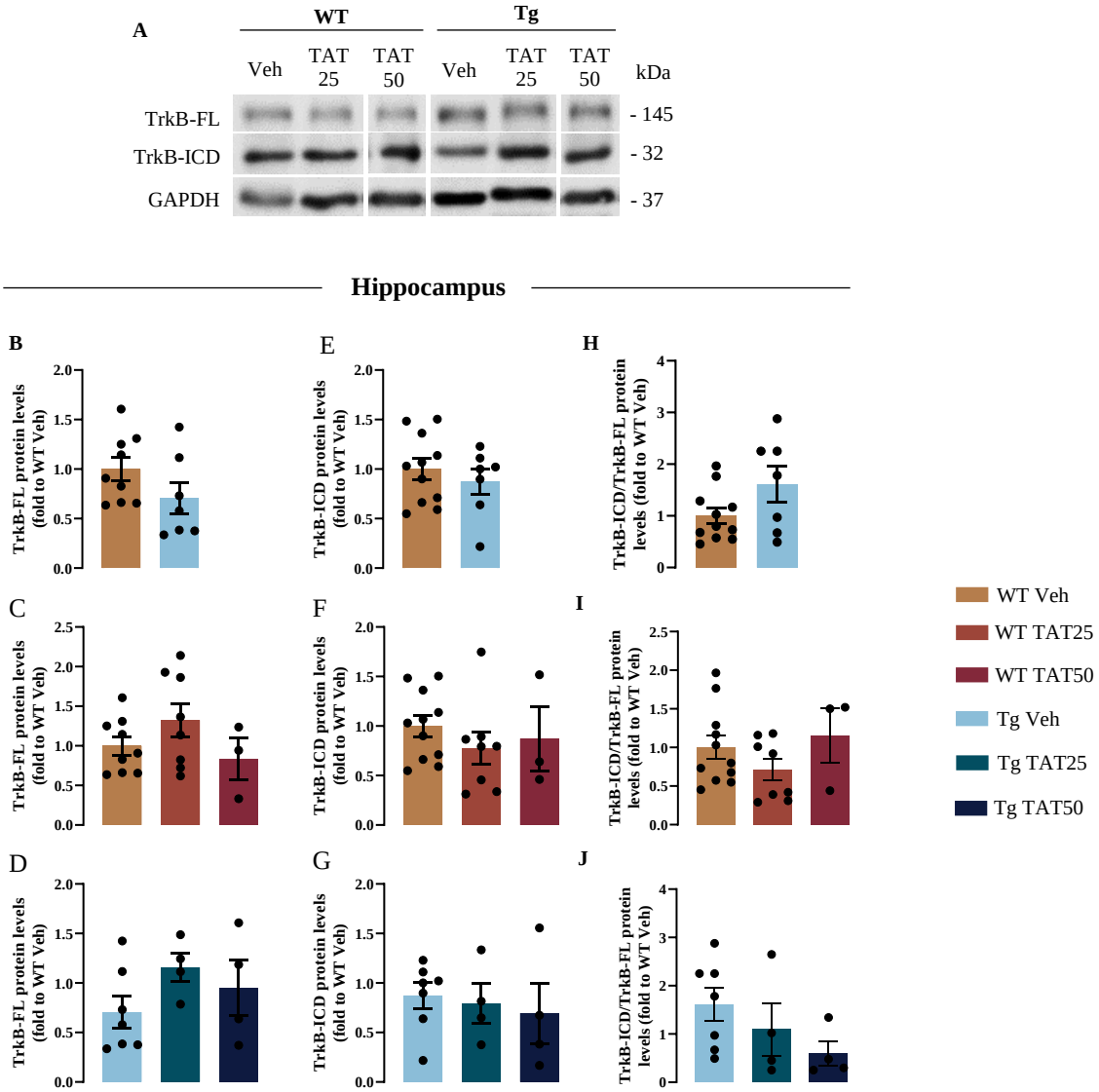

Figure 4. 12 - TrkB-FL and TrkB-ICD protein levels in hippocampal samples of TAT-TrkB-treated 5xFAD mice.

After two months of Veh and TAT-TrkB i.p. injections, control and 5xFAD mice were sacrificed and their hippocampus and cortex used to perform protein analysis. **A.** Representative western-blots of hippocampal samples from TAT-TrkB-treated and non-treated WT and Tg mice. Probing with anti-Trk C-terminal tail (C-14). GAPDH was used as the internal control. **B-G.** Analysis of band intensities represented in **A** from densitometry quantification of TrkB-ICD and TrkB-FL immunoreactivity. Data normalized at WT Veh and represented as mean±SEM. **B, E, H.** Assessment of TrkB-FL and TrkB-ICD levels and TrkB-ICD/TrkB-FL ration within each phenotype (*p*-value>0.05, unpaired *t*-student test, n=7-11 animals per group). **C, F, I.** Assessment of TrkB-FL and TrkB-ICD levels and TrkB-ICD/TrkB-FL ration in WT mice upon treatment with TAT-TrkB (*p*-value>0.05, One-way ANOVA, followed by Tukey's post-test, n=3-11 animals per group). **D, G, J.** Assessment of TrkB-FL and TrkB-ICD levels and TrkB-ICD/TrkB-FL in Tg mice upon treatment with TAT-TrkB (*p*-value>0.05, One-way ANOVA, followed by Tukey's post-test, n=4-7 animals per group). All data represented as mean±SEM. GAPDH - Glyceraldehyde 3-phosphate dehydrogenase; TAT25 - TAT-TrkB 25 mg/kg ; TAT50 – TAT-TrkB 50 mg/kg; TAT-TrkB – peptide capable in preventing TrkB-FL cleavage; TrkB-FL – full-length tropomyosin-related kinase B; TrkB-ICD - TrkB-intracellular domain (calpain-generated); WT – wild-type; Tg – transgenic; Veh – sodium chloride (NaCl) injection;

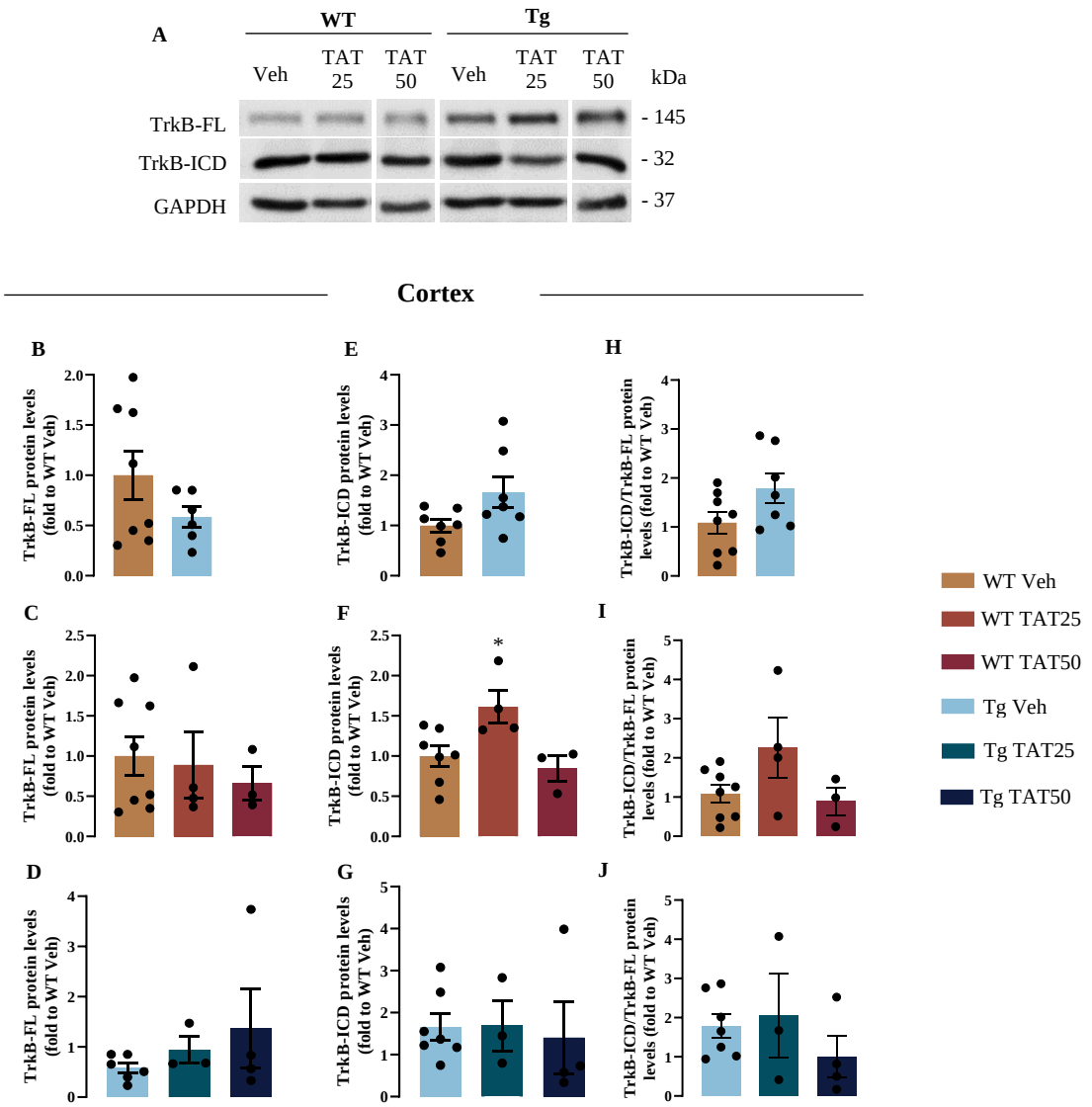

Figure 4. 13 - TrkB-FL and TrkB-ICD protein levels in cortical samples of TAT-TrkB-treated 5xFAD mice.

After two months of Veh and TAT-TrkB i.p. injections, control and 5xFAD mice were sacrificed and their hippocampus and cortex used to perform protein analysis. **A.** Representative western-blots of cortical samples from TAT-TrkB-treated and non-treated WT and Tg mice. Probing with anti-Trk C-terminal tail (C-14). GAPDH was used as the internal control. **B-G.** Analysis of band intensities represented in **A** from densitometry quantification of TrkB-ICD and TrkB-FL immunoreactivity. Data normalized at WT Veh and represented as mean±SEM. **B, E, H.** Assessment of TrkB-FL and TrkB-ICD levels and TrkB-ICD/TrkB-FL ration within each phenotype (*p*-value>0.05, unpaired *t*-student test, n=6-7 animals per group). **C, F, I.** Assessment of TrkB-FL and TrkB-ICD levels and TrkB-ICD/TrkB-FL ration in WT mice upon treatment with TAT-TrkB (*p*-value>0.05, **p*-value<0.05, One-way ANOVA, followed by Tukey's post-test, n=3-8 animals per group). **D, G, J.** Assessment of TrkB-FL and TrkB-ICD levels and TrkB-ICD/TrkB-FL in Tg mice upon treatment with TAT-TrkB (*p*-value>0.05, One-way ANOVA, followed by Tukey's post-test, n=3-7 animals per group). All data represented as mean±SEM. GAPDH - Glyceraldehyde 3-phosphate dehydrogenase; TAT25 - TAT-TrkB 25 mg/kg ; TAT50 – TAT-TrkB 50 mg/kg; TAT-TrkB – peptide capable in preventing TrkB-FL cleavage; TrkB-FL – full-length tropomyosin-related kinase B; TrkB-ICD - TrkB-intracellular domain (calpain-generated); WT – wild-type; Tg – transgenic; Veh – sodium chloride (NaCl) injection;

4.2.3 Discussion

The present work tested for the first time the use of a TAT-TrkB in an *in vivo* set using an AD mouse model. Results obtained upon treatment with two doses of TAT-TrkB showed no behavioural observable differences when comparing in-between WT and Tg mice. Moreover, TrkB-FL and TrkB-ICD protein levels and TrkB-ICD/TrkB-FL ratio were not altered in its majority, within both experimental groups.

As mentioned earlier, our lab designed and developed a small peptide, TAT-TrkB, which is capable in preventing to a degree, the cleavage of TrkB-ICD full receptor. This data has already been described by Fonseca-Gomes, when Aβ-mediated TrkB-FL receptor cleavage was assessed in primary cortical neurons upon TAT-TrkB incubation[117]. Moreover, TrkB-FL and TrkB-ICD protein levels have already also been assessed in rat brain cortex homogenates, showing in both cases a rescue of TrkB-FL and a decrease formation of TrkB-ICD[117].

In this work, we used an AD mouse model, capable of displaying some of the pathological and behavioural-like features of AD. 5xFAD are C57BL/6J-genetic background mice with a total of five mutations in the *APP* and *PSEN1* genes, which as mentioned earlier, are two *loci* known to be mutated in familial AD[82,260]. As such, following the ageing of these animal, specific histopathological hallmarks, alongside behavioural changes begin to appear overtime. Importantly, it is described the appearance of extracellular Aβ plaques in both the hippocampus and cortex within the first 2 months[260]. In a parallel work, our lab was able to confirm the presence of Aβ deposits by WB in both hippocampal and cortical samples, but also by immunohistochemistry of hippocampal slices, corroborating the described Aβ-driven pathology[261].

Given the absence of knowledge regarding the pharmacokinetic profile of TAT-TrkB, the chosen doses reflect those found in the literature for other pharmacological treatments with TAT used in mice, particularly in AD research[262].

Accordingly, 5.5 m.o. Veh- and TAT-TrkB-treated animals were submitted to several behavioural tests, assessing for the efficacy of the peptide. When submitted to the MWM test, WT and Tg Veh-treated mice displayed different behaviours in learning the position of the platform, given by their different latency times. It has been reported that Tg 5xFAD 6-m.o. mice display an impaired spatial memory and learning[263]. As expected, a faster learning in both the 2nd and 3rd training days was observed in WT mice when compared to Tg animals. Interestingly, at the 4th day, the performance of Tg mice was of no statistical difference to that of WT animals. Moreover, WT Veh- and TAT-TrkB-treated mice showed no significant differences among them. Similarly, Tg

Veh- and TAT-TrkB-treated mice also did not show any differences, albeit a small time decrease can be seen in Tg mice treated with TAT25, implying for a possible learning rescue, as TAT25-treated animals presented a learning curve similar to that of WT Veh-treated mice. Notwithstanding, the number of experimental animals must be increased to obtain a more robust data set.

To assess memory and learning integrity, MWM test parameters such as the time that each animal spent on the correct quadrant alongside its platform crossings were also analyzed. Surprisingly and contrary to the literature, no differences were observed when we compared the performance of WT Veh and Tg Veh mice, as according to the literature, Tg mice manifest a decrease in both parameters due to memory impairments[260]. Curiously, there are actually discrepancies regarding memory impairments seen in MWM test, as groups have only reported the occurrence of said impairments in 7 m.o. and older mice, while others describe them appearing in mice young as 1 m.o.[264,265].

As expected, TAT-TrkB-treated WT animals showed no measurable differences in both parameters when compared to WT Veh mice, implying that our compound does not compromise learning and memory. Finally, TAT25-treated Tg mice showed a slight increase in both platform crossings and time spent on the quadrant, yet with no statistical difference relatively to Tg Veh animals. As mentioned above, these mice showed a similar learning curve when compared to WT Veh-treated mice, hinting for a possible learning rescue. Importantly, it must be considered that the MWM test can be stressful to animals due to its nature, environmental and time factors, possibly attenuating differences between experimental groups[266,267]. Moreover, a study also shown that behavioural scores derived from this test may also underlie differences in thigmotaxis performances[268]. Interestingly, it is also known that 5xFAD performance may be also sex-dependent, as female 5xFAD mice exhibit a more pronounce pathology[269]. Again, these studies will need to be remade, increasing the number of animals per group, assessing for all parameters at both 30 and 60s and differentiate the data according to their sex. Studies show that parameters assessed with prolonged time lengths may mask and attenuate small behavioural differences, as mice with a non-compromised memory may abandon the vacated quadrant and explore different areas after a certain time period, as they were unable to find the platform[270]. To ensure that the duration of the test does not bias animal performance, the parameters may be analyzed within the first 30s instead.

To evaluate anxiety-like behaviour, animals were also submitted to an EPM test, assessing paraments such as the number of entries and time spent on open arms. Understandably, due to the nature of these animals, a higher anxiety is reflected

by lower number of entries and time spent on open arms. Nevertheless, studies describe 3 m.o.-6m.o. 5xFAD animals as having progressive decrease in anxiety[271]. Our data shows no differences in WT Veh against Tg Veh mice. Once again, the lack of corroboration by our data to that of previously described, suggest for a need of optimizing this *in vivo* model in our lab. Furthermore, no differences were observed in WT Veh- against WT TAT-TrkB-treated nor in Tg Veh- versus Tg TAT-TrkB-treated animals. As such, we conclude that this novel compound does not promote anxiogenic nor anxiolytic effects.

Taking into consideration the appearance and accumulation of Aβ, we first started by evaluating if WT and Tg Veh-treated mice presented different levels of both TrkB-FL and TrkB-ICD. Despite not observing significant differences among both groups, a slight decrease in TrkB-FL levels was detected in both hippocampal and cortical samples of Tg animals, as expected. Concomitantly, a small increase in TrkB-ICD levels was only observed in cortical samples of Tg mice. Hippocampal levels of TrkB-ICD showed a similar pattern between WT and Tg animals. This last observation might be due to the loss of neuronal density ratio and thus, loss in TrkB-ICD protein levels. Additionally, we also assessed the TrkB-ICD/TrkB-FL ratio and observed that in both sample types, a higher ratio was seen in Tg animals when compared to WT, indicating that levels of TrkB-ICD were superior to those of TrkB-FL.

Next, we evaluated if the administration of two different TAT-TrkB doses had any impact in both TrkB-FL and TrkB-ICD levels in WT groups. We expected to see no significant differences among experimental groups, as WT animals do not display an overaccumulation of Aβ, which eventually leads to TrkB-FL cleavage. Moreover, an observable difference between conditions would suggest a possible toxic action of the novel compound. Surprisingly, an increase in TrkB-ICD protein levels was observed in cortical WT samples upon treatment with TAT25. Albeit not expecting, this result can be easily justified due to the lack of robust experimental data, as the WT TAT25 group only consisted in a total of 4 animals, creating leverage where discrepancies promote a higher mean shift. As such, this data must be re-assessed in a larger higher experimental group of animals. Nevertheless, the remaining TrkB-FL and TrkB-ICD immunoreactivity assays presented no differences, as anticipated. Importantly, TrkB-ICD/TrkB-FL ratio showed no differences among WT animals, suggesting that the increase of TrkB-ICD in TAT25-treated mice was mainly due to intraspecies variability rather than a higher cleavage of TrkB-FL or a TAT-TrkB-mediated toxicity.

Lastly, we evaluated both protein levels in TAT-treated Tg mice, where an Aβ-mediated TrkB-FL receptor cleavage should be triggered. We would expect to see a

rescue of TrkB-FL levels alongside a decrease in TrkB-ICD. In line with the lack of statistical difference when WT Veh and Tg Veh groups were compared, again, no significant measurable changes were observed in this assay. Nonetheless, the hippocampal TrkB-ICD/TrkB-FL ratio suggests that TAT-TrkB drives for a decrease in TrkB-FL cleavage, as mice treated with this compound showed a decrease in TrkB-ICD formation and/or a rescue of TrkB-FL.

Altogether, although both behavioural and immunoreactivity assays presented an overall lack of statistical difference, the same tests must be performed increasing the number of animals per group. Additionally, it is important to mention that TAT-TrkB administration via i.p. may drive for a loss and dispersion of the active compound when translocated into the brain, thus nullifying its neuroprotective effect. As such, pharmacokinetic studies must be performed in the future to evaluate its biodistribution. Regardless, our preliminary data suggest that TAT-TrkB does not drive cellular toxicity in WT animals and hints for a rescue of learning memory alongside a normalization of TrkB-ICD/TrkB-FL ratio.

5 Final Remarks and Future Perspectives

The work presented in this thesis allowed for further characterization of the cleavage-mediated TrkB-FL fragment, TrkB-ICD. TrkB-ICD vesicle incorporation is a potential candidate for its toxic dissemination in the brain, similarly to other major misfolded proteins. Additionally, it also gave insights and awareness on the use of a small peptide capable in preventing, to a degree, TrkB-FL receptor cleavage. Importantly, it must be mentioned that, albeit this thesis was contextualized in AD, TrkB-FL cleavage and TrkB-ICD formation are also present in other disorders with excitotoxic-related events in an acute and focal basis.

Accordingly, in **Section 4.1**, we were able to describe for the first time the presence of both ICD-V5 and the endogenous TrkB-ICD in EVs. Firstly, we began by successfully validating an overexpressing system through ICD-V5-lentiviral transduction of SH-SY5Y neuroblastoma cells, followed by an optimization of a neuron-like differentiation protocol. Next, we isolated the secretome of transduced SH-SY5Y cells and proceeded to the isolation and characterization of differential ultracentrifuged microvesicles and exosomes, alongside protein analysis of EV-depleted secretome. Altogether, we were able to pinpoint the presence of both ICD-V5 and the endogenous TrkB-ICD within both vesicle types. Moreover, TEM and DLS analysis showed no size nor morphological differences within each vesicle population, implying not only their correct isolation but also that ICD-V5 does not alter their native structure. Additionally, preliminary results also showed a detection of TrkB-ICD in the soluble fraction of the secretome. Together, these results may underlie a possible neuronal secretion mechanism, where the dissemination and transmission of TrkB-ICD-containing vesicles intercellularly may help promoting their toxic propagation. Furthermore, we decided to focus special attention on other elimination pathways that may be involved in the clearance of this fragment, aside from its clearance through vesicle secretion. In accordance with previous studies of our lab, we once again corroborated that TrkB-ICD is a stable fragment, with a half-life of 6 hours in SH-SY5Y neuroblastoma cells. This was followed by trying to understand if both the ALP and UPS had any involvement in the clearance of TrkB-ICD. As of now, no robust conclusions can be withdrawn, as both used inhibitors seemed to present an abnormal pharmacological action. That said, it is known that TrkB-FL and other tyrosine kinase receptors are highly ubiquitinated within their intracellular domain. This post-translation modification has been associated with several cellular processes, namely vesicle trafficking and protein degradation. Together, all data points to a

plausible action of one or both systems in the elimination of TrkB-ICD. Lastly, in **Section 4.2** a preliminary efficacy study of the newly designed TAT-TrkB peptide was conducted. As of now, TAT-TrkB has shown strikingly and promising results in the prevention of TrkB-ICD formation in both primary cortical neurons and rat brain cortical homogenates. Our results suggest a potential rescue of the learning curve in TAT-TrkB-treated mice, corroborated with a decrease in hippocampal TrkB-ICD/TrkB-FL ratio in these same animals. Importantly, it must be highlighted the lack of a robust experimental group for each condition, which alongside animal variability, may have causes for a loss of measurable statistical differences. Like TrkB-ICD clearance studies, these assays will be repeated, in order to increase the robustness of the data and respective conclusions.

Taking into consideration the main results of this work, we will continue to dwell on the study of TrkB-ICD in collaboration with Prof. Dora Brites from Faculdade de Farmácia da Universidade de Lisboa, assessing not only its EV-incorporation, but also their incubation in control neuronal, glial, and mixed cell cultures, thus analysing their potential uptake and toxic effects. Furthermore, TrkB-ICD EV presence will be assessed in primary cortical neurons, tissue and in CSF samples of AD patients. TrkB-ICD levels will be evaluated in EVs upon Aβ treatment, studying if a higher TrkB-FL cleavage translates into increased cargo levels of TrkB-ICD in vesicles. Moreover, studies will be performed to observe if TrkB-ICD drives for a modulation of miRNA levels and their altered presence within secreted EVs. Importantly, TrkB-FL and TrkB-ICD ubiquitination studies will also take place, as ubiquitination is a central modification for both vesicle incorporation and protein degradation. As such, new experiments will be conducted to fully disclose the cellular clearance of TrkB-ICD, including cellular degradation and trafficking in EVs. Finally, new TAT-TrkB efficacy studies will be performed based on data from pharmacokinetic studies regarding its biodistribution to better identify an appropriate dose to be administrated. Altogether, our work strives to deeply study the pathology of AD with special focus in a neurotrophin system which, when compromised, drives for a loss of neuroprotection potentiating Aβ-mediated toxicity. Currently, a therapeutic strategy is also being developed with the mindset of rescuing this neuroprotective system.

6 References

1. Segal, R. A. & Greenberg, M. E. Intracellular signaling pathways activated by neurotrophic factors. *Annu. Rev. Neurosci.* **19**, 463–489 (1996).
2. Maness, L. M. *et al.* The neurotrophins and their receptors: Structure, function, and neuropathology. *Neurosci. Biobehav. Rev.* **18**, 143–159 (1994).
3. Skaper, S. The Biology of Neurotrophins, Signalling Pathways, and Functional Peptide Mimetics of Neurotrophins and their Receptors. *CNS Neurol. Disord. - Drug Targets* **7**, 46–62 (2008).
4. Kerschensteiner, M., Stadelmann, C., Dechant, G., Wekerle, H. & Hohlfeld, R. Neurotrophic cross-talk between the nervous and immune systems: Implications for neurological diseases. *Ann. Neurol.* **53**, 292–304 (2003).
5. Baloh, R. H., Enomoto, H., Johnson, E. M. & Milbrandt, J. The GDNF family ligands and receptors - Implications for neural development. *Curr. Opin. Neurobiol.* **10**, 103–110 (2000).
6. Ip, N. The neurotrophins and neuropoietic cytokines: two families of growth factors acting on neural and hematopoieticcells. *Ann N Y Acad Sci* **840**, 97–106 (1998).
7. Levi-Montalcini, R. & Cohen, S. In vitro and in vivo effects of a nerve growth factor-stimulating agent isolated from snake venom. *Proc. Natl. Acad. Sci. USA* **42**, 695–699 (1956).
8. Dawbarn, D. & Allen, S. J. Neurotrophins and neurodegeneration. *Neuropathol. Appl. Neurobiol.* **29**, 211–230 (2003).
9. Autry, A. E. & Monteggia, L. M. Brain-Derived Neurotrophic Factor and Neuropsychiatric Disorders. *Pharmacol. Rev.* **64**, 238–258 (2012).
10. Miranda-Lourenço, C. *et al.* Challenges of BDNF-based therapies: From common to rare diseases. *Pharmacol. Res.* **162**, 105281 (2020).
11. Levi-Montalcini, R. The nerve growth factor: Thirty-five years later. *Vitr. Cell. Dev. Biol.* **23**, 227–238 (1987).
12. Barde, Y. A., Edgar, D. & Thoenen, H. Purification of a new neurotrophic factor from mammalian brain. *EMBO J.* **1**, 549–553 (1982).
13. Hohn, A., Leibrock, J., Bailey, K. & Barde, Y. A. Identification and characterization of a novel member of the nerve growth factor/brain-derived neurotrophic factor family. *Nature* **344**, 339–341 (1990).
14. Maisonpierre, P. C. *et al.* Neurotrophin-3: a Neurotrophic Factor Related to NGF and BDNF. *Science (80-.).* **247**, 1446–1451 (1990).
15. Hallböök, F., Ibáñez, C. F. & Persson, H. Evolutionary studies of the nerve growth factor family reveal a novel member abundantly expressed in Xenopus ovary.

Neuron **6**, 845–858 (1991).

16. Götz, R. *et al.* Neurotrophin-6 is a new member of the nerve growth factor family. *Nature* **372**, 266–269 (1994).
17. Nilsson, A. S., Fainzilber, M., Falck, P. & Ibáñez, C. F. Neurotrophin-7: A novel member of the neurotrophin family from the zebrafish. *FEBS Lett.* **424**, 285–290 (1998).
18. Lai, K. O., Fu, W. Y., Ip, F. C. F. & Ip, N. Y. Cloning and expression of a novel neurotrophin, NT-7, from carp. *Mol. Cell. Neurosci.* **11**, 64–76 (1998).
19. Lessmann, V., Gottmann, K. & Malcangio, M. Neurotrophin secretion: current facts and future prospects. *Prog. Neurobiol.* **69**, 341–374 (2003).
20. Mowla, S. J. *et al.* Differential sorting of nerve growth factor and brain-derived neurotrophic factor in hippocampal neurons. *J. Neurosci.* **19**, 2069–2080 (1999).
21. Al-Qudah, M. A. & Al-Dwairi, A. Mechanisms and regulation of neurotrophin synthesis and secretion. *Neurosciences* **21**, 306–313 (2016).
22. Dechant, G. & Barde, Y. A. Signalling through the neurotrophin receptor p75(NTR). *Curr. Opin. Neurobiol.* **7**, 413–418 (1997).
23. Heymach, J. V. & Shooter, E. M. The biosynthesis of neurotrophin heterodimers by transfected mammalian cells. *J. Biol. Chem.* **270**, 12297–12304 (1995).
24. Arakawa, T. *et al.* Formation of heterodimers from three neurotrophins, nerve growth factor, neurotrophin-3, and brain-derived neurotrophic factor. *J. Biol. Chem.* **269**, 27833–27839 (1994).
25. Miranda, M., Morici, J. F., Zanoni, M. B. & Bekinschtein, P. Brain-Derived Neurotrophic Factor: A Key Molecule for Memory in the Healthy and the Pathological Brain. *Front. Cell. Neurosci.* **13**, 1–25 (2019).
26. Binder, D. K. & Scharfman, H. E. Brain-derived neurotrophic factor. *Growth Factors* **22**, 123–131 (2004).
27. Oliff, H. S., Berchtold, N. C., Isackson, P. & Cotman, C. W. Exercise-induced regulation of brain-derived neurotrophic factor (BDNF) transcripts in the rat hippocampus. *Mol. Brain Res.* **61**, 147–153 (1998).
28. Seidah, N. G., Benjannet, S., Pareek, S., Chrétien, M. & Murphy, R. A. Cellular processing of the neurotrophin precursors of NT3 and BDNF by the mammalian proprotein convertases. *FEBS Lett.* **379**, 247–250 (1996).
29. Pang, P. T. *et al.* Cleavage of proBDNF by tPA/plasmin is essential for long-term hippocampal plasticity. *Science (80-.).* **306**, 487–491 (2004).
30. Mizoguchi, H. *et al.* Matrix metalloproteinase-9 contributes to kindled seizure development in pentylenetetrazole-treated mice by converting pro-BDNF to mature BDNF in the hippocampus. *J. Neurosci.* **31**, 12963–12971 (2011).
31. Brigadski, T. & Leßmann, V. The physiology of regulated BDNF release. *Cell Tissue Res.* **382**, 15–45 (2020).

32. Saha, R. N., Liu, X. & Pahan, K. Up-regulation of BDNF in astrocytes by TNF-α: A case for the neuroprotective role of cytokine. *J. Neuroimmune Pharmacol.* **1**, 212–222 (2006).
33. Nakajima, K. *et al.* Neurotrophin secretion from cultured microglia. *J. Neurosci. Res.* **65**, 322–331 (2001).
34. Roux, P. P. & Barker, P. A. Neurotrophin signaling through the p75 neurotrophin receptor. *Prog. Neurobiol.* **67**, 203–233 (2002).
35. Barker, P. A. p75NTR is positively promiscuous: Novel partners and new insights. *Neuron* **42**, 529–533 (2004).
36. Chao, M. V. Neurotrophins and their receptors: A convergence point for many signalling pathways. *Nat. Rev. Neurosci.* **4**, 299–309 (2003).
37. Shelton, D. L. *et al.* Human trks: Molecular Cloning, Tissue Distribution, and Expression of Extracellular Domain Immunoadhesins. *J. Neurosci.* **15**, 477–491 (1995).
38. Middlemas, D. S., Lindberg, R. A. & Hunter, T. trkB, a Neural Receptor Protein-Tyrosine Kinase: Evidence for a Full-Length and Two Truncated Receptors. *Mol. Cell. Biol.* **11**, 143–153 (1991).
39. Klein, R., Conway, D., Parada, L. F. & Barbacid, M. The trkB Tyrosine Protein Kinase Gene Codes for a Second Neurogenic Receptor That Lacks the Catalytic Kinase Domain. *Cell* **61**, 647–656 (1990).
40. Stoilov, P., Stamm, S. & Castren, E. Analysis of the human TrkB gene genomic organization reveals novel TrkB isoforms, unusual gene length, and splicing mechanism. *Biochem. Biophys. Res. Commun.* **290**, 1054–1065 (2002).
41. Luberg, K., Wong, J., Weickert, C. S. & Timmusk, T. Human TrkB gene: Novel alternative transcripts, protein isoforms and expression pattern in the prefrontal cerebral cortex during postnatal development. *J. Neurochem.* **113**, 952–964 (2010).
42. Wong, J. & Garner, B. Evidence that truncated TrkB isoform, TrkB-Shc can regulate phosphorylated TrkB protein levels. *Biochem. Biophys. Res. Commun.* **420**, 331–335 (2012).
43. Baxter, G. T. *et al.* Signal transduction mediated by the truncated trkB receptor isoforms, trkB.T1 and trkB.T2. *J. Neurosci.* **17**, 2683–2690 (1997).
44. Haapasalo, A. *et al.* Expression of the naturally occurring truncated trkB neurotrophin receptor induces outgrowth of filopodia and processes in neuroblastoma cells. *Oncogene* **18**, 1285–1296 (1999).
45. Rose, C. R. *et al.* Truncated TrkB-T1 mediates neurotrophin-evoked calcium signalling in glia cells. *Nature* **426**, 74–78 (2003).
46. Eide, F. F. *et al.* Naturally occurring truncated trkB receptors have dominant inhibitory effects on brain-derived neurotrophic factor signaling. *J. Neurosci.* **16**,

3123–3129 (1996).

47. Biffo, S., Offenhäuser, N., Carter, B. D. & Barde, Y. A. Selective binding and internalisation by truncated receptors restrict the availability of BDNF during development. *Development* **121**, 2461–2470 (1995).
48. Haapasalo, A., Koponen, E., Hoppe, E., Wong, G. & Castrén, E. Truncated trkB.T1 is dominant negative inhibitor of trkB.TK+-mediated cell survival. *Biochem. Biophys. Res. Commun.* **280**, 1352–1358 (2001).
49. Minichiello, L. TrkB signalling pathways in LTP and learning. *Nat. Rev. Neurosci.* **10**, 850–860 (2009).
50. Qian, X., Riccio, A., Zhang, Y. & Ginty, D. D. Identification and characterization of novel substrates of Trk receptors in developing neurons. *Neuron* **21**, 1017–1029 (1998).
51. Bonni, A. *et al.* Cell survival promoted by the Ras-MAPK signaling pathway by transcription-dependent and -independent mechanisms. *Science (80-.).* **286**, 1358–1362 (1999).
52. Chen, R. H., Abate, C. & Blenis, J. Phosphorylation of the c-Fos transrepression domain by mitogen-activated protein kinase and 90-kDa ribosomal S6 kinase. *Proc. Natl. Acad. Sci. U. S. A.* **90**, 10952–10956 (1993).
53. Tejeda, G. S. & Díaz-Guerra, M. Integral characterization of defective BDNF/TrkB signalling in neurological and psychiatric disorders leads the way to new therapies. *Int. J. Mol. Sci.* **18**, 1–24 (2017).
54. Minichiello, L. *et al.* Mechanism of TrkB-mediated hippocampal long-term potentiation. *Neuron* **36**, 121–137 (2002).
55. Jerónimo-Santos, A. *et al.* Dysregulation of TrkB Receptors and BDNF function by amyloid-β peptide is mediated by calpain. *Cereb. Cortex* **25**, 3107–3121 (2015).
56. Wook, J. Regulation of BDNF-TrkB Signaling and Potential Therapeutic Strategies for Parkinson's Disease. *J. Clin. Med.* **9**, (2020).
57. Weickert, C. S. *et al.* Reductions in neurotrophin receptor mRNAs in the prefrontal cortex of patients with schizophrenia. *Mol. Psychiatry* **10**, 637–650 (2005).
58. Vidaurre, Ó. *et al.* Imbalance of neurotrophin receptor isoforms TrkB-FL/TrkB-T1 induces neuronal death in excitotoxicity. *Cell Death Dis.* **3**, 1–12 (2012).
59. Fonseca-Gomes, J. *et al.* TrkB-ICD fragment, originating from BDNF receptor cleavage, is translocated to cell nucleus and phosphorylates nuclear and axonal proteins. *Front. Mol. Neurosci.* **12**, 4 (2019).
60. Eftekharzadeh, B., Hyman, B. T. & Wegmann, S. Structural studies on the mechanism of protein aggregation in age related neurodegenerative diseases. *Mech. Ageing Dev.* **156**, 1–13 (2016).
61. De Filippis, L. & Binda, E. Concise Review: Self-Renewal in the Central Nervous

System: Neural Stem Cells from Embryo to Adult. *STtem CellsTranslational Med.* **1**, 298–308 (2012).

62. Huang, Y. & Mucke, L. Alzheimer mechanisms and therapeutic strategies. *Cell* **148**, 1204–1222 (2012).
63. Alzheimer, A. Über eine eigenartige Erkrankung der Hirnrinde. *Allg. Zeitschrift für Psychiatr. und Psych. Medizin* **64**, 146–148 (1907).
64. AD Association. 2012 Alzheimer's disease facts and figures. *Alzheimer's Dement.* **8**, 131–168 (2012).
65. Chen, X. Q. & Mobley, W. C. Exploring the pathogenesis of Alzheimer disease in basal forebrain cholinergic neurons: Converging insights from alternative hypotheses. *Front. Neurosci.* **13**, 1–18 (2019).
66. Weller, J. & Budson, A. Current understanding of Alzheimer's disease diagnosis and treatment. *F1000Research* **7**, 1–9 (2018).
67. Raskin, J., Cummings, J., Hardy, J., Schuh, K. & Dean, R. Neurobiology of Alzheimer's Disease: Integrated Molecular, Physiological, Anatomical, Biomarker, and Cognitive Dimensions. *Curr. Alzheimer Res.* **12**, 712–722 (2015).
68. Blennow, K. & Zetterberg, H. Biomarkers for Alzheimer's disease: current status and prospects for the future. *J. Intern. Med.* **284**, 643–663 (2018).
69. Villemagne, V. L. *et al.* Amyloid β deposition, neurodegeneration, and cognitive decline in sporadic Alzheimer's disease: A prospective cohort study. *Lancet Neurol.* **12**, 357–367 (2013).
70. Reiman, E. M. *et al.* Brain imaging and fluid biomarker analysis in young adults at genetic risk for autosomal dominant Alzheimer's disease in the presenilin 1 E280A kindred: A case-control study. *Lancet Neurol.* **11**, 1048–1056 (2012).
71. Massoud, F. & Léger, G. C. Pharmacological treatment of Alzheimer disease. *Can. J. Psychiatry* **56**, 579–588 (2011).
72. Seltzer, B. Donepezil: an update. *Expert Opin Pharmacother* **8**, 1011–1023 (2007).
73. Birks, J. & Harvey, R. Donepezil for dementia due to Alzheimer's disease. *Cochrane Database Syst. Rev.* **CD001190**, (2006).
74. Onor, M. L., Trevisiol, M. & Aguglia, E. Rivastigmine in the treatment of Alzheimer's disease: an update. *Clin. Interv. Aging* **2**, 17–32 (2007).
75. J, B., J, G. E., Birks, J. S. & Evans, J. G. Rivastigmine for Alzheimer's disease. *Cochrane Database Syst. Rev.* **CD001191**, (2009).
76. Robinson, D. M. & Plosker, G. L. Galantamine extended release in Alzheimer's disease: profile report. *Drugs Aging* **23**, 839–842 (2006).
77. Loy, C. & Schneider, L. Galantamine for Alzheimer's disease and mild cognitive impairment. *Cochrane Database Syst. Rev.* (2006). doi:10.1002/14651858.cd001747.pub3
78. Kavirajan, H. Memantine: A comprehensive review of safety and efficacy. *Expert*

Opin. Drug Saf. **8**, 89–109 (2009).

79. Tariot, P. N., Farlow, M. R., Grossberg, G. T., Graham, S. M. & Mcdonald, S. Memantine Treatment in Patients With Moderate to Severe Alzheimer Disease Already Received Donepezil. *J. Am. Med. Assoc.* **291**, 317–324 (2004).
80. Zucchella, C. *et al.* The Multidisciplinary Approach to Alzheimer's Disease and Dementia. A Narrative Review of Non-Pharmacological Treatment. *Front. Neurol.* **9**, 1–22 (2018).
81. Cummings, J., Lee, G., Ritter, A., Sabbagh, M. & Zhong, K. Alzheimer's disease drug development pipeline: 2020. *Alzheimer's Dement. Transl. Res. Clin. Interv.* **6**, 1–29 (2020).
82. Association, A. 2020 Alzheimer's disease facts and figures. *Alzheimer's Dement.* **16**, 391–460 (2020).
83. Swerdlow, R. H. Pathogenesis of Alzheimer's disease. *Clin. Interv. Aging* **2**, 347–359 (2007).
84. Lue, L. F. *et al.* Soluble amyloid β peptide concentration as a predictor of synaptic change in Alzheimer's disease. *Am. J. Pathol.* **155**, 853–862 (1999).
85. DaRocha-Souto, B. *et al.* Brain oligomeric β-amyloid but not total amyloid plaque burden correlates with neuronal loss and astrocyte inflammatory response in amyloid precursor protein/tau transgenic mice. *J. Neuropathol. Exp. Neurol.* **70**, 360–376 (2011).
86. Mokhtar, S. H., Bakhuraysah, M. M., Cram, D. S. & Petratos, S. The beta-amyloid protein of alzheimer's disease: Communication breakdown by modifying the neuronal cytoskeleton. *Int. J. Alzheimers. Dis.* **2013**, (2013).
87. Chen, G. F. *et al.* Amyloid beta: Structure, biology and structure-based therapeutic development. *Acta Pharmacol. Sin.* **38**, 1205–1235 (2017).
88. Milward, E. A. *et al.* The amyloid protein precursor of Alzheimer's disease is a mediator of the effects of nerve growth factor on neurite outgrowth. *Neuron* **9**, 129–137 (1992).
89. Breen, K. C., Bruce, M. & Anderton, B. H. Beta amyloid precursor protein mediates neuronal cell-cell and cell-surface adhesion. *J. Neurosci. Res.* **28**, 90–100 (1991).
90. Wei, W., Norton, D. D., Wang, X. & Kusiak, J. W. Aβ 17-42 in Alzheimer's disease activates JNK and caspase-8 leading to neuronal apoptosis. *Brain* **125**, 2036–2043 (2002).
91. Mucke, L., Masliah, E., Yu, G., Mallory, M. & Rockenstein, E. High-Level Neuronal Expression of Aβ1–42 in Wild-Type Human Amyloid Protein Precursos Transgenic Mice: Synaptotoxicity without Plaque Formation.pdf. *J Neurosci* **20**, 4050–8 (2000).
92. Ma, Y. L., Wang, H. L., Wu, H. C., Wei, C. L. & Lee, E. H. Y. Brain-derived

neurotrophic factor antisense oligonucleotide impairs memory retention and inhibits long-term potentiation in rats. *Neuroscience* **82**, 957–967 (1997).

93. Korte, M. *et al.* Hippocampal long-term potentiation is impaired in mice lacking brain-derived neurotrophic factor. *Proc. Natl. Acad. Sci. U. S. A.* **92**, 8856–8860 (1995).
94. Korte, M. *et al.* Virus-mediated gene transfer into hippocampal CA1 region restores long-term potentiation in brain-derived neurotrophic factor mutant mice. *Proc. Natl. Acad. Sci. U. S. A.* **93**, 12547–12552 (1996).
95. Linnarsson, S., Björklund, A. & Ernfors, P. Learning deficit in BDNF mutant mice. *Eur. J. Neurosci.* **9**, 2581–2587 (1997).
96. Martínez, A. *et al.* TrkB and TrkC signaling are required for maturation and synaptogenesis of hippocampal connections. *J. Neurosci.* **18**, 7336–7350 (1998).
97. Minichiello, L. *et al.* Essential Role for TrkB Receptors in Hippocampus-Mediated Learning below a certain threshold before behavioral defects become apparent. *Neuron* **24**, 401–414 (1999).
98. Saarelainen, T. *et al.* Transgenic mice overexpressing truncated trkB neurotrophin receptors in neurons have impaired long-term spatial memory but normal hippocampal LTP. *Synapse* **38**, 102–104 (2000).
99. Allen, S. J., Watson, J. J. & Dawbarn, D. The Neurotrophins and Their Role in Alzheimer's Disease. *Curr. Neuropharmacol.* **9**, 559–573 (2011).
100. Arancio, O. & Chao, M. V. Neurotrophins, synaptic plasticity and dementia. *Curr. Opin. Neurobiol.* **17**, 325–330 (2007).
101. Salehi, A., Verhaagen, J., Dijkhuizen, P. A. & Swaab, D. F. Co-localization of high-affinity neurotrophin receptors in nucleus basalis of Meynert neurons and their differential reduction in Alzheimer's disease. *Neuroscience* **75**, 373–387 (1996).
102. Jiao, S. S. *et al.* Brain-derived neurotrophic factor protects against tau-related neurodegeneration of Alzheimer's disease. *Transl. Psychiatry* **6**, (2016).
103. Elliott, E., Atlas, R., Lange, A. & Ginzburg, I. Brain-derived neurotrophic factor induces a rapid dephosphorylation of tau protein through a PI-3Kinase signalling mechanism. *Eur. J. Neurosci.* **22**, 1081–1089 (2005).
104. Allen, S. J., Wilcock, G. K. & Dawbarn, D. Profound and selective loss of catalytic TrkB immunoreactivity in Alzheimer's disease. *Biochem. Biophys. Res. Commun.* **264**, 648–651 (1999).
105. Connor, B. *et al.* Trk receptor alterations in Alzheimer's disease. *Mol. Brain Res.* **42**, 1–17 (1996).
106. Ferrer, I. *et al.* BDNF and full-length and truncated TrkB expression in Alzheimer disease. Implications in therapeutic strategies. *J Neuropathol Exp Neurol* **58**, 729–739 (1999).
107. Chakravarthy, B. *et al.* Hippocampal membrane-associated p75ntr levels are

increased in alzheimer's Disease. *J. Alzheimer's Dis.* **30**, 675–684 (2012).

108. Nagahara, A. H. *et al.* Neuroprotective effects of brain-derived neurotrophic factor in rodent and primate models of Alzheimer's disease. *Nat. Med.* **15**, 331–337 (2009).
109. Rohe, M. *et al.* Brain-derived neurotrophic factor reduces amyloidogenic processing through control of SORLA gene expression. *J. Neurosci.* **29**, 15472–15478 (2009).
110. Matrone, C., Ciotti, M. T., Mercanti, D., Marolda, R. & Calissano, P. NGF and BDNF signaling control amyloidogenic route and Aβ production in hippocampal neurons. *Proc. Natl. Acad. Sci. U. S. A.* **105**, 13139–13144 (2008).
111. Marvanová, M. *et al.* The neuroprotective agent memantine induces brain-derived neurotrophic factor and trkB receptor expression in rat brain. *Mol. Cell. Neurosci.* **18**, 247–258 (2001).
112. Tanqueiro, S. R. *et al.* Inhibition of NMDA receptors prevents the loss of BDNF function induced by amyloid β. *Front. Pharmacol.* **9**, 1–14 (2018).
113. Ferreira, A. Calpain Dysregulation in Alzheimer's Disease. *ISRN Biochem.* **2012**, 1–12 (2012).
114. Vaisid, T., Kosower, N. S., Katzav, A., Chapman, J. & Barnoy, S. Calpastatin levels affect calpain activation and calpain proteolytic activity in APP transgenic mouse model of Alzheimer's disease. *Neurochem. Int.* **51**, 391–397 (2007).
115. Lee, M. S. *et al.* Neurotoxicity induces cleavage of p35 to p25 by calpain. *Nature* **405**, 360–364 (2000).
116. Garg, S., Timm, T., Mandelkow, E. M., Mandelkow, E. & Wang, Y. Cleavage of Tau by calpain in Alzheimer's disease: The quest for the toxic 17 kD fragment. *Neurobiol. Aging* **32**, 1–14 (2011).
117. Fonseca-Gomes, J. BDNF receptor cleavage: relevance for Alzheimer's disease pathophysiology. (PhD thesis, Faculdade de Medicina, Universidade de Lisboa, Lisboa, 2020).
118. de Almeida-Borlido, C. Searching for a new biomarker for Alzheimer's Disease based on BDNF receptor cleavage. (MSc thesis, Faculdade de Ciências, Universidade de Lisboa, 2020).
119. Wadia, J. S. & Dowdy, S. F. Transmembrane delivery of protein and peptide drugs by TAT-mediated transduction in the treatment of cancer. *Adv. Drug Deliv. Rev.* **57**, 579–596 (2005).
120. Clausen, L. *et al. Protein stability and degradation in health and disease*. *Advances in Protein Chemistry and Structural Biology* **114**, (Elsevier Inc., 2019).
121. Vilchez, D., Saez, I. & Dillin, A. The role of protein clearance mechanisms in organismal ageing and age-related diseases. *Nat. Commun.* **5**, (2014).
122. Hendrick, J. P. & Hartl, F. U. The role of molecular chaperones in protein folding.

FASEB J. **9**, 1559–1569 (1995).

123. Pinet, S. *et al.* TrkB-containing exosomes promote the transfer of glioblastoma aggressiveness to YKL-40-inactivated glioblastoma cells. *Oncotarget* **7**, 50349–50364 (2016).
124. Sardar Sinha, M. *et al.* Alzheimer's disease pathology propagation by exosomes containing toxic amyloid-beta oligomers. *Acta Neuropathol.* **136**, 41–56 (2018).
125. Brites, D. & Fernandes, A. Neuroinflammation and depression: Microglia activation, extracellular microvesicles and microRNA dysregulation. *Front. Cell. Neurosci.* **9**, 1–20 (2015).
126. Saeedi, S., Israel, S., Nagy, C. & Turecki, G. The emerging role of exosomes in mental disorders. *Transl. Psychiatry* **9**, (2019).
127. Van Niel, G., D'Angelo, G. & Raposo, G. Shedding light on the cell biology of extracellular vesicles. *Nat. Rev. Mol. Cell Biol.* **19**, 213–228 (2018).
128. Johnstone, R. M., Adam, M., Hammond, J. R., Orr, L. & Turbide, C. Vesicle formation during reticulocyte maturation. Association of plasma membrane activities with released vesicles (exosomes). *J. Biol. Chem.* **262**, 9412–9420 (1987).
129. Tjalsma, H., Bolhuis, A., Jongbloed, J. D. H., Bron, S. & van Dijl, J. M. Signal Peptide-Dependent Protein Transport inBacillus subtilis: a Genome-Based Survey of the Secretome. *Microbiol. Mol. Biol. Rev.* **64**, 515–547 (2000).
130. Pinho, A. G., Cibrão, J. R., Silva, N. A., Monteiro, S. & Salgado, A. J. Cell secretome: Basic insights and therapeutic opportunities for CNS disorders. *Pharmaceuticals* **13**, 1–18 (2020).
131. Driscoll, J. & Patel, T. The mesenchymal stem cell secretome as an acellular regenerative therapy for liver disease. *J. Gastroenterol.* **54**, 763–773 (2019).
132. Gnecchi, M. *et al.* Paracrine action accounts for marked protection of ischemic heart by Akt-modified mesenchymal stem cells. *Nat. Med* **11**, 367–368 (2005).
133. Martins, L. F. *et al.* Mesenchymal stem cells secretome-induced axonal outgrowth is mediated by BDNF. *Nat. Sci. Reports* **7**, 1–13 (2017).
134. Salgado, A. J., Reis, R. L., Sousa1, N. & Gimble, J. M. Adipose Tissue Derived Stem Cells Secretome: Soluble Factors and Their Roles in Regenerative Medicine. *Curr. Stem Cell Res. Ther.* **5**, 103–110 (2010).
135. Doyle, L. & Wang, M. Overview of Extracellular Vesicles, Their Origin, Composition, Purpose, and Methods for Exosome Isolation and Analysis. *Cells* **8**, 727 (2019).
136. Théry, C. *et al.* Minimal information for studies of extracellular vesicles 2018 (MISEV2018): a position statement of the International Society for Extracellular Vesicles and update of the MISEV2014 guidelines. *J. Extracell. Vesicles* **7**, (2018).
137. Cai, H., Reinisch, K. & Ferro-Novick, S. Coats, Tethers, Rabs, and SNAREs Work Together to Mediate the Intracellular Destination of a Transport Vesicle. *Dev.*

Cell **12**, 671–682 (2007).

138. Muralidharan-Chari, V., Clancy, J. W., Sedgwick, A. & D'Souza-Schorey, C. Microvesicles: Mediators of extracellular communication during cancer progression. *J. Cell Sci.* **123**, 1603–1611 (2010).
139. Nabhan, J. F., Hu, R., Oh, R. S., Cohen, S. N. & Lu, Q. Formation and release of arrestin domain-containing protein 1-mediated microvesicles (ARMMs) at plasma membrane by recruitment of TSG101 protein. *Proc. Natl. Acad. Sci. U. S. A.* **109**, 4146–4151 (2012).
140. Balakrishnan, A., Roy, S., Fleming, T., Leong, H. S. & Schuurmans, C. The emerging role of extracellular vesicles in the glioma microenvironment: Biogenesis and clinical relevance. *Cancers (Basel).* **12**, 1–25 (2020).
141. Tricarico, C., Clancy, J. & D'Souza-Schorey, C. Biology and biogenesis of shed microvesicles. *Small GTPases* **8**, 220–232 (2017).
142. Alvarez-Erviti, L. *et al.* Lysosomal dysfunction increases exosome-mediated alpha-synuclein release and transmission. *Neurobiol. Dis.* **42**, 360–367 (2011).
143. Hurley, J. H. ESCRT complexes and the biogenesis of multivesicular bodies. *Curr. Opin. Cell Biol.* **20**, 4–11 (2008).
144. Stuffers, S., Sem Wegner, C., Stenmark, H. & Brech, A. Multivesicular endosome biogenesis in the absence of ESCRTs. *Traffic* **10**, 925–937 (2009).
145. van Niel, G. *et al.* The Tetraspanin CD63 Regulates ESCRT-Independent and -Dependent Endosomal Sorting during Melanogenesis. *Dev. Cell* **21**, 708–721 (2011).
146. Colombo, M. *et al.* Analysis of ESCRT functions in exosome biogenesis, composition and secretion highlights the heterogeneity of extracellular vesicles. *J. Cell Sci.* **126**, 5553–5565 (2013).
147. Goñi, F. M. & Alonso, A. Effects of ceramide and other simple sphingolipids on membrane lateral structure. *Biochim. Biophys. Acta - Biomembr.* **1788**, 169–177 (2009).
148. Kajimoto, T., Okada, T., Miya, S., Zhang, L. & Nakamura, S. I. Ongoing activation of sphingosine 1-phosphate receptors mediates maturation of exosomal multivesicular endosomes. *Nat. Commun.* **4**, (2013).
149. Buschow, S. I., Liefhebber, J. M. P., Wubbolts, R. & Stoorvogel, W. Exosomes contain ubiquitinated proteins. *Blood Cells, Mol. Dis.* **35**, 398–403 (2005).
150. Booth, A. M. *et al.* Exosomes and HIV Gag bud from endosome-like domains of the T cell plasma membrane. *J. Cell Biol.* **172**, 923–935 (2006).
151. D'Souza-Schorey Crislyn, C. & Clancy, J. W. Tumor-derived microvesicles: Shedding light on novel microenvironment modulators and prospective cancer biomarkers. *Genes Dev.* **26**, 1287–1299 (2012).
152. Schlienger, S., Campbell, S. & Claing, A. ARF1 regulates the Rho/MLC pathway to

control EGF-dependent breast cancer cell invasion. *Mol. Biol. Cell* **25**, 17–29 (2014).

153. Muralidharan-Chari, V. *et al.* ARF6-Regulated Shedding of Tumor Cell-Derived Plasma Membrane Microvesicles. *Curr. Biol.* **19**, 1875–1885 (2009).
154. Bianco, F. *et al.* Acid sphingomyelinase activity triggers microparticle release from glial cells. *EMBO J.* **28**, 1043–1054 (2009).
155. Hsu, C. *et al.* Regulation of exosome secretion by Rab35 and its GTPase-activating proteins TBC1D10A-C. *J. Cell Biol.* **189**, 223–232 (2010).
156. Jahn, R. & Scheller, R. H. SNAREs - Engines for membrane fusion. *Nat. Rev. Mol. Cell Biol.* **7**, 631–643 (2006).
157. Mulcahy, L. A., Pink, R. C. & Carter, D. R. F. Routes and mechanisms of extracellular vesicle uptake. *J. Extracell. Vesicles* **3**, (2014).
158. Laulagnier, K. *et al.* Amyloid precursor protein products concentrate in a subset of exosomes specifically endocytosed by neurons. *Cell. Mol. Life Sci.* **75**, 757–773 (2018).
159. Yuyama, K., Sun, H., Mitsutake, S. & Igarashi, Y. Sphingolipid-modulated exosome secretion promotes clearance of amyloid-β by microglia. *J. Biol. Chem.* **287**, 10977–10989 (2012).
160. Fernandes, A. *et al.* Secretome from SH-SY5Y APPSwe cells trigger time-dependent CHME3 microglia activation phenotypes, ultimately leading to miR-21 exosome shuttling. *Biochimie* **155**, 67–82 (2018).
161. Feng, D. *et al.* Cellular internalization of exosomes occurs through phagocytosis. *Traffic* **11**, 675–687 (2010).
162. Nakase, I., Kobayashi, N. B., Takatani-Nakase, T. & Yoshida, T. Active macropinocytosis induction by stimulation of epidermal growth factor receptor and oncogenic Ras expression potentiates cellular uptake efficacy of exosomes. *Sci. Rep.* **5**, 1–14 (2015).
163. Tian, T. *et al.* Exosome uptake through clathrin-mediated endocytosis and macropinocytosis and mediating miR-21 delivery. *J. Biol. Chem.* **289**, 22258–22267 (2014).
164. Coleman, B. M. & Hill, A. F. Extracellular vesicles - Their role in the packaging and spread of misfolded proteins associated with neurodegenerative diseases. *Semin. Cell Dev. Biol.* **40**, 89–96 (2015).
165. Valadi, H. *et al.* Exosome-mediated transfer of mRNAs and microRNAs is a novel mechanism of genetic exchange between cells. *Nat. Cell Biol.* **9**, 654–659 (2007).
166. Bissig, C. & Gruenberg, J. ALIX and the multivesicular endosome: ALIX in Wonderland. *Trends Cell Biol.* **24**, 19–25 (2014).
167. Fauré, J. *et al.* Exosomes are released by cultured cortical neurones. *Mol. Cell. Neurosci.* **31**, 642–648 (2006).

168. Krämer-Albers, E. M. *et al.* Oligodendrocytes secrete exosomes containing major myelin and stress-protective proteins: Trophic support for axons? *Proteomics - Clin. Appl.* **1**, 1446–1461 (2007).
169. Lachenal, G. *et al.* Release of exosomes from differentiated neurons and its regulation by synaptic glutamatergic activity. *Mol. Cell. Neurosci.* **46**, 409–418 (2011).
170. Soria, F. N. *et al.* Exosomes, an unmasked culprit in neurodegenerative diseases. *Front. Neurosci.* **11**, 1–12 (2017).
171. Rajendran, L. *et al.* Alzheimer's disease β-amyloid peptides are released in association with exosomes. *Proc. Natl. Acad. Sci. U. S. A.* **103**, 11172–11177 (2006).
172. Sharples, R. A. *et al.* Inhibition of γ-secretase causes increased secretion of amyloid precursor protein C-terminal fragments in association with exosomes. *FASEB J.* **22**, 1469–1478 (2008).
173. Perez-Gonzalez, R., Gauthier, S. A., Kumar, A. & Levy, E. The exosome secretory pathway transports amyloid precursor protein carboxyl-terminal fragments from the cell into the brain extracellular space. *J. Biol. Chem.* **287**, 43108–43115 (2012).
174. Dinkins, M. B., Dasgupta, S., Wang, G., Zhu, G. & Bieberich, E. Exosome reduction invivo is associated with lower amyloid plaque load in the 5XFAD mouse model of Alzheimer's disease. *Neurobiol. Aging* **35**, 1792–1800 (2014).
175. Falker, C. *et al.* Exosomal cellular prion protein drives fibrillization of amyloid beta and counteracts amyloid beta-mediated neurotoxicity. *J. Neurochem.* **137**, 88–100 (2016).
176. Bulloj, A., Leal, M. C., Xu, H., Castaño, E. M. & Morelli, L. Insulin-degrading enzyme sorting in exosomes: A secretory pathway for a key brain amyloid-β degrading protease. *J. Alzheimer's Dis.* **19**, 79–95 (2010).
177. Tamboli, I. Y. *et al.* Statins promote the degradation of extracellular amyloid β-peptide by microglia via stimulation of exosome-associated insulin-degrading enzyme (IDE) secretion. *J. Biol. Chem.* **285**, 37405–37414 (2010).
178. Bahrini, I., Song, J. H., Diez, D. & Hanayama, R. Neuronal exosomes facilitate synaptic pruning by up-regulating complement factors in microglia. *Sci. Rep.* **5**, 1–8 (2015).
179. Joshi, P. *et al.* Microglia convert aggregated amyloid-β into neurotoxic forms through the shedding of microvesicles. *Cell Death Differ.* **21**, 582–593 (2014).
180. Saman, S. *et al.* Exosome-associated tau is secreted in tauopathy models and is selectively phosphorylated in cerebrospinal fluid in early Alzheimer disease. *J. Biol. Chem.* **287**, 3842–3849 (2012).
181. Wang, Y. *et al.* The release and trans-synaptic transmission of Tau via exosomes. *Mol. Neurodegener.* **12**, 1–25 (2017).

182. Wilson, C. M. *et al.* Sortilin mediates the release and transfer of exosomes in concert with two tyrosine kinase receptors. *J. Cell Sci.* **127**, 3983–3997 (2014).
183. Street, J. M. *et al.* Identification and proteomic profiling of exosomes in human cerebrospinal fluid. *J. Transl. Med.* **10**, 1–7 (2012).
184. Cheng, L., Sharples, R. A., Scicluna, B. J. & Hill, A. F. Exosomes provide a protective and enriched source of miRNA for biomarker profiling compared to intracellular and cell-free blood. *J. Extracell. Vesicles* **3**, 1–14 (2014).
185. Cheng, L., Sun, X., Scicluna, B. J., Coleman, B. M. & Hill, A. F. Characterization and deep sequencing analysis of exosomal and non-exosomal miRNA in human urine. *Kidney Int.* **86**, 433–444 (2014).
186. Santa-Maria, I. *et al.* Dysregulation of microRNA-219 promotes neurodegeneration through post-transcriptional regulation of tau. *J. Clin. Invest.* **125**, 681–686 (2015).
187. Song, Z. *et al.* Brain Derived Exosomes Are a Double-Edged Sword in Alzheimer's Disease. *Front. Mol. Neurosci.* **13**, (2020).
188. Yuyama, K. *et al.* A potential function for neuronal exosomes: Sequestering intracerebral amyloid-β peptide. *FEBS Lett.* **589**, 84–88 (2015).
189. Wong, E. & Cuervo, A. M. Integration of clearance mechanisms: the proteasome and autophagy. *Cold Spring Harb. Perspect. Biol.* **2**, 1–19 (2010).
190. Bustamante, H. A. *et al.* Interplay between the autophagy-lysosomal pathway and the ubiquitin-proteasome system: A target for therapeutic development in alzheimer's disease. *Front. Cell. Neurosci.* **12**, 1–18 (2018).
191. Albornoz, N., Bustamante, H., Soza, A. & Burgos, P. Cellular responses to proteasome inhibition: Molecular mechanisms and beyond. *Int. J. Mol. Sci.* **20**, (2019).
192. Wang, X. *et al.* Ubiquitination of serine, threonine, or lysine residues on the cytoplasmic tail can induce ERAD of MHC-I by viral E3 ligase mK3. *J. Cell Biol.* **177**, 613–624 (2007).
193. Callis, J. The Ubiquitination Machinery of the Ubiquitin System. *Arab. B.* **12**, e0174 (2014).
194. Eskelinen, E. L. & Saftig, P. Autophagy: A lysosomal degradation pathway with a central role in health and disease. *Biochim. Biophys. Acta - Mol. Cell Res.* **1793**, 664–673 (2009).
195. Rubinsztein, D. C., Mariño, G. & Kroemer, G. Autophagy and aging. *Cell* **146**, 682–695 (2011).
196. Andersson, V., Hanzén, S., Liu, B., Molin, M. & Nyström, T. Enhancing protein disaggregation restores proteasome activity in aged cells. *Aging (Albany. NY).* **5**, 802–812 (2013).
197. Ferrington, D. A., Husom, A. D. & Thompson, L. V. Altered proteasome structure,

function, and oxidation in aged muscle. *FASEB J.* **19**, 1–24 (2005).

198. Vernace, V. A., Arnaud, L., Schmidt-Glenewinkel, T. & Figueiredo-Pereira, M. E. Aging perturbs 26S proteasome assembly in Drosophila melanogaster . *FASEB J.* **21**, 2672–2682 (2007).
199. Fonseca-Gomes, J. Study the function of the newly discovered TrkB receptor fragment (TrkB-ICD) formed by calpain cleavage. (MSc thesis, Faculdade de Medicina, Universidade de Lisboa, Lisboa, 2016).
200. Schneider, F., Baldauf, K., Wetzel, W. & Reymann, K. G. Behavioral and EEG changes in male 5xFAD mice. *Physiol. Behav.* **135**, 25–33 (2014).
201. Vorhees, C. V *et al.* Adult Learning Deficits after Neonatal Exposure to D - Methamphetamine : Selective Effects on Spatial Navigation and Memory. *J. Neurosci.* **20**, 4732–4739 (2000).
202. Faivre, E. *et al.* Beneficial effect of a selective adenosine A2A receptor antagonist in the APPswe/PS1dE9 mouse model of Alzheimer's disease. *Front. Mol. Neurosci.* **11**, 1–13 (2018).
203. Mouro, F. M. *et al.* Memory deficits induced by chronic cannabinoid exposure are prevented by adenosine A2AR receptor antagonism. *Neuropharmacology* **155**, 10–21 (2019).
204. Biedler, J. L., Helson, L. & Spengler, B. A. Morphology and Growth, Tumorigenicity, and Cytogenetics of Human Neuroblastoma Cells in Continuous Culture. *Cancer Res.* **33**, 2643–2652 (1973).
205. Biedler, J. L., Schachner, M., Roffler-Tarlov, S. & Freedman, L. S. Multiple Neurotransmitter Synthesis by Human Neuroblastoma Cell Lines and Clones. *Cancer Res.* **38**, 3751–3757 (1978).
206. Mingwei, N. & Aschner, M. Neonatal Rat Primary Microglia: Isolation, Culturing and Selected Applications. *Curr Protoc Toxicol* **43**, 12.17.1-12.17.16 (2010).
207. Forster, J. I. *et al.* Characterization of Differentiated SH-SY5Y as Neuronal Screening Model Reveals Increased Oxidative Vulnerability. *J. Biomol. Screen.* **21**, 496–509 (2016).
208. Kobayashi, M., Kurihara, K. & Matsuoka, I. Retinoic acid induces BDNF responsiveness of sympathetic neurons by alteration of Trk neurotrophin receptor expression. *FEBS Lett.* **356**, 60–65 (1994).
209. Dwane, S., Durack, E. & Kiely, P. A. Optimising parameters for the differentiation of SH-SY5Y cells to study cell adhesion and cell migration. *BMC Res. Notes* **6**, (2013).
210. Cardarelli, F. *et al.* The intracellular trafficking mechanism of Lipofectamine-based transfection reagents and its implication for gene delivery. *Sci. Rep.* **6**, 1–8 (2016).
211. Wang, T., Larcher, L. M., Ma, L. & Veedu, R. N. Systematic Screening of Commonly

Used Commercial Transfection Reagents Towards Efficient Transfection of Single-Stranded Oligonucleotides. *Molecules* **23**, 1–15 (2018).

212. Kerridge, D. The Effect of Actidione and other Antifungal Agents on Nucleic Acid and Protein Synthesis in Saccharomyces carlsbergensis. *J. gen. Microbiol* **19**, 497–506 (1958).
213. Belle, A., Tanay, A., Bitincka, L., Shamir, R. & O'Shea, E. K. Quantification of protein half-lives in the budding yeast proteome. *PNAS* **103**, 13004–13009 (2006).
214. Bowman, E. J., Siebers, A. & Altendorf, K. Bafilomycins: A class of inhibitors of membrane ATPases from microorganisms, animal cells, and plant cells. *Proc. Natl. Acad. Sci. USA* **85**, 7972–7976 (1988).
215. Yoshimori, T., Yamamoto, A., Moriyama, Y., Futai, M. & Tashiro, Y. Bafilomycin A1, a Specific Inhibitor of Vacuolar-type H(+)-ATPase, Inhibits Acidification and Protein Degradation in Lysosomes of Cultured Cells. *J. og Biol. Chamistry* **266**, 17707–17712 (1991).
216. Hromadkova, L. *et al.* Brain-derived neurotrophic factor (BDNF) promotes molecular polarization and differentiation of immature neuroblastoma cells into definitive neurons. *Biochim. Biophys. Acta - Mol. Cell Res.* **1867**, 118737 (2020).
217. Filograna, R. *et al.* Analysis of the catecholaminergic phenotype in human SH-SY5Y and BE(2)-M17 neuroblastoma cell lines upon differentiation. *PLoS One* **10**, 1–18 (2015).
218. Rust, A., Leese, C., Binz, T. & Davletov, B. Botulinum neurotoxin type C protease induces apoptosis in differentiated human neuroblastoma cells. *Oncotarget* **7**, 33220–33228 (2016).
219. Rikkert, L. G., Nieuwland, R., Terstappen, L. W. M. M. & Coumans, F. A. W. Quality of extracellular vesicle images by transmission electron microscopy is operator and protocol dependent. *J. Extracell. Vesicles* **8**, (2019).
220. Pinto, S., Cunha, C., Barbosa, M., Vaz, A. R. & Brites, D. Exosomes from NSC-34 Cells Transfected with hSOD1-G93A Are Enriched in miR-124 and Drive Alterations in Microglia Phenotype. *Front. Neurosci.* **11**, 1–21 (2017).
221. Kowal, J. *et al.* Proteomic comparison defines novel markers to characterize heterogeneous populations of extracellular vesicle subtypes. *Proc. Natl. Acad. Sci. U. S. A.* **113**, E968–E977 (2016).
222. Martín-Montañez, E., López-Téllez, J. F., Acevedo, M. J., Pavía, J. & Khan, Z. U. Efficiency of gene transfection reagents in NG108-15, SH-SY5Y and CHO-K1 cell lines. *Methods Find. Exp. Clin. Pharmacol.* **32**, 291–297 (2010).
223. Li, A., Gao, X., Ren, J., Jin, C. & Xue, Y. BDM-PUB: Computational Prediction of Protein Ubiquitination Sites with a Bayesian Discriminant Method. (2009).
224. Hall, G. F. & Saman, S. Death or secretion?: The demise of a plausible assumption

about CSF-tau in alzheimer disease? *Commun. Integr. Biol.* **5**, 623–626 (2012).

225. Kaplan, D. R., Matsumoto, K., Lucarelli, E. & Thielet, C. J. Induction of TrkB by retinoic acid mediates biologic responsiveness to BDNF and differentiation of human neuroblastoma cells. *Neuron* **11**, 321–331 (1993).
226. Janardhanan, A., Sadan, A. & Vanisree, A. J. Synapsin III in Differentiated SH-SY5Y Cell Line as a Potential Tool for Neuropharmacological Evaluations in Schizophrenia. *Electron. J. Biol.* **14**, 67–75 (2018).
227. Shipley, M. M., Mangold, C. A. & Szpara, M. L. Differentiation of the SH-SY5Y human neuroblastoma cell line. *J. Vis. Exp.* **2016**, 1–11 (2016).
228. Cernaianu, G. *et al.* All-trans retinoic acid arrests neuroblastoma cells in a dormant state. Subsequent nerve growth factor/brain-derived neurotrophic factor treatment adds modest benefit. *J. Pediatr. Surg.* **43**, 1284–1294 (2008).
229. Katsetos, C. D., Herman, M. M. & Mörk, S. J. Class III β-tubulin in human development and cancer. *Cell Motil. Cytoskeleton* **55**, 77–96 (2003).
230. Malm, A. V. & Corbett, J. C. W. Improved Dynamic Light Scattering using an adaptive and statistically driven time resolved treatment of correlation data. *Sci. Rep.* **9**, 1–11 (2019).
231. Bosch, S. *et al.* Trehalose prevents aggregation of exosomes and cryodamage. *Sci. Rep.* **6**, 1–11 (2016).
232. Hong, C. S., Funk, S., Muller, L., Boyiadzis, M. & Whiteside, T. L. Isolation of biologically active and morphologically intact exosomes from plasma of patients with cancer. *J. Extracell. Vesicles* **5**, (2016).
233. Murray, S. S. *et al.* Ubiquitin Regulation of Trk Receptor Trafficking and Degradation. *Mol. Neurobiol.* **56**, 1628–1636 (2019).
234. Du, J. *et al.* Regulation of TrkB receptor tyrosine kinase and its internalization by neuronal activity and Ca2+ influx. *J. Cell Biol.* **163**, 385–395 (2003).
235. Grimes, M. L. *et al.* Endocytosis of activated trkA: Evidence that nerve growth factor induces formation of signaling endosomes. *J. Neurosci.* **16**, 7950–7964 (1996).
236. Makkerh, J. P. S. *et al.* p75 neurotrophin receptor reduces ligand-induced Trk receptor ubiquitination and delays Trk receptor internalization and degradation. *EMBO Rep.* **6**, 936–941 (2005).
237. Sánchez-Sánchez, J. & Arévalo, J. C. A review on ubiquitination of neurotrophin receptors: Facts and perspectives. *Int. J. Mol. Sci.* **18**, (2017).
238. Dikic, I. Mechanisms controlling EGF receptor endocytosis and degradation. *Biochem. Soc. Trans.* **31**, 1178–1181 (2003).
239. Berg, M. M., Sternberg, D. W., Parada, L. F. & Chao, M. V. K-252a inhibits nerve growth factor-induced trk proto-oncogene tyrosine phosphorylation and kinase activity. *J. Biol. Chem.* **267**, 13–16 (1992).

240. Carnino, J. M., Ni, K. & Jin, Y. Post-translational Modification Regulates Formation and Cargo-Loading of Extracellular Vesicles. *Front. Immunol.* **11**, 1–8 (2020).
241. Zhang, Y., Wu, X. & Tao, W. A. Characterization and applications of extracellular vesicle proteome with post-translational modifications. *TrAC - Trends Anal. Chem.* **107**, 21–30 (2018).
242. Kumari, S., Mukherjee, A. & Mukhopadhyay, C. K. Dopamine promotes cathepsin B-mediated amyloid precursor protein degradation by reactive oxygen species-sensitive mechanism in neuronal cell. *Mol. Cell. Biochem.* **454**, 153–163 (2019).
243. Chen, W., Smeekens, J. M. & Wu, R. Systematic study of the dynamics and half-lives of newly synthesized proteins in human cells. *Chem. Sci.* **7**, 1393–1400 (2016).
244. Sommerfeld, M. T., Schweigreiter, R., Barde, Y. A. & Hoppe, E. Down-regulation of the neurotrophin receptor TrkB following ligand binding. Evidence for an involvement of the proteasome and differential regulation of TrkA and TrkB. *J. Biol. Chem.* **275**, 8982–8990 (2000).
245. Proenca, C. C., Song, M. & Lee, F. S. Differential effects of BDNF and neurotrophin 4 (NT4) on endocytic sorting of TrkB receptors. *J. Neurochem.* 397–406 (2016). doi:10.1111/jnc.13676
246. Wang, D. *et al.* Proteasome inhibition boosts autophagic degradation of ubiquitinated-AGR2 and enhances the antitumor efficiency of bevacizumab. *Oncogene* **38**, 3458–3474 (2019).
247. Dasgupta, S. *et al.* Proteasome inhibitors alter levels of intracellular peptides in HEK293T and SH-SY5Y cells. *PLoS One* **9**, (2014).
248. Redmann, M. *et al.* Inhibition of autophagy with bafilomycin and chloroquine decreases mitochondrial quality and bioenergetic function in primary neurons. *Redox Biol.* **11**, 73–81 (2017).
249. Pivtoraiko, V. N. *et al.* Low-dose bafilomycin attenuates neuronal cell death associated with autophagy-lysosome pathway dysfunction. *J. Neurochem.* **114**, 1193–1204 (2010).
250. Yamashita, N. & Kuruvilla, R. Neurotrophin signaling endosomes: Biogenesis, regulation, and functions. *Curr. Opin. Neurobiol.* **39**, 139–145 (2016).
251. Geetha, T., Jiang, J. & Wooten, M. W. Lysine 63 polyubiquitination of the nerve growth factor receptor TrkA directs internalization and signaling. *Mol. Cell* **20**, 301–312 (2005).
252. Geetha, T. & Wooten, M. W. TrkA receptor endolysosomal degradation is both ubiquitin and proteasome dependent. *Traffic* **9**, 1146–1156 (2008).
253. Jerónimo-Santos, A. *et al.* Impact of in vivo chronic blockade of adenosine A2A receptors on the BDNF-mediated facilitation of LTP. *Neuropharmacology* **83**, 99–106 (2014).

254. Guo, X., Huang, X. & Chen, M. J. Reversible phosphorylation of the 26S proteasome. *Protein Cell* **8**, 255–272 (2017).
255. Bjørkøy, G. *et al.* p62/SQSTM1 forms protein aggregates degraded by autophagy and has a protective effect on huntingtin-induced cell death. *J. Cell Biol.* **171**, 603–614 (2005).
256. Almeida, C. G., Takahashi, R. H. & Gouras, G. K. Beta-Amyloid Accumulation Impairs Multivesicular Body Sorting By Inhibiting the Ubiquitin-Proteasome System. *J. Neurosci.* **26**, 4277–4288 (2006).
257. Komatsu, M. *et al.* Loss of autophagy in the central nervous system causes neurodegeneration in mice. *Nature* **441**, 880–884 (2006).
258. Korolchuk, V. I., Mansilla, A., Menzies, F. M. & Rubinsztein, D. C. Autophagy Inhibition Compromises Degradation of Ubiquitin-Proteasome Pathway Substrates. *Mol. Cell* **33**, 517–527 (2009).
259. Tseng, B. P., Green, K. N., Chan, J. L., Blurton-Jones, M. & LaFerla, F. M. Aβ inhibits the proteasome and enhances amyloid and tau accumulation. *Neurobiol. Aging* **29**, 1607–1618 (2008).
260. Richard, B. C. *et al.* Gene dosage dependent aggravation of the neurological phenotype in the 5XFAD mouse model of Alzheimer's disease. *J. Alzheimer's Dis.* **45**, 1223–1236 (2015).
261. Ferreira-Manso, M. The impact of BDNF receptor cleavage in Alzheimer's disease-associated Neuroinflammation. (MSc thesis, Faculdade de Ciências, Universidade de Lisboa, 2021).
262. Van Dam, D. & De Deyn, P. P. Animal models in the drug discovery pipeline for Alzheimer's disease. *Br. J. Pharmacol.* **164**, 1285–1300 (2011).
263. Xiao, N. A. *et al.* Reduction of glucose metabolism in olfactory bulb is an earlier Alzheimer's disease-related biomarker in 5XFAD mice. *Chin. Med. J. (Engl).* **128**, 2220–2227 (2015).
264. Gu, L. *et al.* Myelin changes at the early stage of 5XFAD mice. *Brain Res. Bull.* **137**, 285–293 (2018).
265. Wu, D. *et al.* LINGO-1 antibody ameliorates myelin impairment and spatial memory deficits in the early stage of 5XFAD mice. *CNS Neurosci. Ther.* **24**, 381–393 (2018).
266. Francis, D. D., Zaharia, M. D., Shanks, N. & Anisman, H. Stress-induced disturbances in Morris water-maze performance: Interstrain variability. *Physiol. Behav.* **58**, 57–65 (1995).
267. Harrison, F. E., Hosseini, A. H. & McDonald, M. P. Endogenous anxiety and stress responses in water maze and Barnes maze spatial memory tasks. *Behav. Brain Res.* **198**, 247–251 (2009).
268. Wolfer, D. P., Stagljar-Bozicevic, M., Errington, M. L. & Lipp, H. P. Spatial memory

and learning in transgenic mice: Fact or artifact? *News Physiol. Sci.* **13**, 118–123 (1998).

269. Manji, Z. *et al.* 5xFAD Mice Display Sex-Dependent Inflammatory Gene Induction During the Prodromal Stage of Alzheimer's Disease. *J. Alzheimer's Dis.* **70**, 1259–1274 (2019).
270. Blokland, A., Geraerts, E. & Been, M. A detailed analysis of rats' spatial memory in a probe trial of a Morris task. *Behav. Brain Res.* **154**, 71–75 (2004).
271. Jawhar, S., Trawicka, A., Jenneckens, C., Bayer, T. A. & Wirths, O. Motor deficits, neuron loss, and reduced anxiety coinciding with axonal degeneration and intraneuronal Aβ aggregation in the 5XFAD mouse model of Alzheimer's disease. *Neurobiol. Aging* **33**, 196.e29-196.e40 (2012).